UNIVERSITY OF CALIFORNIA

Los Angeles

Nuclear Membrane Ruptures in the Setting of Nuclear Lamin Deficiencies

A dissertation submitted in partial satisfaction of the requirements for the degree

Doctor of Philosophy in Molecular, Cellular, and Integrative Physiology

by

Natalie Yun-Wen Chen

2021

ABSTRACT OF THE DISSERTATION

Nuclear Membrane Ruptures in the Setting of Nuclear Lamin Deficiencies

by

Natalie Yun-Wen Chen

Doctor of Philosophy in Molecular, Cellular, and Integrative Physiology

University of California, Los Angeles, 2021

Professor Stephen G. Young, Chair

The nuclear lamina is an intermediate filament meshwork lining the inner nuclear membrane and is a key component of the nuclear envelope. The nuclear envelope separates the contents of the cell nucleus from the cytoplasm and consists of the inner and outer nuclear membranes, nuclear membrane proteins, nuclear pore complexes, and the nuclear lamina. The principal protein components of the nuclear lamina are lamins A and C (A-type lamins) and lamins B1 and B2 (B-type lamins). B-type lamins are expressed throughout development, whereas the A-type lamins are not expressed until late in development. Mutations in *LMNA* have been linked to a spectrum of human diseases, but only a single disease had been linked to mutations in *LMNB1* or *LMNB2*. Several years ago, our group showed that both lamin B1 and lamin B2 are required for neuronal migration in the developing central nervous system (CNS), and for the survival of neurons. In the developing brain, the processes of neurogenesis and neuronal migration impart considerable

mechanical stress on the cell nucleus. Neurogenesis in the ventricular zone of the developing cortex depends on interkinetic nuclear migration (INM), an oscillatory movement of nuclei between the apical and basal sides of the cell. Once neuronal fate is specified, the migration of neurons from the ventricular zone to the cortical plate depends on nuclear translocation (nucleokinesis) and passage through confined spaces. In cell culture studies, cell nuclei subjected to mechanical stresses (*i.e.*, by physically deforming nuclei or forcing cells to traverse tight constrictions) had been shown to cause nuclear membrane (NM) ruptures. The frequency of NM ruptures was known to be increased in the setting of nuclear lamin deficiencies but the relevance of NM ruptures in cultured cells to pathology in tissues was unknown.

In this dissertation, my goal was to investigate whether deficiencies in nuclear lamins predispose to nuclear membrane ruptures (particularly when the nucleus is subjected to mechanical stress during normal physiological processes, such as cell migration) and whether these ruptures may result in disease phenotypes. In Chapter 2, we showed that fibroblasts lacking all nuclear lamins exhibit spontaneous NM ruptures *in vitro* that are exacerbated by mechanical stress. In Chapter 3, we generated a mouse model with forebrain-specific loss of lamin B1 and expressing a nuclear fluorescent reporter, and showed that forebrain-specific loss of lamin B1 results in NM rupture and cell death *in vivo*. We also showed that both lamin B1– and lamin B2–deficient neuronal progenitor cells exhibit spontaneous NM ruptures, although the frequency and duration of NM ruptures was markedly different. In Chapter 4, we investigated whether overexpression of LAP2β (lamina-associated polypeptide 2, β isoform), a LEM-domain protein of the inner nuclear membrane, could prevent nuclear lamin–deficient fibroblasts and lamin B1–deficient neurons from exhibiting NM ruptures. In tandem, we discovered that reduced expression of LAP2β also rendered nuclear lamin–deficient cells more susceptible to NM ruptures.

The dissertation of Natalie Y. Chen is approved.

Arjun Deb

Karen Reue

Amy C. Rowat

Loren G. Fong

Stephen G. Young, Committee Chair

University of California, Los Angeles

2021

Dedicated to my parents, Vicki Yu and Calvin Chen, and my sister Melanie Chen.

TABLE OF CONTENTS

List of Figures

Chapter 1.

Chapter 2.

Acknowledgments

Undoubtedly, I would like to begin this page by thanking my mentors Dr. Stephen G. Young and Dr. Loren G. Fong. Drs. Young and Fong have provided me with unparalleled support and guidance from the day I joined the lab during my spring quarter rotation. They've directed me in my experiments, my writing, my figure-making, my academic career decisions, and nearly every step I've taken along the way. I do believe that, from the get-go, they believed in me perhaps even more than I believed in myself. Looking back now, what I once considered insurmountable hurdles no longer feel like hurdles, and that is what their mentorship has done for me.

I also could not have done this dissertation without the support of my committee members, Drs. Arjun Deb, Karen Reue, and Amy Rowat. Their feedback has always inspired me to think deeper and further about my dissertation work.

I am so thankful for my lab mates, who have come to feel almost like family to me. I would like to thank Dr. Yiping Tu, who has taught me with so many lab techniques and fundamental practices; Paul H. Kim, who has never hesitated to answer a question or help out when I seek his expertise; my undergraduate assistants, Jazmin Morales and Lovelyn Edillo, who have helped take care of so many lab tasks; Patrick J. Heizer for his help with my mouse studies and his "Mouse Prime Delivery" service; Thomas A. Weston for his help with my electron microscopy studies; Ye Yang for her help with figuring out mouse breeding strategies. I also thank Dr. Anne P. Beigneux and all current and former Young/Fong lab members who have been exceptional colleagues.

Outside of my research group, I am grateful to my collaborators: Jason Belling for his help with designing and building pillar substrates and the UCLA Vector Core's Emmanuelle Faure and Janet Treger for their help with lentiviruses; I acknowledge the Philip Whitcome Training program at UCLA and the UCLA Vascular Biology Training Grant for their financial support during my

studies.

And finally, I want to express my deep appreciation for my friends and family. My parents and sister, who are probably tired of hearing me say the phrase “nuclear lamina” by now, have never ceased to encourage me or cast any doubts on my ability to achieve even at times when I didn’t really think I’d ever finish. Every single time they’ve visited me in LA, I would always take them to lab with me as I took care of my cells or live-cell imaging experiments. Thank you for your patience with me. I moved to LA when I was 20 years old for graduate school and as I’ve progressed through my twenties, I’ve made some of the best friends of my life here. I couldn’t have asked for a better circle of people.

Chapter 1 was reproduced from “Nuclear membrane ruptures, cell death, and tissue damage in the setting of nuclear lamin deficiencies” published in *Nucleus* 2020 11(1):237–249 [DOI: 10.1080/19491034.2020.181540] with some modification. **Chapter 2** contains a reprint of “Fibroblasts lacking nuclear lamins do not have nuclear blebs or protrusions but nevertheless have frequent nuclear membrane ruptures” from *Proc. Natl. Acad. Sci. U. S. A.* 2018, 115(40):10100–10105 [DOI: 10.1073/pnas.1812622115]. **Chapter 3** contains a reprint of “An absence of lamin B1 in migrating neurons causes nuclear membrane ruptures and cell death” from *Proc. Natl. Acad. Sci. U. S. A.* 2019 116(51):25870–15879 [DOI: 10.1073/pnas.1917225116]. **Chapter 4** contains a reprint of “Increased expression of LAP2β, an inner nuclear membrane protein, eliminates nuclear membrane ruptures in nuclear lamin–deficient neurons and fibroblasts” currently under review for publication. All the reproduction and reprints used in this dissertation do not require permission from publishers with proper acknowledgements of the original sources of publication as an author of the articles.

VITA

University of California, Los Angeles **09/2015–present**

Los Angeles, CA

Ph.D. in Molecular, Cellular, Integrative Physiology

University of Washington **09/2009–06/2014**

Seattle, WA

Bachelor of Science in Molecular, Cellular, and Developmental Biology
with Honors

SELECTED PUBLICATIONS

1. **Chen NY,** Kim PH, Fong LG, Young SG. (2020) Nuclear membrane ruptures, cell death, and tissue damage in the setting of nuclear lamin deficiencies. *Nucleus*. 11(1):237–249.
2. Heizer PJ, Yang Y, Tu Y, Kim PH, **Chen NY**, Hu Y, Yoshinaga Y, De Jong P, Vergnes L, Morales JE, Li RL, Jackson N, Reue K, Young SG, Fong LG. (2020) Deficiency in ZMPSTE24 and resulting farnesyl–prelamin A accumulation only modestly affect mouse adipose tissue stores. *Journal of Lipid Research*. 61(3):413–421.
3. **Chen NY**, Yang Y, Weston TA, Belling JN, Heizer P, Tu Y, Kim PH, Edillo L, Jonas SJ, Weiss PS, Fong LG, Young SG. (2019) An absence of lamin B1 in migrating neurons causes nuclear membrane ruptures and cell death. *Proc. Natl. Acad. Sci. USA* 116(51):25870–25879.
4. Belling JN, Heidenreich LK, Tian Z, Mendoza AM, Chiou T, Gong Y, **Chen NY**, Young TD, Wattanatorn N, Park JH, Scarabelli L, Chiang N, Takahashi J, Young SG, Stieg AZ, De Oliveira S, Huang TJ, Weiss PS, Jonas SJ. (2019) Acoustofluidic gene delivery to human hematopoietic stem and progenitor cells. *Proc. Natl. Acad. Sci. USA* 117(20):10976–10982.
5. Nmezi BS, Xu J, Fu R, Armiger T, Rodriguez-Bey G, Schneider JM, Ma H, Tu Y, **Chen NY**, Young SG, Dahl K, Liu, Y., & Padath, Q. (2018). A concentric model for the spatial organization of the nuclear lamina predicts distinct functional roles for the A and B1 type networks. *Proc. Natl. Acad. Sci. USA* 116(10):4307–4315.

6. Kim P, Luu J, Heizer P, Tu Y, Weston TA, Lim C, **Chen N**, Li RL, Lin P-Y, Dunn J, Hodzic D, Young SG, Fong, LG (2018). Disrupting the LINC Complex in Aortic Smooth Muscle Cells Ameliorates Vascular Disease in a Mouse Model of Hutchinson-Gilford Progeria Syndrome. *Science Translational Medicine*. 10(460):eaat7163.
7. **Chen NY**, Kim P, Weston T, Edillo L, Tu Y, Fong LG, Young SG. (2018) Fibroblasts lacking nuclear lamins do not have nuclear blebs but nevertheless have frequent nuclear membrane ruptures. *Proc. Natl. Acad. Sci. USA* 115(40):10100–10105.
8. Dapp MJ, Chen L, Hall BM, Westfall D, Wong K, Zhao H, Deng W, Sibley T, Ghoral T, Kim K, **Chen N**, McHugh S, Au L, Kober KM, Cohen M, Anastos K, Mullins JI. (2017). Patterns and rates of viral evolution in HIV-1 subtype infected females and males. *PLoS ONE*. 12(1):e0182443.

Chapter 1:

Introduction

The Nuclear Lamina in Health and Disease

The nuclear lamina is an intermediate filament meshwork of nuclear lamin proteins underlying the inner nuclear membrane of the nuclear envelope. Nuclear lamins, the proteins that make up the nuclear lamina supporting the cell nucleus, were discovered more than 35 years ago (1, 2). Since then, the structural and genetic properties of these proteins have been thoroughly examined. Mutations in *LMNA* (the gene for lamins A and C) cause more than a dozen human disorders (3, 4), including muscular dystrophy, lipodystrophy, and premature aging syndromes, such as Hutchinson-Gilford progeria syndrome. In contrast, only a single *LMNB1* mutation has been confirmed to cause human disease (duplication of *LMNB1* causing autosomal dominant leukodystrophy)(5). While B-type lamins (lamin B1 and lamin B2) were once believed to play essential roles, such as mitosis and DNA replication (6–9), in all cells, Drs. Stephen Young and Loren Fong generated tissue-specific models of B-type lamin deficiencies that proved to be completely viable (10, 11). More importantly, they made a critical discovery that both B-type lamins held crucial and independent roles in central nervous system (CNS) development: loss of either B-type lamin impaired neuronal migration in the cerebral cortex and the retina—and loss of either B-type lamin lead to varying degrees of neuronal death (12–15).

Forces on the Cell Nucleus During Neuronal Migration

Investigating the developing brain as a model to study the role of nuclear lamins in neuronal migration was intriguing. First, neurons in the developing mouse brain (before E18.5) express *Lmnb1* and *Lmnb2* (the genes for lamin B1 and lamin B2) at high levels, but the expression of *Lmna* (the gene for lamin A and lamin C) is absent (16–19). There is no reason to believe that the "natural deficiency" of lamin A and lamin C in cortical neurons would impair neuronal migration, but we suspected that a deficiency of one additional nuclear lamin protein (either lamin B1 or

lamin B2) might render neurons susceptible to nuclear membrane ruptures (20). Second, the glial-directed migration of neurons from the ventricular zone (where neurons are born) to their final position within the cortical plate, subjects neurons to mechanical stress. The migration of neurons is utterly dependent on nucleokinesis—a process by which cytoplasmic motors pull the nucleus forward (along microtubules) into the leading edge of the cell. Nucleokinesis is central for two developmental processes in the CNS. The first is interkinetic nuclear migration (INM), which is required for the birth of new neurons (21). During INM, the nuclei of neuronal progenitors move in an oscillatory, cell-cycle–dependent pattern between the apical and basal sides of the ventricular zone. Dynein motors tug on the nucleus via nucleoporins within the nuclear envelope. Without nucleoporins, apical movement of nuclei is abolished. When nuclear movement is incomplete, cell-cycle progression does not occur and neurons are not born. The second form of nuclear movement takes place as newborn neurons migrate to their final laminar position in the CNS. In this process, the centrosome moves into the leading edge of the cells and cytoplasmic motors pull the nucleus towards the centrosome. After the nucleus is pulled forward, the trailing edge of the cell remodels, resulting in net forward movement of the neuron (21–25). Multiple cycles of nucleokinesis, followed by remodeling of the trailing edge of the cell, results in saltatory movement of the neuron to its final position within the cortical plate. The forces required for nuclear translocation are exerted on the "linker of nucleoskeleton and cytoskeleton" (LINC) complex which is anchored to the nuclear lamina (15, 26–29).

Coffinier and coworkers discovered, using immunohistochemistry and BrdU birthdating experiments, that the glial-directed migration of neurons from the ventricular zone to the cortical plate is defective in both *Lmnb1*- and *Lmnb2*-deficient embryos (12, 18). The defective migration of neurons results in markedly abnormal layering of neurons in the cerebral cortex. Defective

neuronal migration is likely caused by ineffective nucleokinesis. Because a deficiency of lamin B1 or lamin B2 reduces the integrity of the nuclear lamina, the cytoplasmic motors that normally pull the nucleus into the leading edge of the cell are ineffective. Rather than moving the nucleus, they simply "stretch out" and deform the nucleus (18). Misshapen nuclei are common in the cortical plate of *Lmnb1*$^{-/-}$ and *Lmnb2*$^{-/-}$ embryos (18). In addition to defective layering of cortical plate neurons, there was another noteworthy finding in *Lmnb1*$^{-/-}$ and *Lmnb2*$^{-/-}$ embryos—fewer neurons and evidence of neuronal cell death (18). Decreased cellularity of the cortical plate was striking in E18.5 *Lmnb1*$^{-/-}$ embryos but subtle in E18.5 *Lmnb2*$^{-/-}$ embryos (12, 18). While *Lmnb1*$^{-/-}$ and *Lmnb2*$^{-/-}$ embryos die at birth, forebrain-specific knockout models survive normally. Inactivation of *Lmnb1* or *Lmnb2* in these forebrain-specific knockout models still resulted in a progressive loss of neurons. By two months of age, forebrains in forebrain-specific knockout mice were very small and the numbers of viable neurons were markedly reduced. In two-month-old forebrain-specific *Lmnb1*/*Lmnb2* double-knockout mice, neurons were undetectable (18). Thus, lamin B1 and lamin B2 are crucial for the postnatal survival of cortical neurons (12, 18). In neurons, we hypothesized that mechanical stresses associated with nucleokinesis result in nuclear membrane ruptures in the setting of nuclear lamin deficiencies, and that the interspersion of nuclear and cytoplasmic contents ultimately causes DNA damage and neuronal death (Figure 1.1).

Early Descriptions of Nuclear Membrane Ruptures

Nuclear membrane ruptures were observed in 2001 by de Noronha *et al.* (30) while working to elucidate how Vpr, a multifunctional HIV-1 protein, affects nuclear–cytoplasmic trafficking. They found that overexpression of Vpr in HeLa cells resulted in herniations of nuclear chromatin (nuclear blebs) and noted that blebs appeared in segments of the nuclear envelope that were deficient in lamin C and nuclear pore complexes. Vpr overexpression was accompanied by

ruptures of nuclear membranes, resulting in the escape of nuclear contents into the cytoplasm. They assumed that nuclear membrane ruptures originated from the nuclear blebs. In 2006, Cohen *et al.* (31) examined parvovirus-infected fibroblasts and observed evidence of nuclear membrane ruptures. Immunofluorescence microscopy studies with antibodies against lamins A/C revealed gaps in the nuclear lamina, and electron microscopy studies identified discontinuities in the nuclear envelope (31).

Subsequently, nuclear membrane ruptures were identified in human fibroblasts harboring missense or nonsense mutations in *LMNA* and in cancer cell lines (osteosarcoma cells, HeLa cells) (32–34). In 2011, De Vos *et al*. (32) observed spontaneous nuclear membrane ruptures in fibroblasts from patients with *LMNA* missense mutations (including mutations causing familial partial lipodystrophy, cardiomyopathy, and a progeroid disorder). In 2013, Tamiello *et al.* (33) observed nuclear membrane ruptures in fibroblasts from a two-year-old child with a progeroid disorder resulting from compound heterozygosity for p.T528M and p.M540T mutations in *LMNA*. The fibroblasts in the latter study contained a nuclear-localized yellow fluorescent protein (EYFP-NLS), and nuclear membrane ruptures were visualized by the escape of the EYFP-NLS into the cytoplasm. Vargas *et al.* (34) observed spontaneous nuclear membrane ruptures in cultured osteosarcoma and HeLa cells, which have baseline abnormalities in nuclear shape and where nuclear lamin proteins can be distributed unevenly along the nuclear rim. Using osteosarcoma cells that had been transfected with GFP containing a nuclear localization signal (GFP_3-NLS), they observed, by videomicroscopy, nuclear membrane ruptures in ~8% of the cells, with most ruptures undergoing repair within 30 min (allowing for return of GFP_3-NLS into the nucleus). The frequency of nuclear membrane ruptures increased to ~25% when the cells were transiently transfected with an siRNA cocktail against lamin A/C, lamin B1, and lamin B2—or when the cells

were stably transfected with a short hairpin RNA (shRNA) against lamin B1(34). These studies provided the first clues that nuclear lamin deficiencies could be linked to nuclear membrane ruptures or loss of nuclear membrane integrity.

Nuclear Membrane Rupture Frequency in Cells Subjected to Mechanical Stress

Several studies have examined the impact of mechanical stress on nuclear membrane ruptures (35–37). Harada *et al.* (38) found that serum-driven migration of lung carcinoma–derived A549 cells through 3-μm pores resulted in a large increase in caspase 3–positive cell death in the setting of lamin-A knockdown. In 2016, Raab *et al*. (35) found, by videomicroscopy, that bone marrow–derived mouse dendritic cells expressing a nuclear-localized GFP (NLS-GFP) exhibited nuclear membrane ruptures as they migrated through collagen-filled channels containing 5-μm constrictions and when the cells migrated within a mouse ear explant. During cell migration, the nuclei became deformed, followed by nuclear membrane ruptures, evident from reduced NLS-GFP in the nucleoplasm and escape of NLS-GFP into the cytoplasm. To define the site of nuclear membrane rupture, Raab *et al*. (35) examined the localization of a GFP-tagged cytoplasmic DNA-binding probe (cyclic guanosine monophosphate-adenosine monophosphate synthase; cGAS) in RPE1 cells as the cells migrated across narrow constrictions. They identified GFP-cGAS foci at the leading edge of the cell—the same site where nuclear protrusions were observed. When RPE1 cells with a lamin A/C knockdown were forced to traverse narrow constrictions, nuclear membrane ruptures were accompanied by reduced cell survival.

At the same time, Denais *et al.* (36) observed nuclear membrane ruptures in human fibroblasts, breast cancer cells, and fibrosarcoma cells migrating in a microfluidic device with 2-μm constrictions. They documented nuclear membrane ruptures by the escape of NLS-GFP into the cytoplasm and by visualizing the distribution of a GFP containing a nuclear export signal (NES-

GFP), which is normally confined to the cytoplasm. In the setting of nuclear membrane ruptures, NES-GFP appeared in the nucleus. They also observed cGAS at sites of nuclear membrane ruptures. Both Raab *et al.* (35) and Denais *et al.* (36) found that nuclear membrane ruptures in migrating cells were accompanied by an accumulation of fluorescently-labelled 53BP, a protein that is recruited to double-stranded DNA breaks and to regions of low chromatin density (37). In migrating osteosarcoma cells with nuclear membrane ruptures, Irianto *et al.* (37) observed increased numbers of γH2AX foci in the nucleus and DNA breaks, as well as escape of DNA repair factors into the cytoplasm.

Cytoskeletal–Nuclear Force Transmission Triggers Nuclear Membrane Ruptures

The transmission of cytoskeletal forces to the nucleus increases the frequency of nuclear membrane ruptures. For example, Raab *et al.* (35) observed that increased force transmission to the cell nucleus as mouse dendritic cells migrate through dense extracellular matrices resulted in more nuclear membrane ruptures (35). Also, an uncontrolled accumulation of contractile actin stress fibers over the cell nucleus (39) resulted in nuclear deformation and increased numbers of nuclear membrane ruptures. Conversely, Hatch *et al*. (40) showed that depolymerizing actin filaments with cytochalasin D or latrunculin—or inhibiting the actomyosin network with blebbistatin—reduced nuclear membrane ruptures in osteosarcoma cells with a knockdown of lamin B1. Additionally, Xia *et al.* (41) showed that blebbistatin suppressed nuclear membrane ruptures when A549 cells (with a lamin A knockdown) migrated through small pores (42). Disrupting the (LINC) complex, either by reducing SUN protein expression or by disrupting nesprin–SUN protein interactions with a KASH domain, also reduced the frequency of nuclear membrane ruptures (40). The LINC complex, located in the perinuclear space, is crucial for transmitting forces from the cytoskeleton to the nuclear lamina (29).

While multiple studies have documented nuclear membrane ruptures when the nuclear lamina is weakened or compromised by reduced expression of nuclear lamins or by the expression of mutant nuclear lamin proteins (32–36, 40), my thesis work has helped advanced our knowledge on the role of nuclear lamins in nuclear membrane ruptures. At this point we know that fibroblasts lacking nuclear lamins exhibit frequent spontaneous nuclear membrane ruptures and DNA damage. (43), The impressive vitality of TKO MEFs raised a provocative question: Are nuclear membrane ruptures innocuous in living animals or do they adversely affect cell vitality in the setting of physiologic or developmental processes in living animals? To define the importance of nuclear membrane ruptures *in vivo*, we investigated migrating neurons in the developing brain. In the setting of lamin B1 or lamin B2 deficiency, we hypothesized that the mechanical stress associated with nucleokinesis and cell migration could trigger nuclear membrane ruptures and lead inexorably to cell death. We investigated this hypothesis in cell culture models and in the developing cerebral cortex of mouse embryos. Our studies uncovered, for the first time, a link between nuclear membrane ruptures, neuronal survival, and tissue pathology (20).

Physiologic Relevance of Nuclear Membrane Ruptures

We doubt that the relevance of ruptures is restricted to the developing brain. Sooner or later, we suspect that nuclear membrane ruptures will be shown to be important in the pathophysiology of multiple laminopathies, particularly those associated with cell death and overt tissue pathology. In recent years, there has been considerable interest in the arterial pathology of Hutchinson-Gilford progeria syndrome (HGPS) (44), a progeroid disorder caused by a mutant form of prelamin A (progerin) (45–47) that cannot be processed to mature lamin A (45–47). In a 2018 paper, we (48) made a seminal observation about nuclear lamin gene expression in the aorta. In medial SMCs, we found that the expression of *Lmna* is quite high, whereas *Lmnb1* expression is very low. In HGPS

mice, we observed very high levels of progerin protein in the medial SMCs of the aorta but very low levels of lamin B1 protein (48). In contrast, both proteins were expressed at high levels in the endothelial cells of the arterial intima. We hypothesized that this combination—high levels of progerin but low levels of lamin B1—rendered SMCs susceptible to injury in the setting of mechanical stress—and that it might be possible to prevent SMC death by blocking transmission of cytoskeleton forces to the nucleus. To explore that hypothesis, we examined the effects of disrupting the LINC complex in both progerin-expressing SMCs in cell culture and in the aortas of HGPS mice. To disrupt the LINC complex, we expressed the KASH (Klarischt/Anc-1, Syne Homology) domain of Nesprin2 (KASH2) (48) in SMCs, which interferes with Nesprin–Sun protein interactions in the perinuclear space and limits transmission of cytoskeletal forces to the nucleus. The hypothesis that interrupting force transmission to the nucleus would ameliorate disease phenotypes was confirmed—both in progerin-expressing SMCs in culture and in histopathologic studies of HGPS mice (48). In cultured progerin-expressing SMCs, KASH2 expression eliminated nuclear blebs and markedly reduced DNA damage and, in HGPS mice harboring a transgene encoding a *Cre*-activatable KASH2 domain, activation of KASH2 expression in aortic SMCs significantly reduced death of SMCs in the medial layer of the aorta and reduced the compensatory thickening of the adventitial layer (48). It seems possible that nuclear membrane ruptures occur in SMCs and underlie the progressive loss of SMCs in the medial layer of the aorta in HGPS mice. This scenario is plausible, particularly since our electron microscopy studies (48) uncovered profound morphological defects in the nuclear membranes of medial SMCs in aortas of HGPS mice.

More recently, Earle *et al*. (49) investigated the relevance of nuclear membrane ruptures to myopathy in *Lmna*$^{-/-}$ mice and gene-targeted mice harboring lamin A/C missense mutations

known to cause myopathy in humans. In cultured myotubes (generated from myoblasts isolated from the mutant mice), they observed misshapen nuclei, DNA damage, and frequent nuclear membrane ruptures. In myofibers harvested from mutant mice, they found that expression of a KASH2 domain reduced DNA damage, consistent with our earlier studies (48). They also found indirect evidence for nuclear membrane ruptures in myofibers harvested from mice (cGAS foci and the presence of heat shock protein 90 in the nucleus). We suggest that future studies of mouse models of *LMNA*-related muscular dystrophies should take advantage of the ROSA$^{td\text{-}Tomato}$ transgene (20) and examine, in a more direct fashion, the frequency of nuclear membrane ruptures in specific skeletal muscle beds under different experimental conditions. Directly assessing the frequency of nuclear membrane ruptures in skeletal muscle beds, combined with quantification of dystrophic changes in skeletal muscles, could add considerably to our understanding of the *LMNA*-related myopathies.

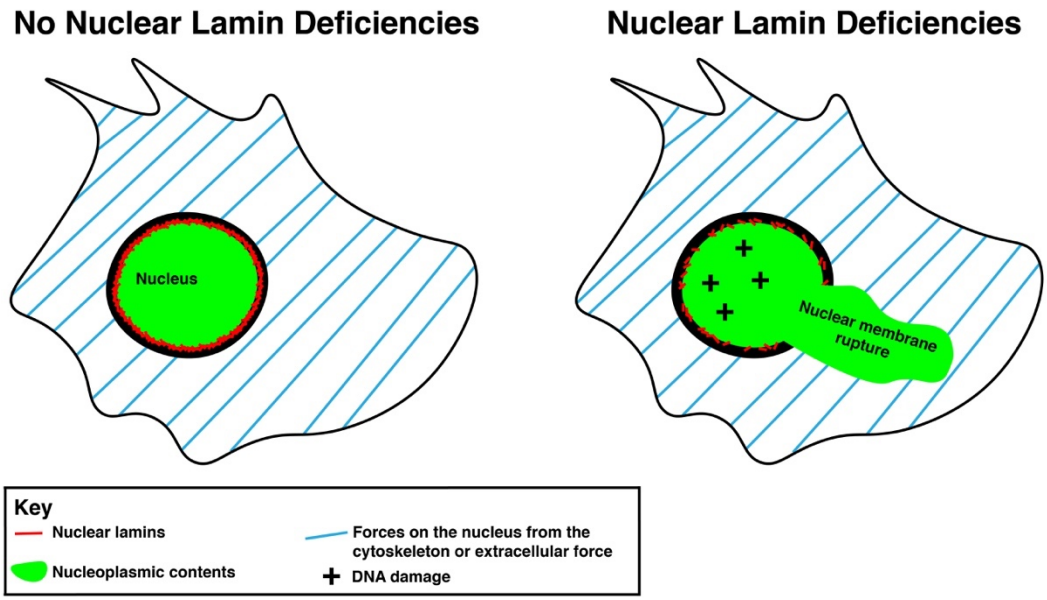

Figure 1.1. Schematic diagram of nuclear membrane rupture. The nuclear lamina (red) is a meshwork underlying the nuclear membranes surrounding the nucleus (nucleoplasmic contents are denoted by green). With an intact nuclear lamina, even when the nucleus is subject to forces from the cytoskeleton or extracellular forces (blue), the nucleoplasmic contents stay localized to the nucleus because nuclear membrane integrity is not disrupted. Without a nuclear lamina (or in the absence of some nuclear lamins resulting in a functionally compromised nuclear lamina), we hypothesized that forces on the nucleus would result in a loss of nuclear membrane integrity as judged by the leakage of nucleoplasmic contents (green) into the cytoplasm. This is what we call a nuclear membrane rupture. When nuclear membrane integrity is lost, we suspect that the mixing of nucleoplasmic and cytoplasmic contents would result in DNA damage within the nucleus (black crosses). This is perhaps an underlying mechanism for disease in the setting of nuclear lamin deficiencies or defects.

References

1. Gerace L & Blobel G (1982) Nuclear lamina and the structural organization of the nuclear envelope. *Cold Spring Harb Symp Quant Biol* 46 Pt 2:967–978.
2. Gerace L, Blum A, & Blobel G (1978) Immunocytochemical localization of the major polypeptides of the nuclear pore complex-lamina fraction. Interphase and mitotic distribution. *J Cell Biol* 79(2 Pt 1):546–566.
3. Worman HJ, Fong LG, Muchir A, & Young SG (2009) Laminopathies and the long strange trip from basic cell biology to therapy. *J Clin Invest* 119(7):1825–1836.
4. Worman HJ & Bonne G (2007) "Laminopathies": a wide spectrum of human diseases. *Exp Cell Res* 313(10):2121–2133.
5. Padiath QS*, et al.* (2006) Lamin B1 duplications cause autosomal dominant leukodystrophy. *Nat Genet* 38(10):1114–1123.
6. Martin C*, et al.* (2009) Lamin B1 maintains the functional plasticity of nucleoli. *J Cell Sci* 122(Pt 10):1551–1562.
7. Tsai MY*, et al.* (2006) A mitotic lamin B matrix induced by RanGTP required for spindle assembly. *Science* 311(5769):1887–1893.
8. Moir RD, Montag-Lowy M, & Goldman RD (1994) Dynamic properties of nuclear lamins: lamin B is associated with sites of DNA replication. *J Cell Biol* 125(6):1201–1212.
9. Dechat T*, et al.* (2007) Alterations in mitosis and cell cycle progression caused by a mutant lamin A known to accelerate human aging. *Proc Natl Acad Sci USA* 104(12):4955–4960.
10. Yang SH*, et al.* (2011) An absence of both lamin B1 and lamin B2 in keratinocytes has no effect on cell proliferation or the development of skin and hair. *Hum Mol Genet* 20(18):3537–3544.

11. Yang SH, Jung HJ, Coffinier C, Fong LG, & Young SG (2011) Are B-type lamins essential in all mammalian cells? *Nucleus* 2(6):562–569.

12. Coffinier C*, et al.* (2010) Abnormal development of the cerebral cortex and cerebellum in the setting of lamin B2 deficiency. *Proc Natl Acad Sci USA* 107(11):5076–5081.

13. Jung HJ*, et al.* (2013) Farnesylation of lamin B1 is important for retention of nuclear chromatin during neuronal migration. *Proc Natl Acad Sci U S A* 110(21):E1923–1932.

14. Lee JM*, et al.* (2014) Reciprocal knock-in mice to investigate the functional redundancy of lamin B1 and lamin B2. *Mol Biol Cell* 25(10):1666–1675.

15. Coffinier C, Fong LG, & Young SG (2010) LINCing lamin B2 to neuronal migration: growing evidence for cell-specific roles of B-type lamins. *Nucleus* 1(5):407–411.

16. Dechat T*, et al.* (2008) Nuclear lamins: major factors in the structural organization and function of the nucleus and chromatin. *Genes Dev.* 22(7):832–853.

17. Coffinier C*, et al.* (2010) Direct synthesis of lamin A, bypassing prelamin a processing, causes misshapen nuclei in fibroblasts but no detectable pathology in mice. *J Biol Chem* 285(27):20818–20826.

18. Coffinier C*, et al.* (2011) Deficiencies in lamin B1 and lamin B2 cause neurodevelopmental defects and distinct nuclear shape abnormalities in neurons. *Mol Biol Cell* 22(23):4683–4693.

19. Jung HJ*, et al.* (2012) Regulation of prelamin A but not lamin C by miR-9, a brain-specific microRNA. *Proc Natl Acad Sci USA* 109(7):E423–431.

20. Chen NY*, et al.* (2019) An absence of lamin B1 in migrating neurons causes nuclear membrane ruptures and cell death. *Proc Natl Acad Sci USA* 116(51):25870–25879.

21. Hu DJ*, et al.* (2013) Dynein recruitment to nuclear pores activates apical nuclear migration and mitotic entry in brain progenitor cells. *Cell* 154(6):1300–1313.

22. Vallee RB & Tsai JW (2006) The cellular roles of the lissencephaly gene LIS1, and what they tell us about brain development. *Genes Dev* 20(11):1384–1393.

23. Tsai JW, Bremner KH, & Vallee RB (2007) Dual subcellular roles for LIS1 and dynein in radial neuronal migration in live brain tissue. *Nat Neurosci* 10(8):970–979.

24. Wynshaw-Boris A (2007) Lissencephaly and LIS1: insights into the molecular mechanisms of neuronal migration and development. *Clin Genet* 72(4):296–304.

25. Tsai LH & Gleeson JG (2005) Nucleokinesis in neuronal migration. *Neuron* 46(3):383–388.

26. Razafsky D, Zang S, & Hodzic D (2011) UnLINCing the nuclear envelope: towards an understanding of the physiological significance of nuclear positioning. *Biochem Soc Trans* 39(6):1790–1794.

27. Razafsky D & Hodzic D (2009) Bringing KASH under the SUN: the many faces of nucleo-cytoskeletal connections. *J Cell Biol* 186(4):461–472.

28. Hale CM*, et al.* (2008) Dysfunctional connections between the nucleus and the actin and microtubule networks in laminopathic models. *Biophys J* 95(11):5462–5475.

29. Crisp M*, et al.* (2006) Coupling of the nucleus and cytoplasm: role of the LINC complex. *J Cell Biol* 172(1):41–53.

30. de Noronha CM*, et al.* (2001) Dynamic disruptions in nuclear envelope architecture and integrity induced by HIV-1 Vpr. *Science* 294(5544):1105–1108.

31. Cohen S, Behzad AR, Carroll JB, & Pante N (2006) Parvoviral nuclear import: bypassing the host nuclear-transport machinery. *J Gen Virol* 87(Pt 11):3209–3213.

32. De Vos WH, *et al.* (2011) Repetitive disruptions of the nuclear envelope invoke temporary loss of cellular compartmentalization in laminopathies. *Hum Mol Genet* 20(21):4175–4186.

33. Tamiello C, *et al.* (2013) Soft substrates normalize nuclear morphology and prevent nuclear rupture in fibroblasts from a laminopathy patient with compound heterozygous LMNA mutations. *Nucleus* 4(1):61–73.

34. Vargas JD, Hatch EM, Anderson DJ, & Hetzer MW (2012) Transient nuclear envelope rupturing during interphase in human cancer cells. *Nucleus* 3(1):88–100.

35. Raab M, *et al.* (2016) ESCRT III repairs nuclear envelope ruptures during cell migration to limit DNA damage and cell death. *Science* 352(6283):359–362.

36. Denais CM, *et al.* (2016) Nuclear envelope rupture and repair during cancer cell migration. *Science* 352(6283):353–358.

37. Irianto J, *et al.* (2017) DNA Damage Follows Repair Factor Depletion and Portends Genome Variation in Cancer Cells after Pore Migration. *Curr Biol* 27(2):210–223.

38. Harada T, *et al.* (2014) Nuclear lamin stiffness is a barrier to 3D migration, but softness can limit survival. *J Cell Biol* 204(5):669–682.

39. Kanellos G, *et al.* (2015) ADF and Cofilin1 Control Actin Stress Fibers, Nuclear Integrity, and Cell Survival. *Cell Rep* 13(9):1949–1964.

40. Hatch EM & Hetzer MW (2016) Nuclear envelope rupture is induced by actin-based nucleus confinement. *J Cell Biol* 215(1):27–36.

41. Xia Y, *et al.* (2018) Nuclear rupture at sites of high curvature compromises retention of DNA repair factors. *J Cell Biol* 217(11):3796–3808.

42. Xia Y*, et al.* (2019) Rescue of DNA damage after constricted migration reveals a mechano-regulated threshold for cell cycle. *J Cell Biol* 218(8):2545–2563.

43. Chen NY*, et al.* (2018) Fibroblasts lacking nuclear lamins do not have nuclear blebs or protrusions but nevertheless have frequent nuclear membrane ruptures. *Proc Natl Acad Sci USA* 115(40):10100–10105.

44. DeBusk FL (1972) The Hutchinson-Gilford progeria syndrome. Report of 4 cases and review of the literature. *J Pediatr* 80(4):697–724.

45. Eriksson M*, et al.* (2003) Recurrent de novo point mutations in lamin A cause Hutchinson-Gilford progeria syndrome. *Nature* 423(6937):293–298.

46. Young SG, Fong LG, & Michaelis S (2005) Prelamin A, Zmpste24, misshapen cell nuclei, and progeria--new evidence suggesting that protein farnesylation could be important for disease pathogenesis. *J Lipid Res* 46(12):2531–2558.

47. De Sandre-Giovannoli A*, et al.* (2003) Lamin a truncation in Hutchinson-Gilford progeria. *Science* 300(5628):2055.

48. Kim PH*, et al.* (2018) Disrupting the LINC complex in smooth muscle cells reduces aortic disease in a mouse model of Hutchinson-Gilford progeria syndrome. *Sci Transl Med* 10(460).

49. Earle AJ*, et al.* (2020) Mutant lamins cause nuclear envelope rupture and DNA damage in skeletal muscle cells. *Nat Mater* 19(4):464–473.

Chapter 2:

Fibroblasts Lacking Nuclear Lamins Do Not Have Nuclear Blebs or Protrusions but Nevertheless Have Frequent Nuclear Membrane Ruptures

Fibroblasts lacking nuclear lamins do not have nuclear blebs or protrusions but nevertheless have frequent nuclear membrane ruptures

Natalie Y. Chen[a], Paul Kim[a], Thomas A. Weston[a], Lovelyn Edillo[a], Yiping Tu[a], Loren G. Fong[a,1,2], and Stephen G. Young[a,b,c,1,2]

[a]Department of Medicine, University of California, Los Angeles, CA 90095; [b]Department of Human Genetics, University of California, Los Angeles, CA 90095; and [c]The Molecular Biology Institute, University of California, Los Angeles, CA 90095

Contributed by Stephen G. Young, August 14, 2018 (sent for review July 23, 2018; reviewed by William T. Dauer and Howard J. Worman)

The nuclear lamina, an intermediate filament meshwork lining the inner nuclear membrane, is formed by the nuclear lamins (lamins A, C, B1, and B2). Defects or deficiencies in individual nuclear lamin proteins have been reported to elicit nuclear blebs (protrusions or outpouchings of the nuclear envelope) and increase susceptibility for nuclear membrane ruptures. It is unclear, however, how a complete absence of nuclear lamins would affect nuclear envelope morphology and nuclear membrane integrity (i.e., whether nuclear membrane blebs or protrusions would occur and, if not, whether cells would be susceptible to nuclear membrane ruptures). To address these issues, we generated mouse embryonic fibroblasts (MEFs) lacking all nuclear lamins. The nuclear lamin-deficient MEFs had irregular nuclear shapes but no nuclear blebs or protrusions. Despite a virtual absence of nuclear blebs, MEFs lacking nuclear lamins had frequent, prolonged, and occasionally nonhealing nuclear membrane ruptures. By transmission electron microscopy, the inner nuclear membrane in nuclear lamin-deficient MEFs have a "wavy" appearance, and there were discrete discontinuities in the inner and outer nuclear membranes. Nuclear membrane ruptures were accompanied by a large increase in DNA damage, as judged by γ-H2AX foci. Mechanical stress increased both nuclear membrane ruptures and DNA damage, whereas minimizing transmission of cytoskeletal forces to the nucleus had the opposite effects.

nuclear lamina | nuclear envelope | nuclear membrane rupture

The nuclear lamina is an intermediate filament meshwork lining the inner nuclear membrane and is composed of A-type and B-type nuclear lamins (1, 2). The nuclear lamina provides structural support for the cell nucleus and interacts with the nuclear chromatin, transcription factors, and proteins of the inner nuclear membrane (1, 2).

For years, the nuclear lamins were thought to play essential roles in the cell nucleus. In particular, B-type lamins were thought to play roles in DNA synthesis (3–5) and in the assembly of the mitotic spindle (6, 7). Recent studies by Jung et al. (8) showed that this is not the case; keratinocytes and fibroblasts proliferate normally and survive in the absence of nuclear lamins. Studies with embryonic stem cells support the idea that nuclear lamin-deficient cells can proliferate and differentiate (9, 10). These newer insights demand a better understanding of the physiologic importance of the nuclear lamina.

One clue into the function of the nuclear lamina is that deficiencies in nuclear lamins or structural defects in nuclear lamins result in nuclear blebs (protrusions or outpouchings of the nuclear envelope) (11–14). Nuclear blebs occur in fibroblasts from patients with Hutchinson–Gilford progeria syndrome (a progeroid syndrome caused by a mutant form of prelamin A) (15), and blebs are common in lamin B1-deficient fibroblasts (16). The mechanisms for nuclear bleb formation are not fully understood, but Funkhouser et al. (11) proposed that separations of nuclear lamin filamentous networks cause nuclear blebs.

Another clue to the function of the nuclear lamina is the observation that defects or deficiencies in nuclear lamins result in nuclear membrane ruptures, leading to intermixing of nucleoplasmic and cytoplasmic contents (17–21) and DNA damage (21, 22). The assumption has been that nuclear membrane ruptures originate from nuclear blebs (19, 22–26).

In the current study, we generated mouse embryonic fibroblasts (MEFs) lacking all nuclear lamins. We wanted to determine whether those cells would manifest nuclear blebs (or protrusions of the chromatin beyond the bounds of the nuclear membranes). We also wanted to determine whether cells lacking nuclear lamins would be susceptible to nuclear membrane ruptures—or whether the absence of nuclear lamin filaments might actually protect from nuclear membrane ruptures.

Results

Nuclear Lamin-Deficient Mouse Embryonic Fibroblasts. We generated *Lmna*$^{+/+}$*Lmnb1* $^{/}$ *Lmnb2*$^{+/+}$ MEFs [lamin B1 knockout (B1KO)], *Lmna*$^{+/}$ *Lmnb1* $^{/}$ *Lmnb2* $^{/}$ MEFs [expressing lamin A/C from one allele but no B-type lamins (A1B0)], and *Lmna* $^{/}$ *Lmnb1* $^{/}$ *Lmnb2* $^{/}$ MEFs [triple knockout (TKO)]. TKO MEFs were created by treating *Lmna* $^{/}$ *Lmnb1*$^{fl/fl}$*Lmnb2*$^{fl/fl}$ MEFs (8, 27) with *Cre* adenovirus. TKO MEFs did not express transcripts for prelamin A, lamin C, lamin B1, or lamin B2, as judged by qRT-PCR (Fig. 1*A*). As expected, nuclear lamin proteins were absent from TKO MEFs, as judged by Western blots (Fig. 1*B*) and immunofluorescence microscopy (Fig. 1 *C* and *D*). B1KO MEFs lacked lamin B1 but had normal levels of lamins A, C, and B2. A1B0 MEFs lacked lamins B1 and B2 but had half-normal amounts of lamins A and C (Fig. 1 *B*–*D*).

Significance

Genetic defects in nuclear lamins or reduced expression of nuclear lamins is accompanied by nuclear blebs and an increased susceptibility for nuclear membrane ruptures. Nuclear membrane ruptures are exacerbated by subjecting cells to mechanical forces. Here, we demonstrate that cells lacking nuclear lamins have oblong nuclei, but no nuclear blebs and no protrusions of the chromatin beyond the bounds of the nuclear membranes. Nevertheless, the cells displayed frequent and prolonged nuclear membrane ruptures, associated with DNA damage and occasionally by cell death. Thus, the nuclear lamina is crucial for the integrity of the nuclear membranes and for limiting damage to DNA. We suspect that our observations could be relevant to disease caused by defects or deficiencies in the nuclear lamins.

Author contributions: N.Y.C., L.G.F., and S.G.Y. designed research; N.Y.C., P.K., T.A.W., L.E., and Y.T. performed research; N.Y.C. and P.K. contributed new reagents/analytic tools; N.Y.C. and S.G.Y. analyzed data; and N.Y.C., L.G.F., and S.G.Y. wrote the paper.

Reviewers: W.T.D., University of Michigan; and H.J.W., Columbia University.

The authors declare no conflict of interest.

[1]L.G.F. and S.G.Y. contributed equally to this work.

[2]To whom correspondence may be addressed. Email: lfong@mednet.ucla.edu or sgyoung@mednet.ucla.edu.

This article contains supporting information online at www.pnas.org/lookup/suppl/doi:10.1073/pnas.1812622115/-/DCSupplemental.

Published online September 17, 2018.

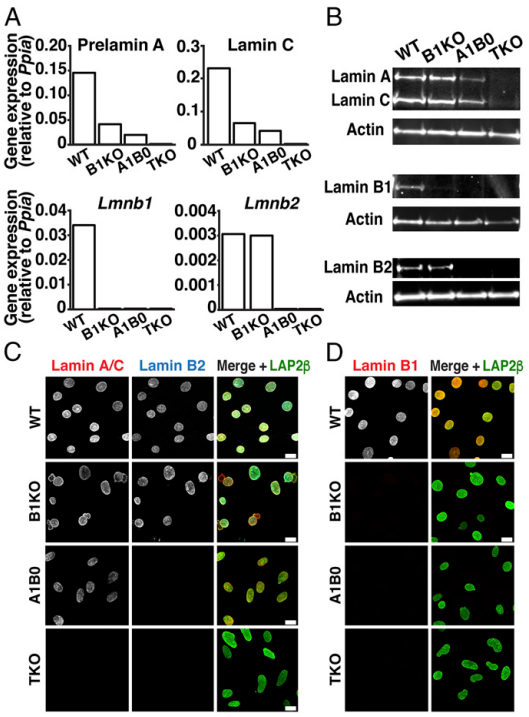

Fig. 1. Mouse embryonic fibroblasts (MEFs) lacking nuclear lamins. (*A*) Transcript levels for prelamin A, lamin C, lamin B1, and lamin B2 in *Lmna*$^{+/+}$*Lmnb1*$^{+/+}$*Lmnb2*$^{+/+}$ [wild-type (WT)], *Lmna*$^{+/+}$*Lmnb1*$^{-/-}$*Lmnb2*$^{+/+}$ [lamin B1 knockout (B1KO)], *Lmna*$^{+/-}$*Lmnb1*$^{-/-}$*Lmnb2*$^{-/-}$ [expressing lamin A/C from one allele but no B-type lamins (A1B0)], and *Lmna*$^{-/-}$*Lmnb1*$^{-/-}$*Lmnb2*$^{-/-}$ [triple-knockout (TKO)] MEFs. Expression was normalized to *Ppia*; mean of two independent experiments. (*B*) Western blots showing nuclear lamin expression in MEFs. Actin was used as a loading control. (*C*) Immunofluorescence microscopy of MEFs with antibodies against lamin A/C (red), lamin B2 (blue), and LAP2β (green). (Scale bars, 20 μm.) (*D*) Immunofluorescence microscopy of MEFs with antibodies against lamin B1 (red) and LAP2β (green). (Scale bars, 20 μm.)

An Absence of Nuclear Blebs in TKO MEFs. Nuclei of WT MEFs were round or oval, and nuclear blebs were very rare (Fig. 2 *A* and *B*). Nuclei from B1KO and A1B0 MEFs were round or oval, but 10.7 ± 3.3% of B1KO MEFs and 16.2 ± 5.3% of A1B0 MEFs had nuclear blebs (Fig. 2 *A* and *B*). Nuclear blebs in TKO MEF nuclei were rare (2.0 ± 1.2%; n = 527 cells), but 84.0 ± 4.1% of nuclei were oblong or irregularly shaped (Fig. 2 *A*, *C*, and *D*). In TKO MEFs, we never observed herniation or protrusion of chromatin beyond the bounds of the nuclear membranes [visualized with the inner nuclear membrane marker LAP2β (lamina-associated polypeptide 2, β isoform)]. Nuclear pore complexes (NPCs) were asymmetrically distributed in TKO MEFs (*SI Appendix*, Fig. S1 *A* and *B*), in keeping with results in an earlier study (9).

By transmission electron microscopy (TEM), both inner and outer nuclear membranes of TKO MEFs were "wavy," whereas only the outer nuclear membrane was wavy in WT MEFs (Fig. 2 *E* and *F* and *SI Appendix*, Fig. S2*A*).

Frequent Nuclear Ruptures in TKO MEFs. To assess susceptibility of TKO MEFs to nuclear membrane ruptures, we expressed an NLS-GFP reporter (green fluorescent protein with a nuclear localization signal) (22) in MEFs and visualized cells by fluorescence microscopy (*SI Appendix*, Fig. S3*A*). In WT MEFs, NLS-GFP was nearly always confined to the nucleus, but the NLS-GFP in TKO MEFs was often present in the cytoplasm, indicating the presence of a nuclear membrane rupture (19, 20, 22). Nuclear membrane ruptures were also rare in wild-type MEFs as they moved across the substrate (Fig. 3*A*, *Top*, and Movie S1). In contrast, nuclear membrane ruptures were frequent in migrating TKO MEFs (Fig. 3*A*, *Bottom*, and Movie S2). In most cases, the ruptures were repaired, and the NLS-GFP returned to the nucleus. Nuclear membrane ruptures often occurred repetitively in the same fibroblast.

To determine the frequency of nuclear membrane ruptures in TKO MEFs, we imaged NLS-GFP–expressing TKO MEFs for 20 h. Numbers of nuclear membrane ruptures and the percentage

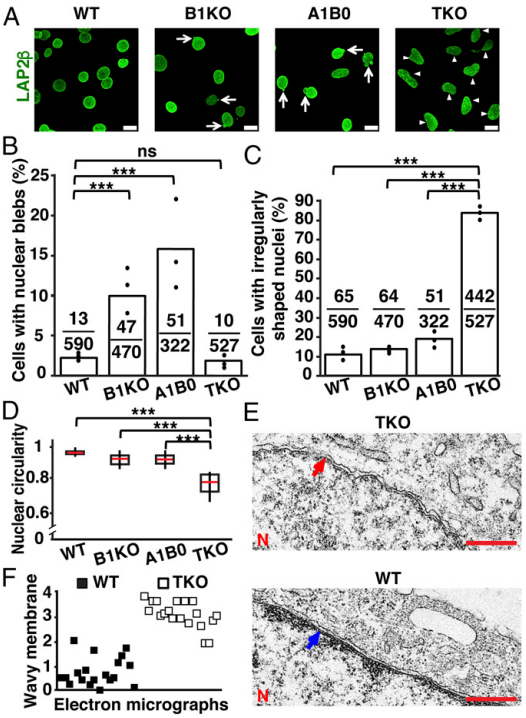

Fig. 2. Morphological abnormalities in WT, B1KO, A1B0, and TKO MEFs. (*A*) Immunofluorescence microscopy of MEFs stained with an antibody against LAP2β (green). The arrows point to nuclear blebs; the arrowheads point to irregularly shaped nuclei. (Scale bars, 20 μm.) (*B*) Percentages of cells with nuclear blebs. The black circles show the averages for three independent experiments; fractions show numbers of cells with blebs divided by the total number of cells examined. ***P < 0.0001 by χ^2 test; ns, nonsignificant, P > 0.05. (*C*) Percentages of cells with irregularly shaped nuclei. The black circles indicate the averages for three independent experiments; fractions show the numbers of cells with irregularly shaped nuclei divided by the total number of cells examined. ***P < 0.0001 by χ^2 test. (*D*) Box plots showing reduced circularity of the nucleus in TKO MEFs. The red line denotes the population median; boxes show 25th and 75th percentiles; and vertical lines show the 10th and 90th percentiles. ***P < 0.0001 by unpaired Student's t test. (*E*) Electron micrographs showing that the inner nuclear membrane in TKO MEFs is wavy (*red* arrow), whereas it is straighter in WT MEFs (blue arrow). N, nuclei. (Scale bar, 500 nm.) (*F*) Scatter plot showing the average "wavy membrane score" for 38 electron micrographs (19 WT and 19 TKO MEFs) by 10 observers blinded to genotype. Each square represents the average score for an image (0 representing the "least wavy" and 4 representing the "most wavy"). WT MEFs (black squares); TKO MEF electron micrographs (white squares).

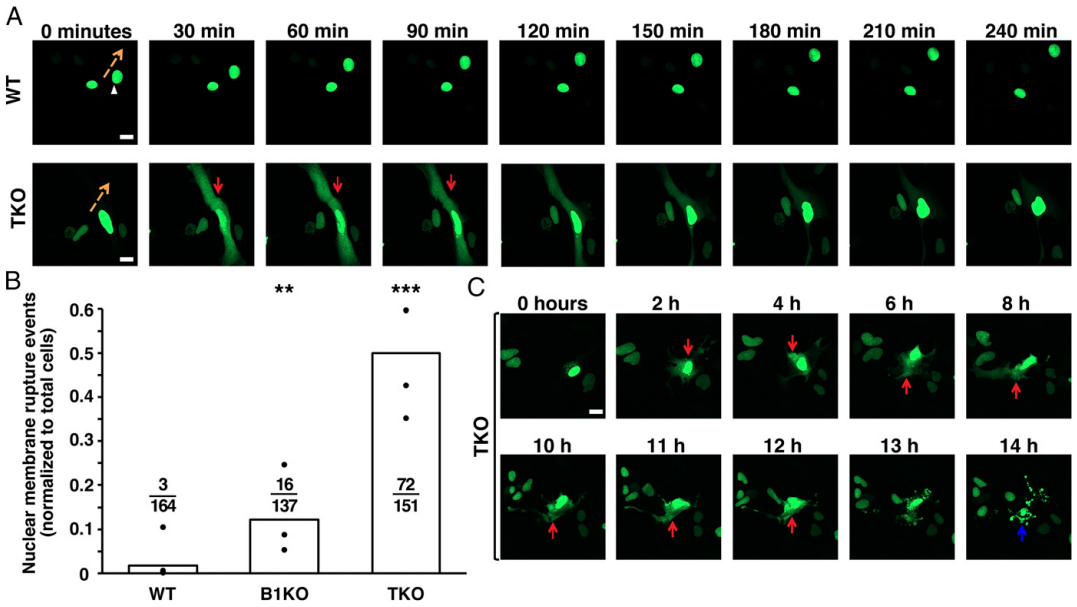

Fig. 3. Nuclear membrane ruptures in TKO MEFs. (*A*) Sequential images of WT and TKO MEFs expressing a green fluorescent protein fused to a nuclear localization signal (NLS-GFP) (green) and imaged by live-cell fluorescence microscopy for 240 min. Images at 30-min intervals are shown. The orange arrows indicate the direction of nuclear movement, and the red arrows point to a nuclear membrane rupture event in a TKO MEF. (*B*) Bar graph showing the number of nuclear membrane ruptures as a percentage of the total number of cells evaluated. The black circles show the averages for three independent experiments. Ratios above each genotype show the total number of nuclear membrane rupture events divided by the total number of cells evaluated. Nuclear membrane ruptures were more frequent in TKO and B1KO MEFs than in WT MEFs. $^{**}P < 0.001$; $^{***}P < 0.0001$ by χ^2 test. (*C*) Sequential images showing a nonhealing nuclear membrane rupture in a TKO MEF (NLS-GFP remains in the cytoplasm) and cell death after 14 h. (Scale bars: *A* and *C*, 20 μm.)

of fibroblasts with nuclear membrane ruptures were higher in TKO MEFs than in WT or B1KO MEFs ($P < 0.0001$) (Fig. 3*B* and *SI Appendix*, Fig. S3*B*). We observed 72 nuclear membrane ruptures in 151 TKO MEFs. Also, nuclear membrane ruptures were more prolonged in TKO MEFs (241 ± 66 min in TKO MEFs vs. 94.4 ± 39 min in B1KO MEFs) (*SI Appendix*, Fig. S3*C*). When TKO MEFs were seeded at high density, nuclear membrane ruptures were observed in migrating cells squeezing between closely packed cells (*SI Appendix*, Fig. S3*D* and Movie S3).

Earlier studies suggested that nuclear membrane ruptures occurred at sites of nuclear blebs (12, 19, 22, 25), but ruptures were common in TKO MEFs despite a virtual absence of blebs. To determine whether nuclear membrane blebs formed before nuclear membrane ruptures, TKO MEFs were imaged at 15-s intervals (*SI Appendix*, Fig. S4*A* and Movies S4–S6). We never observed nuclear blebs or protrusions before nuclear membrane ruptures, suggesting that nuclear blebs are not a prerequisite for nuclear membrane ruptures. Also, we observed no apparent correlation between nuclear membrane ruptures and nuclear blebs in B1KO MEFs (*SI Appendix*, Fig. S4*B*). We identified 16 nuclear membrane ruptures in 137 B1KO MEFs (6.5 ± 1.4%) (Fig. 3*B*), but only 3 of the 16 ruptures occurred in cells harboring a nuclear bleb (*SI Appendix*, Fig. S4 *B* and *C* and Movies S7–S9).

We observed examples of nonhealing nuclear membrane ruptures in TKO MEFs, and those cells invariably died (Fig. 3*C* and Movies S10 and S11), implying that persistent interspersion of cytoplasmic and nucleoplasmic contents is incompatible with cell survival. We suspected that nuclear membrane ruptures in TKO MEFs might lead to DNA damage. Indeed, γ-H2AX foci were far more frequent in TKO MEFs than in WT MEFs (*SI Appendix*, Fig. S5).

TKO and B1KO MEFs harboring nuclear membrane ruptures had gaps and irregularities in the distribution of LAP2β (Fig. 4*A* and *B* and *SI Appendix*, Fig. S6*A*). In WT MEFs (Fig. 2*A*) and mutant MEFs without ruptures (*SI Appendix*, Fig. S6*B*), LAP2β was homogenously distributed at the nuclear rim. In MEFs with nuclear membrane ruptures, we occasionally observed significant colocalization of NLS-GFP with the ER-resident protein calreticulin, presumably reflecting a ruptured inner nuclear membrane and entry of NLS-GFP into the ER (Fig. 4*C*). More frequently, there was minimal colocalization with calreticulin and NLS-GFP was located throughout the cytoplasm, reflecting ruptures of both inner and outer nuclear membranes (*SI Appendix*, Fig. S6*C*). By TEM, we identified short discontinuities in either the inner or the outer nuclear membranes in TKO MEFs (Fig. 4*D* and *SI Appendix*, Fig. S7), but we never found a gaping hole involving both the inner and outer nuclear membranes.

Disrupting the Cytoskeleton Reduces Nuclear Membrane Ruptures in TKO MEFs. Cytochalasin D reduced the percentage of TKO MEFs with irregularly shaped nuclei (11.3 ± 0.9% vs. 73.2 ± 1.2% in untreated cells) (Fig. 5 *A*, *B*, and *G*), likely by reducing transmission of cytoskeletal forces to the nucleus. Similarly, disrupting the LINC complex with the KASH domain of nesprin 2 (KASH2) (28) reduced the percentage of cells with irregularly shaped nuclei (Fig. 5 *C* and *G*). Neither cytochalasin D nor KASH2 corrected the distribution of NPCs in TKO MEFs (*SI Appendix*, Fig. S1 *C* and *D*), nor did those interventions normalize the wavy inner nuclear membrane phenotype (*SI Appendix*, Fig. S2 *B* and *C*).

We examined the frequency of nuclear membrane ruptures in WT and TKO MEFs under static conditions and with biaxial stretching. Under static conditions, nuclear membrane ruptures were detected in 1.9 ± 0.2% of WT MEFs and 10.7 ± 1.7% of TKO MEFs. When stretched, the frequency of nuclear membrane ruptures was 3.2 ± 1.7% in WT cells vs. 37.3 ± 6.4% in TKO MEFs

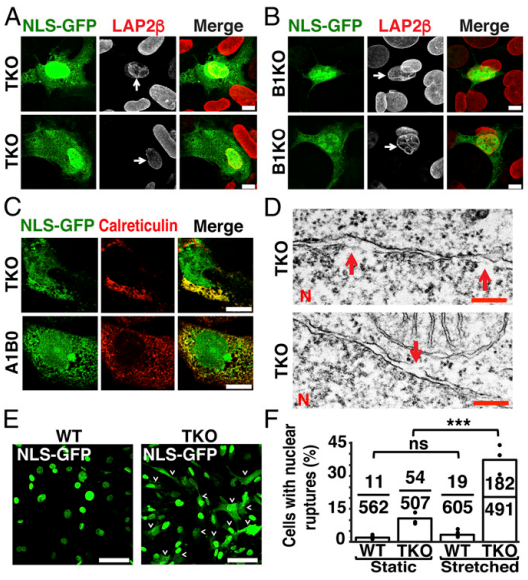

Fig. 4. Increased nuclear membrane ruptures in MEFs lacking nuclear lamins. (*A* and *B*) Immunofluorescence microscopy showing abnormal LAP2β distribution (red) in TKO (*A*) and B1KO (*B*) cells harboring nuclear membrane ruptures (arrows). (Scale bars, 10 μm.) (*C*) Fluorescence microscopy of MEFs with nuclear membrane ruptures (i.e., NLS-GFP in the cytoplasm) and stained with an antibody against calreticulin (ER marker; red). Cytoplasmic NLS-GFP was detected within the ER (yellow) and outside the ER (green). (Scale bars, 10 μm.) (*D*) Electron micrographs showing breaks (red arrows) in the inner (*Top*) and the outer nuclear membrane (*Bottom*) of TKO MEFs. N, nuclei. (Scale bars, 200 nm.) (*E*) Fluorescence microscopy showing larger numbers of nuclear membrane ruptures in TKO MEFs subjected to biaxial stretching. WT and TKO MEFs were subjected to biaxial stretching for 24 h. Nuclear membrane ruptures were frequent, as judged by NLS-GFP (green) in the cytoplasm (arrowheads). (Scale bars, 50 μm.) (*F*) Bar graph showing effects of stretching on nuclear membrane ruptures in WT and TKO MEFs. The black circles indicate frequencies in three independent experiments. Ratios above each genotype show the number of cells with NLS-GFP in the cytoplasm divided by the number of cells scored. ***$P < 0.0005$; ns, nonsignificant, $P > 0.05$ by χ^2 test.

(Fig. 4 *E* and *F*). Cytochalasin D reduced the frequency of nuclear membrane ruptures in TKO MEFs (Fig. 5 *H* and *I*). Under static conditions, 13 ± 7.2% of untreated TKO MEFs had nuclear membrane ruptures vs. 2.8 ± 1.7% in cells treated with cytochalasin D (Movie S12). When TKO MEFs were subjected to biaxial stretching, 43 ± 11.1% of untreated cells had nuclear membrane ruptures vs. 6.8 ± 4.2% in cells treated with cytochalasin D (Fig. 5*I*). Cytochalasin D also reduced the frequency of DNA damage (as judged by γ-H2AX foci), both under static conditions and with stretching ($P < 0.0005$) (Fig. 5 *J*–*L* and *SI Appendix*, Fig. S8).

Partial Rescue of Nuclear Abnormalities in TKO MEFs by Individual Nuclear Lamins. We expressed individual nuclear lamins in TKO MEFs at levels comparable to those in wild-type MEFs (*SI Appendix*, Fig. S9 *A*–*C*). The expression of each nuclear lamin improved the distribution of NPCs, with the NPC distribution mirroring the distribution of the nuclear lamin (*SI Appendix*, Fig. S1 *E*–*G*). Lamin A expression, but not lamin B1 or B2 expression, reversed the wavy inner nuclear membrane phenotype (*SI Appendix*, Fig. S2 *D*–*F*). Expression of either lamin A or lamin B1 reduced the percentage of cells with irregularly shaped nuclei ($P < 0.0001$) but simultaneously elicited nuclear blebs (Fig. 5 *D*, *E*, and *G* and *SI Appendix*, Fig. S9*G*). Lamin A in transfected TKO MEFs was distributed in a "honeycomb" pattern, in contrast to the even distribution pattern of lamin A in WT MEFs (*SI Appendix*, Fig. S9*D*) and the even distribution of lamin B1 in transfected TKO MEFs (*SI Appendix*, Fig. S9*E*). Lamin B2 was unevenly distributed in lamin B2-expressing TKO MEFs, and lamin B2 did not correct the irregular nuclear shape phenotype (Fig. 5 *F* and *G* and *SI Appendix*, Fig. S9*F*). Lamin B1 expression reduced the frequency of nuclear membrane ruptures, whereas lamin B2 expression did not (Fig. 5*H* and Movies S13 and S14). Unexpectedly, lamin A expression in TKO MEFs increased the frequency of nuclear membrane ruptures (Fig. 5*H* and Movie S15). The duration of ruptures in lamin A-expressing TKO MEFs was shorter than in nontransfected TKO MEFs (*SI Appendix*, Fig. S9*H*), but the shorter duration of ruptures was not accompanied by reduced DNA damage (*SI Appendix*, Fig. S9*I*).

Discussion

We examined nuclear membrane morphology and nuclear membrane ruptures in fibroblasts lacking all nuclear lamins (TKO MEFs) and gleaned five insights. First, nuclei in TKO MEFs are oblong and irregularly shaped but nuclear blebs are virtually absent. Cytochalasin D normalized nuclear shape, implying that cytoskeletal forces cause the abnormal nuclear shape. Second, the absence of nuclear lamins in TKO MEFs was accompanied by discrete discontinuities in either the inner or outer nuclear membranes but no gaping holes, as judged by TEM. A hallmark of TKO MEFs is a wavy inner nuclear membrane. The expression of lamin A largely normalized that phenotype, while the effects of the B-type lamins were far less impressive. Third, despite a virtual absence of nuclear blebs in TKO MEFs, nuclear membrane ruptures were frequent. These ruptures were prolonged and accompanied by DNA damage. In most cases, the nuclear membrane ruptures eventually healed, but in some cells the ruptures persisted, resulting in cell death. Fourth, nuclear membrane ruptures and the accompanying DNA damage were exaggerated by mechanical stretching and minimized by interventions that reduce force transmission to the nucleus (e.g., actin depolymerization, disrupting the LINC complex). These observations support earlier reports that external forces on the nucleus promote nuclear membrane ruptures (19, 22–26, 29). Fifth, transfection of TKO MEFs with individual nuclear lamin proteins did not abolish nuclear membrane ruptures, implying that a combination of several nuclear lamins is required for maintaining nuclear membrane integrity.

Earlier studies showed that mutations or deficiencies in nuclear lamin proteins can elicit nuclear blebs and nuclear membrane ruptures (11–14), leading to the assumption that nuclear membrane ruptures originate from weak segments of the nuclear envelope (i.e., blebs). However, we found that nuclear membrane ruptures in TKO MEFs are frequent despite an absence of blebs. Our data from live-cell imaging at 15-s intervals provided no indication that blebs or protrusions precede nuclear membrane ruptures, although we cannot exclude the possibility that the blebs are so evanescent that they simply cannot be visualized with this approach. Also, in B1KO MEFs, only a few of the nuclear membrane ruptures occurred in cells harboring nuclear blebs. Also, the expression of lamin B1 in TKO MEFs increased the frequency of nuclear blebs while reducing the frequency of nuclear membrane ruptures.

Expressing lamin A in TKO MEFs increased the frequency of nuclear membrane ruptures, whereas lamin B1 reduced the frequency of ruptures. In the case of lamin B1, we suspect that the association of its farnesyl lipid anchor with the inner nuclear membrane serves to immobilize lamin B1 filaments and thereby preserve the integrity of the inner nuclear membrane. Mature lamin A lacks a lipid anchor; consequently, lamin A filaments have greater mobility and might even pierce the nuclear membranes (particularly when the membranes are not buffered by a layer of lamin B1 filaments). We believe that this scenario is plausible. In keratinocytes lacking nuclear lamins, keratin filaments can be visualized in the cell nucleus, raising the possibility that those filaments may have pierced the nuclear membranes (8).

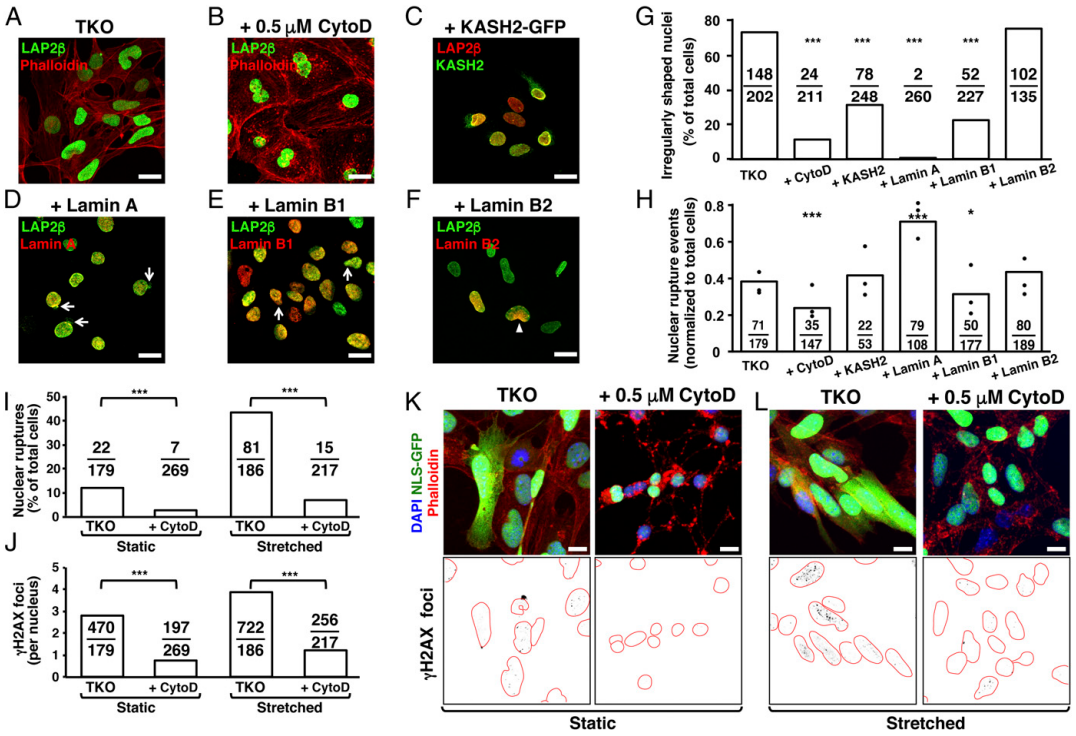

Fig. 5. Impact of actin depolymerization, disrupting the LINC complex, and nuclear lamin expression on nuclear morphology, nuclear membrane ruptures, and DNA damage in TKO MEFs. (*A–F*) Fluorescence microscopy images of TKO MEFs treated with 0.5 μM cytochalasin D (to disrupt the cytoskeleton); TKO MEFs expressing the KASH domain of nesprin 2 (KASH2-EGFP; to disrupt the LINC complex); and expressing human prelamin A (pTRIPZ-hu-prelamin A), human lamin B1 (pTRIPZ-*LMNB1*), or human lamin B2 (pTRIPZ-*LMNB2*). Cells were stained to visualize LAP2β, actin (with phalloidin), KASH2, lamin A, lamin B1, or lamin B2. Expression of lamin A and lamin B1 elicited nuclear blebs (arrows). In most cells, lamin B2 was not expressed uniformly in the nucleus (arrowhead). (Scale bars, 20 μm.) (*G*) Percentage of TKO MEFs with irregularly shaped nuclei. The ratios show the number of cells with irregularly shaped nuclei divided by the total number of cells examined. Treatment groups vs. control: $***P < 0.0001$ by χ^2 test. (*H*) Number of nuclear membrane ruptures in TKO MEFs. The results were analyzed as described in *G*. Treatment groups vs. control: $*P < 0.01$, $***P < 0.0001$ by χ^2 test. (*I*) Bar graph showing that cytochalasin D reduces the frequency of nuclear membrane ruptures in static and stretched TKO MEFs. The results were analyzed as described in *G*. $***P < 0.0001$ by χ^2 test. (*J*) Bar graph showing that cytochalasin D reduces γ-H2AX foci in static and stretched TKO MEFs. The results were analyzed as described in *G*. $***P < 0.0005$ by Student's *t* test. (*K* and *L*) Fluorescence microscopy images showing that cytochalasin D reduces γ-H2AX foci in static (*K*) and stretched (*L*) TKO MEFs. Panels below images show γ-H2AX foci (black) inside nuclei (outlined in red). (Scale bars: *K* and *L*, 10 μm.)

By TEM, we observed short discontinuities in the inner nuclear membrane and the outer nuclear membrane, but despite exhaustive efforts found no gaping holes involving both inner and outer nuclear membranes. However, it is conceivable that we simply overlooked large breaches, given that only ~15% of the cells have nuclear membrane ruptures at any given time. Also, we imaged only a small portion of the cell nucleus; our TEM sections were 65 nm thick, while the nucleus is several micrometers thick.

Our studies underscored functional differences between lamin B1 and lamin B2. Both lamin B1 and lamin B2 are uniformly distributed along the nuclear rim in wild-type cells (13, 14, 30). When those proteins are expressed in TKO MEFs, lamin B1 is uniformly distributed along the nuclear rim, whereas in many cells lamin B2 is distributed in an inhomogeneous fashion. Also, in contrast to lamin B1, lamin B2 had no capacity to elicit nuclear blebs in TKO MEFs or to correct the wavy inner nuclear membrane phenotype. The distinct properties of the two B-type lamins are consistent with our earlier findings. In lamin B1-deficient neurons, the distribution of lamin B2 is inhomogeneous, whereas lamin B1 is distributed normally in lamin B2-deficient neurons (13). Also, the farnesyl lipid anchor is crucial for lamin B1 stability and function, whereas lamin B2's farnesyl lipid tail is dispensable (30).

By immunofluorescence microscopy, we observed two intriguing findings. The first is that occasional TKO MEFs with nuclear membrane ruptures displayed substantial colocalization of NLS-GFP and calreticulin. In those cells, we suspect that an inner nuclear membrane rupture allowed NLS-GFP to enter the perinuclear space and then enter the ER lumen (where calreticulin resides). The second observation is that TKO MEFs with nuclear membrane ruptures invariably had gaps and irregularities in the distribution of LAP2β, whereas LAP2β was evenly distributed in cells without nuclear membrane ruptures. We do not know whether the profoundly abnormal distribution of LAP2β preceded the nuclear membrane ruptures or was a consequence of the ruptures. We cannot completely exclude the possibility that the gaps in LAP2β distribution reflected gaping holes in the nuclear membranes, but our TEM studies provided no support for that possibility.

In summary, our studies demonstrate that an absence of nuclear lamins leads to frequent and prolonged nuclear membrane ruptures and DNA damage. Ultimately, we suspect that our findings will prove relevant to disease phenotypes, for example

the progressive loss of cortical neurons accompanying deficiencies of lamin B1 or lamin B2 (13, 14, 30, 31).

Materials and Methods

Cell Culture. To generate TKO MEFs (*Lmna*$^{-/-}$*Lmnb1*$^{-/-}$*Lmnb2*$^{-/-}$), we treated *Lmna*$^{-/-}$*Lmnb1*$^{fl/fl}$*Lmnb2*$^{fl/fl}$ MEFs as described previously (8, 27) with *Cre* adenovirus. To generate fluorescently labeled cell lines with the nuclear rupture reporter NLS-GFP (22), we transduced cells with lentivirus by UCLA's Vector Core Facility.

RNA Studies. qRT-PCR (qPCR) studies were performed with the primers listed in *SI Appendix*, Table S1.

Western Blots. Urea-soluble protein extracts from cells were prepared (32), and Western blots were performed with the antibodies listed in *SI Appendix*, Table S2.

Immunofluorescence Microscopy. Cells on coverslips were fixed with 4% paraformaldehyde in PBS or ice-cold methanol followed by one dip in acetone and permeabilized with 0.2% Triton. The cells were then processed for confocal immunofluorescence microscopy (27) using antibodies listed in *SI Appendix*, Table S2.

Nuclear Shape Analysis. To quantify percentages of cells with nuclear blebs and cells with irregularly shaped nuclei, we stained MEFs with an antibody against LAP2β (*SI Appendix*, Table S2). Fluorescence images of randomly selected nuclei were acquired at 20× on a Zeiss LSM700 laser-scanning microscope. Nuclei of WT, B1KO, A1B0, and TKO MEFs were scored as normal, having one or more nuclear blebs, or irregularly shaped (deviating from a spherical shape, oblong) by an independent observer blinded to genotype. At least 300 cells were scored per group.

Electron Microscopy. Cells were prepared by fixing and scraping monolayers of cells or by en face embedding of adherent cells grown on Thermanox (Ted Pella) coverslips. Details are included in *SI Appendix, SI Materials and Methods*.

Live-Cell Imaging. Live-cell imaging was performed with 35-mm glass-bottom microwell Petri dishes (MatTek) or six-well plates containing 2-mm glass wells (MatTek) on a Zeiss LSM 800 confocal microscope with a Plan Apochromat 10×/0.45 or a Plan Apochromat 20×/0.80 objective at 37 °C with 5% CO_2 maintained by TempModule S1 (Zeiss) and CO_2 Module S1 (Zeiss). *Z* stacks were acquired from fluorescence and transmission channels in sequential order at indicated time steps.

Cell Stretching. Stretching MEFs on polydimethylsiloxane (PDMS) membranes was performed as described (33). Cells were seeded on flexible PDMS membranes (1 mm thick). The membranes were stretched 5 mm at 0.5 Hz for 24 h. To test the effects of cytochalasin D on nuclear membrane ruptures, the membranes were stretched 2 mm at 0.5 Hz for 2 h.

Treatment of Cells with Cytochalasin D. MEFs were treated with 0.5 μM cytochalasin D (Tocris) for 1 h before live-cell imaging or fixation for immunofluorescence microscopy. For cell-stretching experiments, MEFs were treated with 0.5 μM cytochalasin D for 3 h before being stretched 2 mm at 0.5 Hz for 3 h.

Expression Vectors for Nuclear Lamins and KASH2. pTRIPZ-Prelamin A was generated with a human prelamin A cDNA (#SC101048; Origene) (33). pTRIPZ-*LMNB1* and pTRIPZ-*LMNB2* were generated by introducing a human lamin B1 cDNA (#SC116661; Origene) or a human lamin B2 cDNA (#SC106163; Origene) into the pTRIPZ vector with Infusion Cloning (Clontech). The EGFP-KASH2 sequence was amplified from pEGFP-C1-KASH2 (34) subcloned into the pLenti6/v5-DEST plasmid (Thermo Fisher).

Statistical Analyses. Statistical analyses were performed with GraphPad QuickCalcs (https://www.graphpad.com/). Differences in nuclear morphologies (blebs, irregularly shaped nuclei) and nuclear membrane rupture frequency were analyzed with a χ^2 test. Differences in nuclear circularity and numbers of γ-H2AX foci were assessed by two-tailed Student's *t* test.

See *SI Appendix, SI Materials and Methods* for more details on the methods we used.

ACKNOWLEDGMENTS. We thank Dr. Dino Di Carlo (UCLA) for the use of the membrane cleaning device. We thank Dr. Jan Lammerding for sharing the NLS-GFP plasmid and for observations that inspired us to embark on this project. Virus production and transduction were performed by the Integrated Molecular Technologies Core/UCLA Vector Core, which is supported by Center for Ulcer Research and Education/P30 DK041301. This work was supported by National Institutes of Health Grant HL126551 (to S.G.Y.) and Grant AG047192 (to L.G.F.), National Institutes of Health Ruth L. Kirschstein National Research Service Award T32GM065823 (to N.Y.C.), and a Whitcome Fellowship award from UCLA's Molecular Biology Institute.

1. Worman HJ, Fong LG, Muchir A, Young SG (2009) Laminopathies and the long strange trip from basic cell biology to therapy. *J Clin Invest* 119:1825–1836.
2. Burke B, Stewart CL (2013) The nuclear lamins: Flexibility in function. *Nat Rev Mol Cell Biol* 14:13–24.
3. Moir RD, Montag-Lowy M, Goldman RD (1994) Dynamic properties of nuclear lamins: Lamin B is associated with sites of DNA replication. *J Cell Biol* 125:1201–1212.
4. Moir RD, et al. (2000) Review: The dynamics of the nuclear lamins during the cell cycle—relationship between structure and function. *J Struct Biol* 129:324–334.
5. Ellis DJ, Jenkins H, Whitfield WG, Hutchison CJ (1997) GST-lamin fusion proteins act as dominant negative mutants in *Xenopus* egg extract and reveal the function of the lamina in DNA replication. *J Cell Sci* 110:2507–2518.
6. Tsai MY, et al. (2006) A mitotic lamin B matrix induced by RanGTP required for spindle assembly. *Science* 311:1887–1893.
7. Harborth J, Elbashir SM, Bechert K, Tuschl T, Weber K (2001) Identification of essential genes in cultured mammalian cells using small interfering RNAs. *J Cell Sci* 114:4557–4565.
8. Jung HJ, et al. (2014) An absence of nuclear lamins in keratinocytes leads to ichthyosis, defective epidermal barrier function, and intrusion of nuclear membranes and endoplasmic reticulum into the nuclear chromatin. *Mol Cell Biol* 34:4534–4544.
9. Guo Y, Zheng Y (2015) Lamins position the nuclear pores and centrosomes by modulating dynein. *Mol Biol Cell* 26:3379–3389.
10. Kim Y, Zheng X, Zheng Y (2013) Proliferation and differentiation of mouse embryonic stem cells lacking all lamins. *Cell Res* 23:1420–1423.
11. Funkhouser CM, et al. (2013) Mechanical model of blebbing in nuclear lamin meshworks. *Proc Natl Acad Sci USA* 110:3248–3253.
12. Hatch E, Hetzer M (2014) Breaching the nuclear envelope in development and disease. *J Cell Biol* 205:133–141.
13. Coffinier C, et al. (2011) Deficiencies in lamin B1 and lamin B2 cause neurodevelopmental defects and distinct nuclear shape abnormalities in neurons. *Mol Biol Cell* 22:4683–4693.
14. Coffinier C, et al. (2010) Abnormal development of the cerebral cortex and cerebellum in the setting of lamin B2 deficiency. *Proc Natl Acad Sci USA* 107:5076–5081.
15. Eriksson M, et al. (2003) Recurrent de novo point mutations in lamin A cause Hutchinson–Gilford progeria syndrome. *Nature* 423:293–298.
16. Vergnes L, Péterfy M, Bergo MO, Young SG, Reue K (2004) Lamin B1 is required for mouse development and nuclear integrity. *Proc Natl Acad Sci USA* 101:10428–10433.
17. Hatch EM (2018) Nuclear envelope rupture: Little holes, big openings. *Curr Opin Cell Biol* 52:66–72.
18. De Vos WH, et al. (2011) Repetitive disruptions of the nuclear envelope invoke temporary loss of cellular compartmentalization in laminopathies. *Hum Mol Genet* 20:4175–4186.
19. Vargas JD, Hatch EM, Anderson DJ, Hetzer MW (2012) Transient nuclear envelope rupturing during interphase in human cancer cells. *Nucleus* 3:88–100.
20. Hatch EM, Fischer AH, Deerinck TJ, Hetzer MW (2013) Catastrophic nuclear envelope collapse in cancer cell micronuclei. *Cell* 154:47–60.
21. Raab M, et al. (2016) ESCRT III repairs nuclear envelope ruptures during cell migration to limit DNA damage and cell death. *Science* 352:359–362.
22. Denais CM, et al. (2016) Nuclear envelope rupture and repair during cancer cell migration. *Science* 352:353–358.
23. Lammerding J, Wolf K (2016) Nuclear envelope rupture: Actin fibers are putting the squeeze on the nucleus. *J Cell Biol* 215:5–8.
24. Isermann P, Lammerding J (2017) Consequences of a tight squeeze: Nuclear envelope rupture and repair. *Nucleus* 8:268–274.
25. Hatch EM, Hetzer MW (2016) Nuclear envelope rupture is induced by actin-based nucleus confinement. *J Cell Biol* 215:27–36.
26. de Noronha CMC, et al. (2001) Dynamic disruptions in nuclear envelope architecture and integrity induced by HIV-1 Vpr. *Science* 294:1105–1108.
27. Yang SH, et al. (2011) An absence of both lamin B1 and lamin B2 in keratinocytes has no effect on cell proliferation or the development of skin and hair. *Hum Mol Genet* 20:3537–3544.
28. Razafsky D, Hodzic D (2014) Temporal and tissue-specific disruption of LINC complexes in vivo. *Genesis* 52:359–365.
29. McGregor AL, Hsia CR, Lammerding J (2016) Squish and squeeze-the nucleus as a physical barrier during migration in confined environments. *Curr Opin Cell Biol* 40:32–40.
30. Jung HJ, et al. (2013) Farnesylation of lamin B1 is important for retention of nuclear chromatin during neuronal migration. *Proc Natl Acad Sci USA* 110:E1923–E1932.
31. Young SG, Jung HJ, Coffinier C, Fong LG (2012) Understanding the roles of nuclear A- and B-type lamins in brain development. *J Biol Chem* 287:16103–16110.
32. Fong LG, et al. (2004) Heterozygosity for Lmna deficiency eliminates the progeria-like phenotypes in Zmpste24-deficient mice. *Proc Natl Acad Sci USA* 101:18111–18116.
33. Kim P, et al. Disrupting the LINC complex in smooth muscle cells ameliorates aortic disease in a mouse model of Hutchinson–Gilford progeria syndrome. *Sci Transl Med*, in press.
34. Stewart-Hutchinson PJ, Hale CM, Wirtz D, Hodzic D (2008) Structural requirements for the assembly of LINC complexes and their function in cellular mechanical stiffness. *Exp Cell Res* 314:1892–1905.

SI Materials and Methods

Cell Culture. To generate triple-knockout (TKO) MEFs (*Lmna*$^{-/-}$*Lmnb1*$^{-/-}$*Lmnb2*$^{-/-}$) and A1B0 MEFs (*Lmna*$^{+/-}$*Lmnb1*$^{-/-}$*Lmnb2*$^{-/-}$), *Lmna*$^{-/-}$*Lmnb1*$^{fl/fl}$ *Lmnb2*$^{fl/fl}$ and *Lmna*$^{+/-}$*Lmnb1*$^{fl/fl}$ *Lmnb2*$^{fl/fl}$ MEFs, respectively, were treated with *Cre* adenovirus (Gene Transfer Vector Core) three times at 1,000 MOI each. To generate B1KO MEFs (*Lmna*$^{+/+}$*Lmnb1*$^{-/-}$*Lmnb2*$^{+/+}$), E13.5 mouse embryos were harvested from *Lmnb1*$^{+/-}$ breeder pairs. Cultures of MEFs were grown in monolayer cultures at 37°C with 5–7% CO2 and maintained in DMEM (Gibco) containing 10% fetal bovine serum (FBS; Hyclone) and 100 units/ml of penicillin and 100 μg/ml of streptomycin.

Quantitative RT-PCR Studies. Total RNA was isolated and treated with DNase I (Ambion). RNA was reverse-transcribed with random primers, oligo(dT), and SuperScript III (Invitrogen). qPCR reactions were performed on a 7900 Fast Real-Time PCR system (Applied Biosystems) with SYBR Green PCR Master Mix (Bioline). Transcript levels were determined by the comparative cycle threshold method and normalized to levels of cyclophilin A. All primers used are listed in Table S1.

Western Blots. Proteins were size-fractionated on 4–12% gradient polyacrylamide Bis-Tris gels (Invitrogen) and transferred to a nitrocellulose membrane. Membranes were blocked with Odyssey Blocking solution (LI-COR Biosciences) for 1 h at RT and then incubated with primary antibodies at 4°C overnight. After washing the membranes with PBS containing 0.1% Tween-20, they were incubated with infrared dye (IR)–labeled secondary antibodies for 1 h at RT. The IR signals were quantified with an Odyssey infrared scanner (LI-COR Biosciences).

Immunofluorescence Microscopy and Image Analysis. For confocal immunofluorescence microscopy, images were obtained with a Zeiss LSM700 laser-scanning microscope with a Plan Apochromat 20×/0.80 objective (air) or a Plan Apochromat 100×/1.40 oil-immersion objective. Images along the *z*-axis were processed by Zen 2010 software (Zeiss). For live-cell imaging, image sequences were analyzed with ZEN (Zeiss) using only linear adjustments uniformly applied to the entire image region. For confocal image stacks, images were three-dimensionally reconstructed and displayed as maximum intensity projections. A nuclear rupture event was defined as NLS-GFP entry into the cytoplasm (in interphase cells only).

Nuclear Circularity. To quantify the variation in nuclear morphology, we computed nuclear circularity ($4\pi \times \text{area}/\text{perimeter}^2$) by measuring nuclear areas and perimeters of 100 cells for each genotype. The circularity measurement reaches a maximum value of 1.0 for a circle and decreases with shape irregularities (1).

Electron Microscopy. Cells were prepared for transmission electron microscopy (TEM) in two ways: 1) Embedding of non-adherent cells. Cell monolayers were fixed for 1 h in fixative solution containing 4% paraformaldehyde (EMS) and 2.5% glutaraldehyde (EMS) buffered with 0.1 M sodium cacodylate (Sigma) and then gently scraped from the dishes with a cell scraper (Corning). The suspension was centrifuged at 350 *g* for 15 min to generate a pellet. The pellets were allowed to fix for another 45 min before rinsing three times with 0.1 M sodium cacodylate and post-fixing with 1% osmium tetroxide (EMS) buffered with 0.1 M sodium cacodylate for 1 h at room temperature. Next, samples were rinsed three times with distilled water and stained overnight with 2% uranyl acetate (SPIChem) at 4°C. Samples were rinsed three times with distilled water and dehydrated through a series of increasing acetone concentrations (30%, 50%, 70%, 85%, 95%, 100%; 3 × 10 min each) before infiltration with increasing concentrations of EMBed812 epoxy resin (EMS) in acetone (33% for 2 h; 66% overnight; 100% for 4 h). Next, samples were embedded in fresh resin and polymerized in a vacuum oven for 24 h at 65°C. 2) *En face* embedding of adherent cells. Cells were grown on Thermanox (Ted Pella) coverslips. Cells on coverslips were rinsed once with fixative solution (2.5% glutaraldehyde in 0.1 M sodium cacodylate), and then fresh fixative was added for 1 h on ice. Next, cells were rinsed 5 × 2 min each with cold 0.1 M sodium cacodylate and then post-fixed with 2% osmium tetroxide in 0.1 M sodium cacodylate for 30 min on ice. Next, cells were rinsed 5 × 2 min with distilled water and stained overnight with 2% uranyl acetate at 4°C. Cells were rinsed 5 × 2 min with distilled water and dehydrated through a series of increasing ethanol concentrations (30%, 50%, 70%, 85%, 95%, 100%; 3 × 2 min each) before being infiltrated with increasing

concentrations of EMBed812 epoxy resin in acetone (33% for 1 h; 66% overnight; 100% for 2 h). Next, coverslips were inverted onto a BEEM capsule filled to the top with fresh EMBed812 and polymerized in an oven at 65°C for 48 h. Once polymerized, coverslips were peeled off of the block, leaving the monolayer of cells behind. For both methods, the polymerized blocks were removed from the tubes, were trimmed and 65-nm sections were generated with a Leica UC6 ultramicrotome and picked up on freshly glow-discharged copper grids (Ted Pella) that were coated with formvar and carbon. Sections were then stained with Reynold's lead citrate solution for 10 min. Images were acquired with an FEI T12 transmission electron microscope set to 120kV accelerating voltage using a Gatan 2kX2k digital camera.

Cell Stretching. Flexible polydimethylsiloxane (PDMS) membranes were prepared in 150-mm culture dishes with the Sylgard 184 silicone elastomer kit (Dow-Corning #3097358-1004). Membranes strips (7 × 0.8 cm) were activated with a plasma cleaning machine, treated with 2% 3-aminopropy-triethoxysilane at RT for 45 min, and then dried at 55° C for 30 min. The membranes were incubated with 0.5 mg/ml sulfo-SANPAH in HEPES buffer and crosslinked with UV exposure (300–460 nm) for 30 sec. The washed membranes were stored at 4° C in a 100 μg/ml collagen solution (PureCol 5005; Advanced Biomatrix). Cells (1×10^5) were added to individual membrane strips in molds and incubated in media for 24 h and then clamped into a custom-built stretching device. The brackets holding the membranes were attached to an L12 linear actuator (Actuonix) controlled by a multifunction DAQ device (National Instruments) and LabVIEW 2015 software (National Instruments).

pTRIPZ–Prelamin A, pTRIPZ-*LMNB1*, pTRIPZ-*LMNB2*, and pLenti6-EGFP-KASH2 Lentiviral Vectors. The doxycycline-inducible vector pTRIPZ-hDDX5/17 (Addgene) was digested with restriction enzymes *Age*I and *Eco*RI and gel-purified. For the pTRIPZ–Prelamin A vector, a human prelamin A cDNA in pCMV-XL5 vector (#SC101048; Origene) was subcloned into pTRIPZ with Infusion Cloning (Clontech). For the pTRIPZ-*LMNB1*, a human lamin B1 cDNA in pCMB6-XL4 vector (#SC116661; Origene) was amplified with the Titanium Taq PCR kit (Clontech) and sequence-specific primers (forward primer, 5′–GTCAGATCGCACCGGATGGCGACTG–3′; reverse primer, 5′–GTAGCCCCTTGAATTTTACATAATTGCACAGC–3′). For the pTRIPZ-*LMNB2*, a human lamin B2 cDNA in pCMV6-XL4 vector (#SC106163; Origene) was amplified with the Titanium Taq PCR kit (Clontech) and sequence-specific primers (forward primer, 5′–ATGCGTGTGGACCTGGAGAAA–3′; reverse primer, 5′–GTAGCCCCTTGAATTTCACATCACGTAGCAGCCTCTTGA–3′). Each fragment (*LMNB1* and *LMNB2*) was purified with UltraClean15 (Qiagen; Germantown, MD) and subcloned into pTRIPZ vector with Infusion Cloning (Clontech). The products were amplified in XL10-Gold Ultracompetent cells (Agilent; Santa Clara, CA), and plasmids with the correct sequence were isolated with plasmid kits (Qiagen). Packaging of lentivirus and transduction of cells were performed by UCLA's Vector Core. Transduced cells were selected for one week with 1.5 μg/ml puromycin (Gibco) and serially diluted to isolate clones. Doxycycline (Fisher Scientific) was added at the indicated doses to induce expression. The EGFP-KASH2 sequence was amplified from pEGFP-C1-KASH2 (2) as described (3). Briefly, gel-purified fragments were subcloned into the pLenti6/v5-DEST plasmid (ThermoFisher). Packaging of lentivirus and transduction of cells were performed by UCLA's Vector Core. Transduced cells were selected for one week with 2 μg/ml blasticidin (Gibco). Packaging of lentivirus and transduction of cells were performed by UCLA's Vector Core. Transduced cells were subjected to selection for one week with 1.5 μg/ml puromycin or 2 μg/ml blasticidin (Gibco). Doxycycline (Fisher Scientific) was added to induce protein expression.

Supplementary Figures

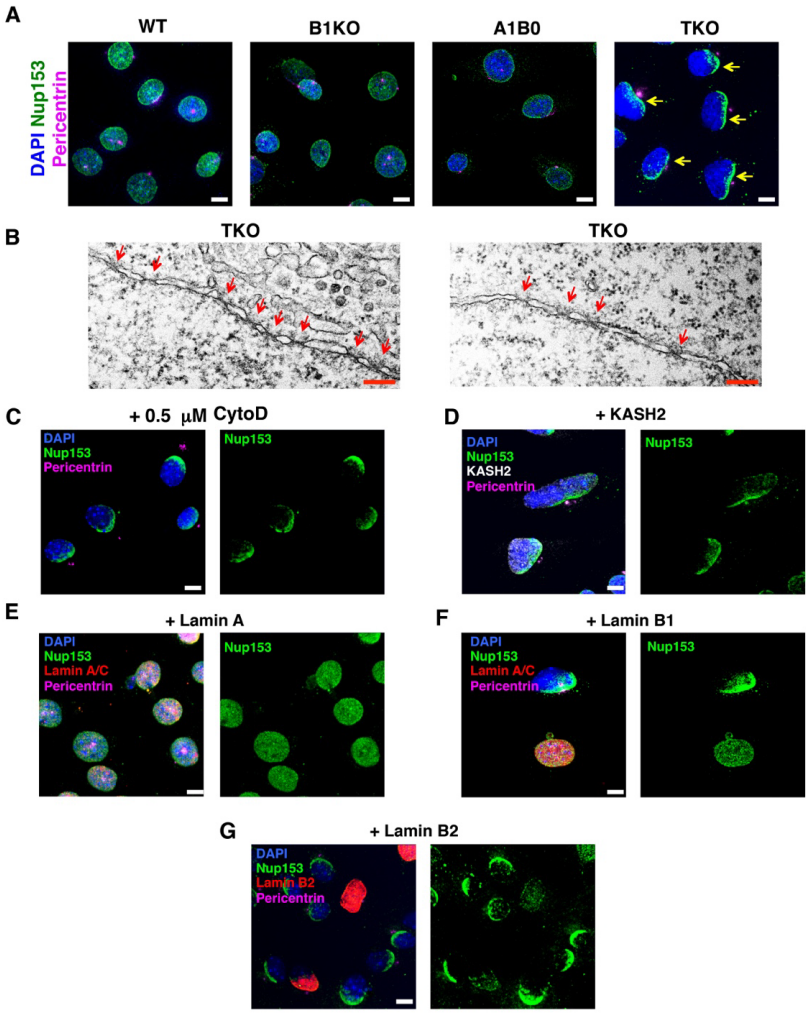

Fig. S1. Abnormal nuclear pore complex (NPC) distribution in TKO MEFs and rescue with individual nuclear lamins. (*A*) Confocal immunofluorescence micrographs showing asymmetric distribution of NPCs (close to the centrosome; *yellow* arrows) in MEFs lacking all nuclear lamins but an even distribution in WT, *Lmna*$^{+/+}$*Lmnb1*$^{-/-}$*Lmnb2*$^{+/+}$ (B1KO), and *Lmna*$^{+/-}$*Lmnb1*$^{-/-}$*Lmnb2*$^{-/-}$ (A1B0) MEFs. MEFs were stained with antibodies against the nuclear pore protein Nup153 (*green*) and the centrosome marker pericentrin (*magenta*). (Scale bars, 10 μm.) (*B*) Electron micrographs showing a high density of NPCs (*red* arrows) in segments of the nuclear envelope in TKO MEFs (Scale bars, 200 nm.) (*C*) Treating TKO MEFs with cytochalasin D made the nuclei rounder but did not rescue nucleoporin distribution. MEFs

were stained with antibodies against the NPC protein Nup153 and pericentrin. (*D*) KASH2-EGFP expression did not rescue nucleoporin distribution in TKO MEFs. MEFs were stained with antibodies against the nuclear pore protein Nup153 and pericentrin. (*E*) Prelamin A expression normalized NPC distribution in TKO MEFs. MEFs were stained with antibodies against lamin A/C (*red*), Nup 153, and pericentrin. (*F*) Lamin B1 expression normalized NPC distribution in TKO MEFs. MEFs were stained with antibodies against lamin B1 (*red*), Nup 153, and pericentrin. (*G*) Lamin B2 expression in TKO MEFs resulted in a change in NPC distribution that matched lamin B2's expression pattern. MEFs were stained with antibodies against lamin B2 (*red*), Nup 153, and pericentrin. In panels *C–E*, Nup153 is in *green*, pericentrin is in *magenta*, and DNA was stained with DAPI (*blue*). (Scale bars in panels *C–G*, 10 μm.)

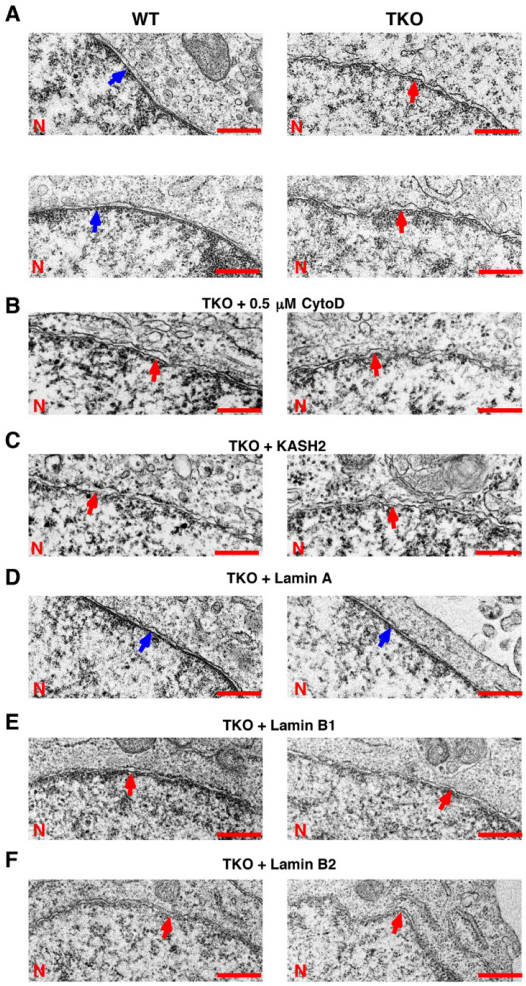

Fig. S2. (*A*) Electron micrographs showing "wavy" inner nuclear membranes in *Lmna*$^{-/-}$*Lmnb1*$^{-/-}$*Lmnb2*$^{-/-}$ (TKO) mouse embryonic fibroblasts (MEFs) (*red* arrows), and relatively straight inner nuclear membranes in wild-type (WT) MEFs (*blue* arrows). (Scale bars, 500 nm.) (*B–F*) Cytochalasin D treatment (*B*) or KASH2-EGFP expression (*C*) did not normalize the wavy inner nuclear membrane phenotype in TKO MEFs. Prelamin A expression (*D*) normalized the wavy inner nuclear membrane phenotype but lamin B1 (*E*) or lamin B2 (*F*) had little or no effect. (Scale bars, 500 nm.)

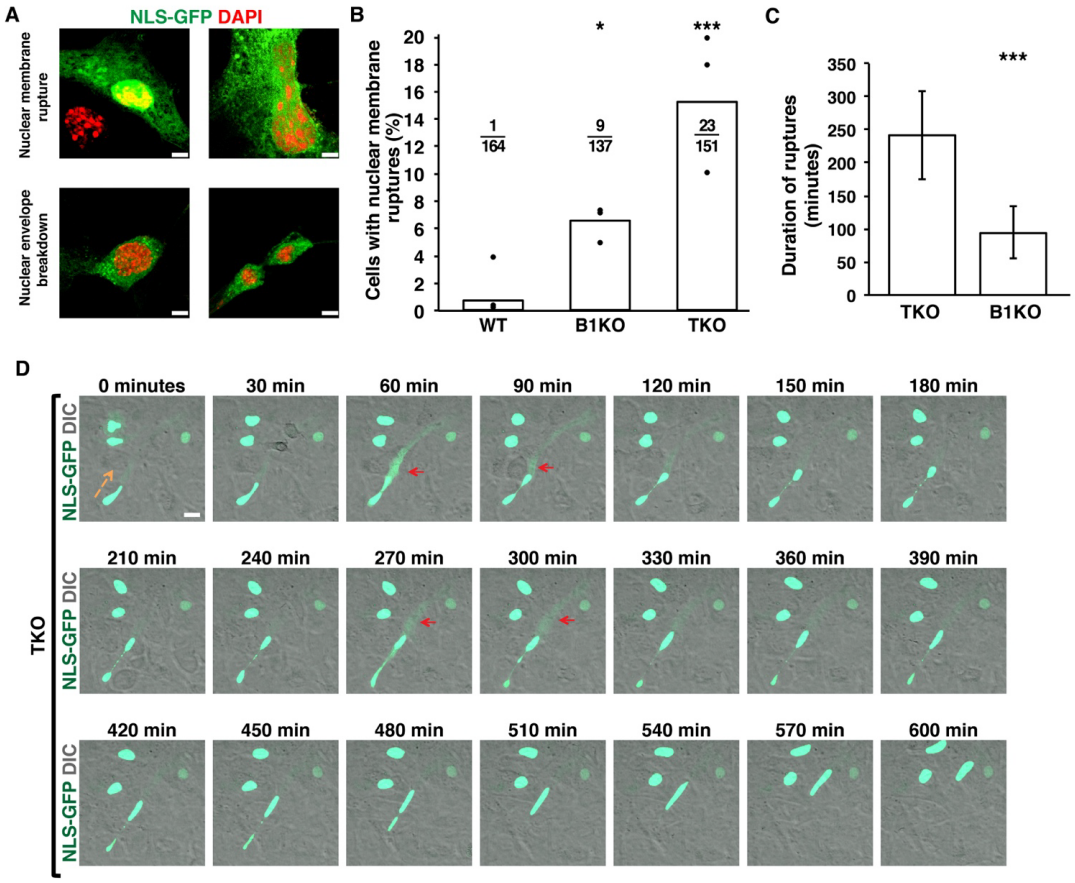

Fig. S3. Nuclear membrane ruptures in *Lmna*$^{+/+}$*Lmnb1*$^{+/+}$*Lmnb2*$^{+/+}$ (wild-type; WT), *Lmna*$^{+/+}$*Lmnb1*$^{-/-}$ *Lmnb2*$^{+/+}$ (lamin B1 knockout; B1KO), and *Lmna*$^{-/-}$*Lmnb1*$^{-/-}$*Lmnb2*$^{-/-}$ (TKO) mouse embryonic fibroblasts (MEFs). (*A*) Confocal micrographs showing TKO MEFs expressing NLS-GFP (*green*) and DNA stained with DAPI (*red*). Nuclear membrane ruptures (*top*) are easily distinguished from mitotic nuclear envelope breakdown (*bottom*) by the DNA staining pattern (*i.e.*, condensed chromatin in mitotic cells), the cytoplasmic shape, and the presence of two nuclei at the end of cell division. (Scale bars, 5 μm.) (*B*) Bar graph showing percentages of MEFs with nuclear membrane ruptures during 20 h of imaging. Nuclear membrane ruptures were more frequent in B1KO and TKO MEFs than in WT MEFs. *$P < 0.05$, ***$P < 0.0005$ by χ^2 test. (*C*) Bar graph showing the average duration of nuclear membrane ruptures in TKO and B1KO MEFs (average of 10 nuclear membrane ruptures per group). ***$P < 0.0001$ by Student's *t* test. (*D*) Image sequence showing multiple nuclear membrane ruptures (*red* arrows) in a migrating TKO MEF. NLS-GFP is in *green* and DIC is in *gray*. (Scale bar, 20 μm.)

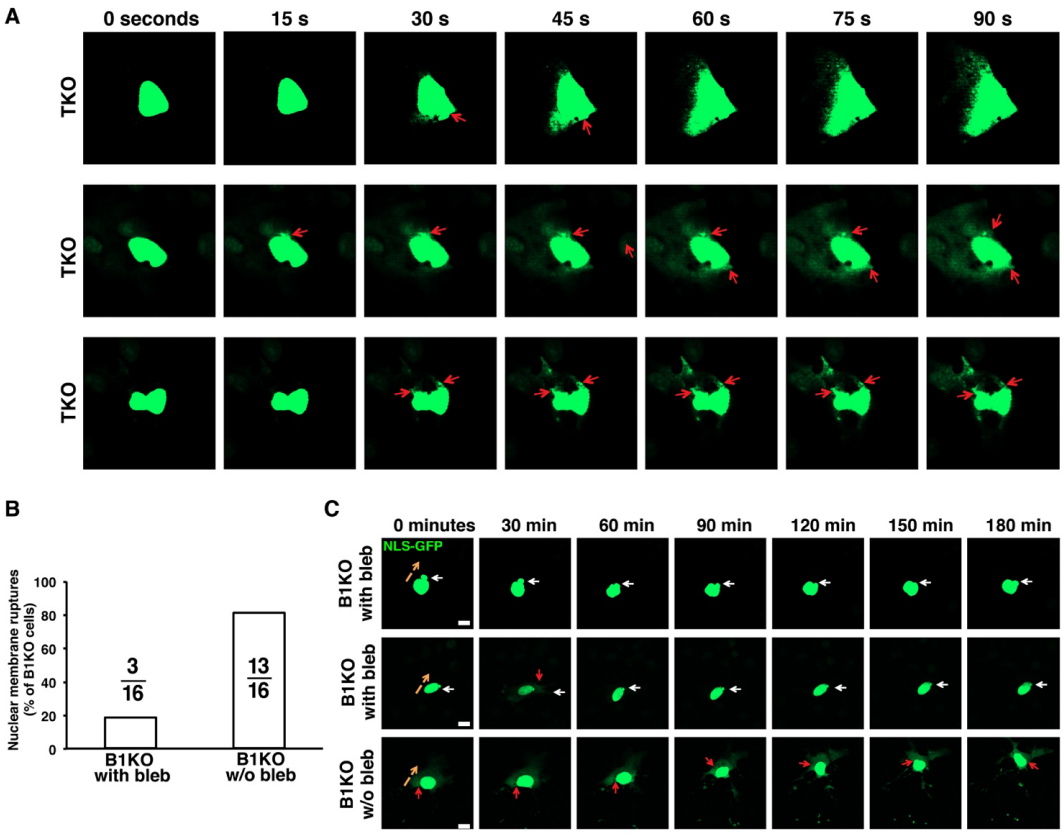

Fig. S4. Nuclear blebs are not a prerequisite for nuclear membrane ruptures. (*A*) Image sequences of three separate nuclear membrane rupture events in TKO MEFs (*top*, *middle*, *bottom*), where nuclear membrane ruptures occur in cells lacking a nuclear bleb. *Red* arrows show where nuclear membrane ruptures first appear in each cell. (*B*) Bar graph showing percentages of nuclear membrane ruptures in B1KO MEFs in cells with nuclear blebs *vs.* cells without nuclear blebs during 20 h of imaging. Only three of 33 nuclear membrane rupture events occurred in nuclei with a nuclear bleb. (*C*) Three image sequences of B1KO MEFs: (*top*) a B1KO nucleus with a nuclear bleb but no nuclear membrane ruptures; (*middle*) a B1KO nucleus with a nuclear bleb and one rupture event (*red arrow*); (*bottom*) a B1KO nucleus without a nuclear bleb but with a nuclear membrane rupture (*red arrow*). *Orange* arrows indicate direction of nuclear translocation. (Scale bars, 20 μm.)

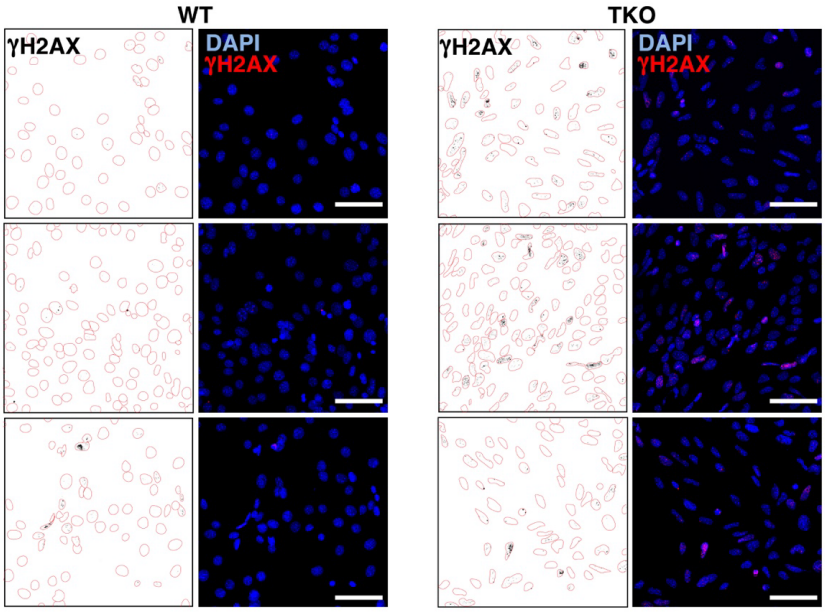

Fig. S5. Confocal immunofluorescence micrographs of wild-type (WT) and *Lmna*$^{-/-}$*Lmnb1*$^{-/-}$*Lmnb2*$^{-/-}$ (TKO) MEFs, revealing larger numbers of γ-H2AX foci in TKO MEFs than in WT MEFs. In the fluorescence microscopy images, γ-H2AX foci are colored *red*, and the nuclei are stained with DAPI (blue). To better visualize the γ-H2AX foci, drawings of the microscopy images were generated. In the drawings, the perimeter of each nucleus is outlined in *red* and γ-H2AX foci are shown in *black*. (Scale bars, 50 μm.)

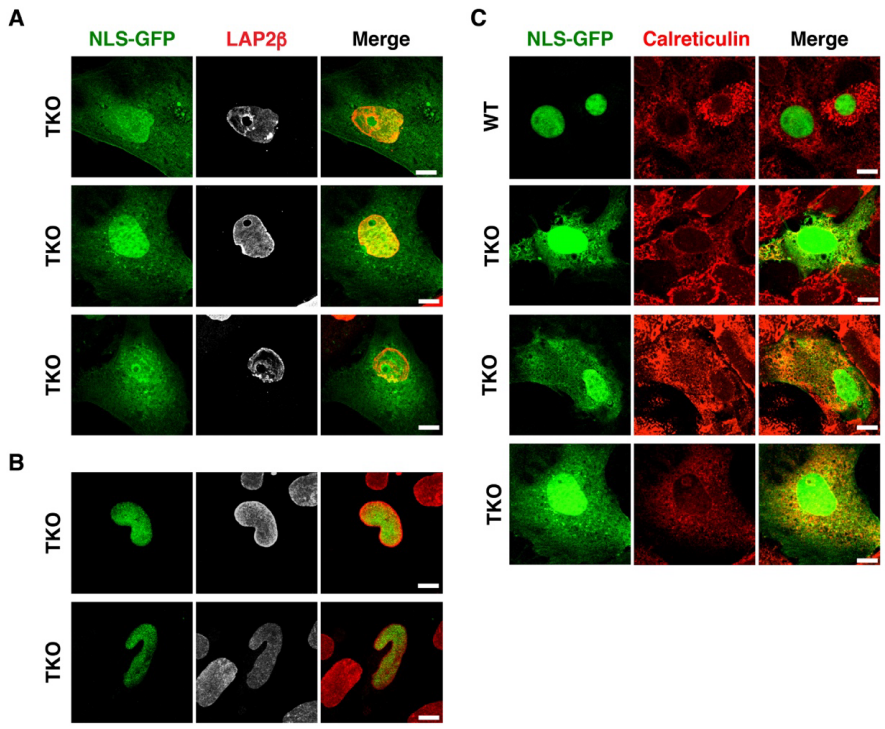

Fig. S6. Abnormal nuclear morphology in *Lmna*$^{-/-}$*Lmnb1*$^{-/-}$*Lmnb2*$^{-/-}$ (TKO) mouse embryonic fibroblasts (MEFs). (*A*) Confocal immunofluorescence micrographs showing an abnormal distribution of LAP2β (an inner nuclear membrane marker; *red*) in TKO MEFs with nuclear membrane ruptures, where NLS-GFP escapes into the cytoplasm. (*B*) Confocal immunofluorescence micrographs showing LAP2β is uniformly distributed in TKO MEFs without nuclear membrane ruptures. Note the abnormal nuclear shape. (*C*) Confocal immunofluorescence micrographs of WT and TKO MEFs that have been stained with an antibody against calreticulin (*red*), a resident protein of the endoplasmic reticulum. NLS-GFP is located exclusively in the nucleus of WT MEFs (*top*), with negligible colocalization with calreticulin. In TKO MEFs, the degree of colocalization between NLS-GFP and calreticulin was variable. (Scale bars in *A*–*C*, 10 μm.)

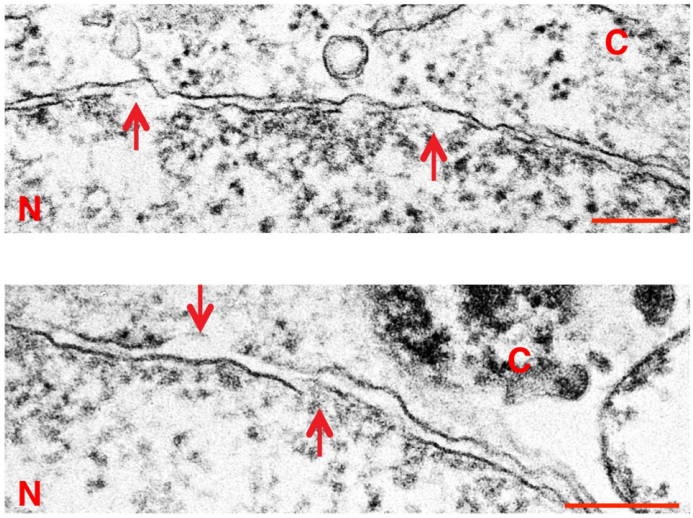

Fig. S7. Electron micrographs of adherent TKO MEFs showing examples of discrete inner and outer nuclear membrane discontinuities (*red* arrows). (Scale bars, 200 nm.) N, nucleus; C, cytoplasm.

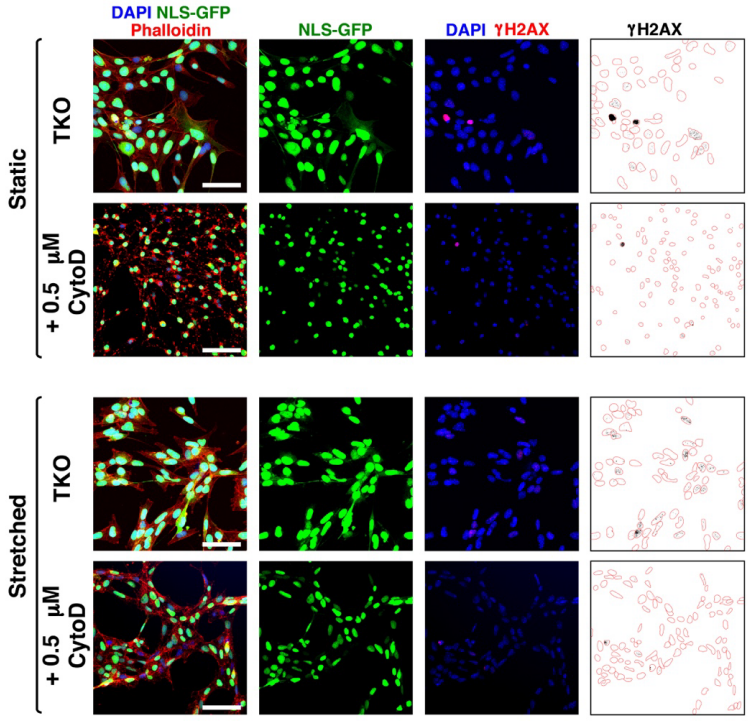

Fig. S8. Confocal immunofluorescence micrographs of TKO MEFs under static conditions (*top*) and with mechanical stretching (*bottom*). Actin depolymerization in TKO MEFs with cytochalasin D results in rounder nuclei, fewer nuclear membrane ruptures [as judged by the escape of NLS-GFP into the cytoplasm], and reduced numbers of γ-H2AX foci in TKO MEFs, both under static and stretched conditions. In the far right panel, the nuclei of TKO MEFs stained with an antibody against γ-H2AX are outlined in *red* and γ-H2AX foci are colored in *black*. The drawings reveal fewer γ-H2AX foci in cells treated with cytochalasin D, both under static and stretched conditions. (Scale bars, 50 μm.)

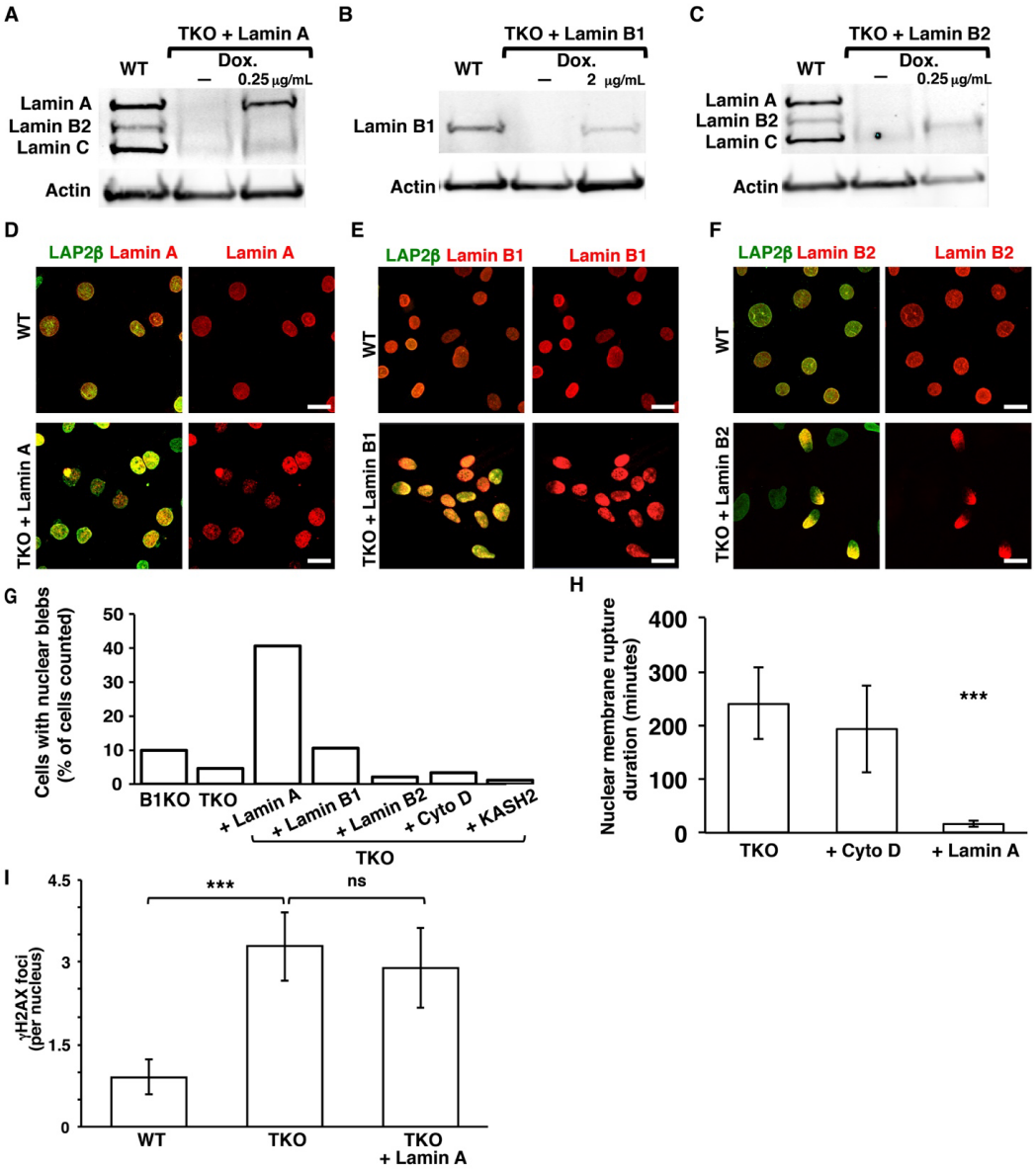

Fig. S9. (*A–C*) Western blot studies of TKO MEFs after introducing expression vectors for prelamin A (pTRIPZ–hu-prelamin A), lamin B1 (pTRIPZ-*LMNB1*), or lamin B2 (pTRIPZ-*LMNB2*) and then inducing expression with doxycycline (Dox.). Lamin expression was compared to wild-type (WT) MEFs. Actin was used as a loading control. (*D*) Immunofluorescence micrographs showing a homogeneous distribution of lamin A in WT MEFs and an uneven ("honeycomb") distribution of lamin A in TKO MEFs that express lamin A (*i.e.*, after being transduced with pTRIPZ–hu-prelamin A). LAP2β is in *green* and lamin A is in

red. (*E*) Immunofluorescence micrographs showing lamin B1 distribution in WT MEFs, and in TKO MEFs that express lamin B1 (*i.e.*, after being transduced with pTRIPZ–*LMNB1*). LAP2β is in *green* and lamin B1 is in *red*. (*F*) Immunofluorescence micrographs showing an even distribution of lamin B2 in WT MEFs and an asymmetric distribution of lamin B2 in TKO MEFs expressing lamin B2. LAP2β is in *green* and lamin B2 is in *red*. (Scale bars in *D–F*, 20 μm.). (*G*) Bar graph showing the percentage of cells with nuclear blebs in TKO MEFs with lamin A expression, lamin B1 expression, lamin B2 expression, cytochalasin D treatment, and KASH2 expression. B1KO MEFs are include as a control. (*H*) Bar graph shows the average duration of nuclear membrane ruptures in TKO MEFs, TKO MEFs treated with 0.5 μM cytochalasin D, and TKO MEFs expressing lamin A. Nuclear membrane rupture duration was shorter in TKO MEFs expressing lamin A. ***$P < 0.0001$ by Student's *t* test. (*I*) Bar graph showing that expression of lamin A does not reduce γ-H2AX foci in TKO MEFs. The results were analyzed as described in *G*. ***$P < 0.0005$; nonsignificant (ns, $P > 0.05$ by Student's *t* test).

Supplementary Tables S1–S2

Table S1

Gene	Species	Sequences (5′–3′)
Lamin A	Mouse	ggttgaggacaatgaggatga tgagcgcaggttgtactcag
Lamin B1	Mouse	caactgacctcatctggaagaac tgaagactgtgcttctctgagc
Lamin B2	Mouse	aggtgcaggctgagctagag tgattccagatccttcactcg
Lamin C	Mouse	cctatcgaaagctgctggag cctgagactgggatgagtgg
Cyclophilin A	Mouse	tgagcactggagagaaagga ccattatggcgtgtaaagtca

Table S2

Antigen	Antibody	Species	Company	WB	ICC
Lap2β [27]	Monoclonal	Mouse	BD Transduction Lab		1:500
Lamin B1 [M-20]	Polyclonal	Goat	Santa Cruz Biotech.	1:2000	1:500
Pericentrin	Polyclonal	Rabbit	Abcam		1:1000
Lamin A/C	Polyclonal	Goat	Santa Cruz Biotech.		1:500
Lamin A	Monoclonal	Mouse	Santa Cruz. Biotech	1:2000	
Lamin B2	Monoclonal	Rabbit	Abcam		1:1000
Lamin B2	Monoclonal	Mouse	Invitrogen		1:50
Lamin B2	Polyclonal	Rabbit	Proteintech	1:300	
Actin	Polyclonal	Goat	Santa Cruz Biotech.	1:5000	
Nup 153	Monoclonal	Mouse	Abcam		1:250
TurboGFP	Polyclonal	Rabbit	Thermo Fisher Scientific		1:1000
eGFP	Polyclonal	Rabbit	Invitrogen		1:1000
Phalloidin-546			Invitrogen		1:2000
γ-H2AX	Monoclonal	Rabbit	EMD Millipore		1:1000

Captions for Movies S1–S15

Movies S1 and S2. TKO MEFs exhibit transient nuclear membrane ruptures. TKO MEFs (Movie S2) expressing NLS-GFP (*green*) were imaged over 240 min and exhibit transient nuclear membrane ruptures (flooding of NLS-GFP into the cytoplasm). WT MEFs (Movie S1) imaged over 240 min do not exhibit nuclear membrane ruptures. DIC is in *gray*.

Movie S3. A TKO MEF exhibits nuclear membrane rupture and nuclear fragmentation. TKO MEFs expressing NLS-GFP (*green*) were plated at high density and imaged over 500 min. A TKO MEF exhibits a nuclear membrane rupture and subsequent nuclear fragmentation. DIC is in *gray*.

Movies S4–6. Nuclear membrane ruptures do not occur through nuclear blebs/herniations in TKO MEFs. TKO MEFs expressing NLS-GFP (*green*) were imaged over 150 sec at 15-sec intervals. Each movie (S6, S7, S8) documents a distinct example of a nuclear membrane rupture in the absence of a nuclear bleb. DIC is in *gray*.

Movies S7–S9. B1KO MEFs occasionally exhibit nuclear membrane ruptures but they do not always coincide with the presence of a nuclear bleb. B1KO MEFs expressing NLS-GFP (*green*) were imaged over 180 min. A B1KO MEF with a nuclear bleb does not have a nuclear membrane rupture (Movie S3). An occasional B1KO MEF with a nuclear bleb does exhibit a nuclear membrane rupture (Movie S4). More often, B1KO MEFs without a nuclear bleb have nuclear membrane ruptures (Movie S5). DIC is in *gray*.

Movies S10 and S11. TKO MEFs with nuclear membrane ruptures leading to cell death. TKO MEFs expressing NLS-GFP (*green*) were imaged over time. (Movie S10) NLS-GFP persists in the cytoplasm. Time interval, 890 min. (Movie S11) In Movie S11, NLS-GFP in the cytoplasm was as intense as in the nucleoplasm. Time interval: 1120 min.

Movie S12. Cytochalasin D prevents nuclear membrane ruptures in TKO MEFs. TKO MEFs expressing NLS-GFP (*green*) were treated with 0.5 mM of cytochalasin D for 1 h and then imaged for 240 min. In the presence of cytochalasin D, the nucleus is rounder and does not exhibit nuclear membrane ruptures. DIC is in *gray*. Time interval: 240 min.

Movies S13–15. Expression of lamin A, lamin B1, or lamin B2 in TKO MEFs does not prevent nuclear membrane ruptures. TKO MEFs expressing NLS-GFP (*green*) were transduced with an inducible expression vector for lamin B1 (Movie S13), lamin B2 (Movie S14), or lamin A (Movie S15). Each movie captures a nuclear membrane rupture. DIC is in *gray*. Time interval: 240 min.

References for SI

1. Rowat AC, Jaalouk DE, Zwerger M, Ung WL, Eydeinant IA, Olins DE, Olins AL, Herrmann H, Weltz DA, Lammerding J (2013) Nuclear envelope composition determines the ability of neutrophil-type cells to passage through micron-scale constrictions. *J Biol Chem* **288**:8610–8618.
2. Stewart-Hutchinson PJ, Hale CM, Wirtz D, Hodzic D (2008) Structural requirements for the assembly of LINC complexes and their function in cellular mechanical stiffness. *Exp Cell Res* **314**:1892–1905.
3. Kim P, *et al.* Disrupting the LINC complex in smooth muscle cells ameliorates aortic disease in a mouse model of Hutchinson-Gilford progeria syndrome. *Sci. Transl. Med. (in press)*.

Chapter 3:

An Absence of Lamin B1 in Migrating Neurons Causes Nuclear Membrane Ruptures and Cell Death

An absence of lamin B1 in migrating neurons causes nuclear membrane ruptures and cell death

Natalie Y. Chen[a], Ye Yang[a], Thomas A. Weston[a], Jason N. Belling[b,c], Patrick Heizer[a], Yiping Tu[a], Paul Kim[a], Lovelyn Edillo[a], Steven J. Jonas[d,e,f], Paul S. Weiss[b,c,g,h], Loren G. Fong[a,1,2], and Stephen G. Young[a,i,j,1,2]

[a]Department of Medicine, David Geffen School of Medicine, University of California, Los Angeles, CA 90095; [b]California NanoSystems Institute, David Geffen School of Medicine, University of California, Los Angeles, CA 90095; [c]Department of Chemistry and Biochemistry, David Geffen School of Medicine, University of California, Los Angeles, CA 90095; [d]Department of Pediatrics, David Geffen School of Medicine, University of California, Los Angeles, CA 90095; [e]Children's Discovery and Innovation Institute, University of California, Los Angeles, CA 90095; [f]Eli and Edythe Broad Center of Regenerative Medicine and Stem Cell Research, University of California, Los Angeles, CA 90095; [g]Department of Bioengineering, University of California, Los Angeles, CA 90095; [h]Department of Materials Science and Engineering, University of California, Los Angeles, CA 90095; [i]Department of Human Genetics, David Geffen School of Medicine, University of California, Los Angeles, CA 90095; and [j]Molecular Biology Institute, David Geffen School of Medicine, University of California, Los Angeles, CA 90095

Contributed by Stephen G. Young, November 4, 2019 (sent for review October 3, 2019; reviewed by William T. Dauer and Howard J. Worman)

Deficiencies in either lamin B1 or lamin B2 cause both defective migration of cortical neurons in the developing brain and reduced neuronal survival. The neuronal migration abnormality is explained by a weakened nuclear lamina that interferes with nucleokinesis, a nuclear translocation process required for neuronal migration. In contrast, the explanation for impaired neuronal survival is poorly understood. We hypothesized that the forces imparted on the nucleus during neuronal migration result in nuclear membrane (NM) ruptures, causing interspersion of nuclear and cytoplasmic contents—and ultimately cell death. To test this hypothesis, we bred *Lmnb1*-deficient mice that express a nuclear-localized fluorescent *Cre* reporter. Migrating neurons within the cortical plate of E18.5 *Lmnb1*-deficient embryos exhibited NM ruptures, evident by the escape of the nuclear-localized reporter into the cytoplasm and NM discontinuities by electron microscopy. The NM ruptures were accompanied by DNA damage and cell death. The NM ruptures were not observed in nonmigrating cells within the ventricular zone. NM ruptures, DNA damage, and cell death were also observed in cultured *Lmnb1*$^{-/-}$ and *Lmnb2*$^{-/-}$ neurons as they migrated away from neurospheres. To test whether mechanical forces on the cell nucleus are relevant to NM ruptures in migrating neurons, we examined cultured *Lmnb1*$^{-/-}$ neurons when exposed to external constrictive forces (migration into a field of tightly spaced silicon pillars). As the cells entered the field of pillars, there were frequent NM ruptures, accompanied by DNA damage and cell death.

nuclear lamins | nuclear envelope | nuclear membrane rupture | B-type lamins

For several decades, the prevailing view among cell biologists was that B-type lamins (lamin B1 and lamin B2) play multiple essential roles in the cell nucleus, including in DNA replication and mitosis (1–7). Over the past decade, studies of genetically modified mouse models have cast considerable doubt on this view (8–12). For example, the fact that a deficiency of both lamin B1 and lamin B2 in keratinocytes (a rapidly dividing cell type) has no perceptible effect on the skin or hair of mice is inconsistent with B-type lamins having essential roles in DNA replication or mitosis (8). Perhaps more importantly, the analysis of mouse models yielded fresh insights into the functional relevance of B-type lamins in mammals. For example, a combination of immunohistochemical studies and BrdU birthdating experiments revealed defective migration of cortical neurons in lamin B1- and lamin B2-deficient embryos, resulting in a neuronal layering abnormality in the cerebral cortex along with neonatal mortality (10–13).

Finding that B-type lamins have a role in neuronal migration was unexpected, particularly in light of prevailing views about the role of B-type lamins in cell biology (3, 5, 14–16), but in hindsight the neurodevelopmental abnormalities made sense. The migration of neurons from the ventricular zone to the cortical plate during embryogenesis depends on nucleokinesis—a process in which the cell nucleus is moved forward by cytoplasmic motors toward the leading edge of migrating neurons (17–21). In the setting of lamin B1 or lamin B2 deficiency, the nuclear envelope is weakened and nucleokinesis is impaired. Elongated nuclei or nuclei with large blebs were present in cortical neurons, both in mutant mouse embryos and mutant neurospheres (12, 22), suggesting that cytoplasmic motors were effective in pulling on the nucleus (as judged by the distorted nuclear shape) but less effective in moving the nucleus toward the leading edge of the cell

In addition to the neuronal migration defect in *Lmnb1*- and *Lmnb2*-deficient mice, there was a more perplexing phenotype—reduced neuronal density in the cerebral cortex. This loss of cortical neurons was mild in *Lmnb2*-deficient embryos but severe in *Lmnb1*-deficient embryos (11, 12). The explanation for the reduced cellularity in the cerebral cortex was not clear, but the fact that the phenotype progressed after birth in forebrain-specific *Lmnb1* and *Lmnb2* knockout (KO) mice (12) implied that it was likely a consequence of reduced neuronal survival.

We hypothesized that reduced neuronal survival in *Lmnb1* and *Lmnb2* knockout mice might be caused by reduced integrity

Significance

Deficiencies in lamin B1 or lamin B2 in mice result in markedly reduced neuronal density in the cerebral cortex, but the mechanism has been unclear. We found that deficiencies of either lamin B1 or lamin B2 cause nuclear membrane (NM) ruptures in migrating neurons, accompanied by DNA damage and cell death. Our studies were informative because they uncovered large differences in the frequency of NM repair in lamin B1- and lamin B2-deficient neurons, implying unique functions for the 2 nuclear lamins in maintaining NM integrity. Also, our studies uncovered an important role for mechanical stresses in eliciting NM ruptures, helping to explain the increased frequency of NM ruptures in migrating neurons.

Author contributions: N.Y.C., P.S.W., L.G.F., and S.G.Y. designed research; N.Y.C., Y.Y., T.A.W., J.N.B., P.H., Y.T., P.K., L.E., and S.J.J. performed research; N.Y.C. contributed new reagents/analytic tools; N.Y.C., L.G.F., and S.G.Y. analyzed data; and N.Y.C. and S.G.Y. wrote the paper.

Reviewers: W.T.D., University of Michigan; and H.J.W., Columbia University.

The authors declare no competing interest.

[1]L.G.F. and S.G.Y. contributed equally to this work.

[2]To whom correspondence may be addressed. Email: lfong@mednet.ucla.edu or sgyoung@mednet.ucla.edu.

This article contains supporting information online at https://www.pnas.org/lookup/suppl/doi:10.1073/pnas.1917225116/-/DCSupplemental.

First published December 3, 2019.

of the nuclear membranes, resulting in nuclear membrane (NM) ruptures, intermixing of nuclear and cytoplasmic contents, DNA damage, and ultimately cell death. This scenario seemed possible, for 2 reasons. First, reducing nuclear lamin expression in tumor cell lines or fibroblasts renders the cells more susceptible to NM ruptures in response to external mechanical forces (23–27), and it seemed plausible that the forces imparted on the nucleus during nucleokinesis (or the constrictive forces imparted on cells as they migrate to the cortical plate) could have similar consequences, particularly when the nuclear envelope is weakened by the absence of a B-type lamin. Second, unlike peripheral cell types, migrating neurons in the developing brain do not express lamin A or lamin C (13, 28–30), and the absence of those protein likely renders neurons more susceptible to NM ruptures.

In the current study, we took advantage of both genetically modified mice and cultured cell models to examine the hypothesis that deficiencies in B-type lamins render neurons susceptible to NM ruptures and ultimately to cell death.

Results

NM Ruptures in Neurons of *Lmnb1*-Deficient Mice. To investigate the reduced density of cortical neurons in *Lmnb1*-deficient embryos, we stained the cerebral cortex of embryonic day 18.5 (E18.5) *Lmnb1*-deficient embryos for active caspase 3, a marker of apoptotic cell death. Substantial amounts of caspase 3 staining were observed within the cortical plate of *Lmnb1*-deficient embryos (Fig. 1*A*). Also, staining with the LIVE/DEAD fluorescent vital dye revealed widespread cell death in the forebrain (but not cerebellum) of forebrain-specific *Lmnb1* knockout embryos (Fig. 1*B*). We suspected that the cell death might be a consequence of NM ruptures and intermixing of nuclear and cytoplasmic contents. To explore that idea, we bred *Lmnb1*-deficient mice harboring a nuclear-localized fluorescent reporter (*SI Appendix*, Fig. S1). In neurons of wild-type (WT) mice, the reporter was confined to the cell nucleus (Fig. 1 *C* and *D* and *SI Appendix*, Fig. S2, *Upper*). However, in *Lmnb1*-deficient embryos, we observed escape of the reporter into the cytoplasm of many neurons (Fig. 1 *C* and *E* and *SI Appendix*, Fig. S2, *Lower*). Interestingly, no NM ruptures were observed in cells of the ventricular zone (Fig. 1 *C* and *E* and *SI Appendix*, Fig. S3). By transmission electron microscopy (EM), we had no difficulty identifying discontinuities in the nuclear membranes of cortical plate neurons in *Lmnb1*-deficient embryos (Fig. 1 *F* and *G* and *SI Appendix*, Fig. S1).

NM ruptures in cortical plate neurons of *Lmnb1*-deficient embryos were accompanied by an inhomogeneous distribution of lamin B2. In cortical plate neurons, lamin B2 was mislocalized to 1 pole of the nuclear rim (*SI Appendix*, Fig. S4), leaving a large fraction of the nuclear rim devoid of nuclear lamins. In contrast, lamin B2 distribution was uniformly distributed along the nuclear rim in cells of the ventricular zone (where NM ruptures were not observed) (*SI Appendix*, Fig. S4*A*). The asymmetric distribution of lamin B2 is likely due to the forces of nucleokinesis, given that lamin B2 was largely confined to the leading edge of neurons as they migrated away from cultured neurospheres (*SI Appendix*, Fig. S4*B*) (22). In the forebrain of adult forebrain-specific *Lmnb1* knockout mice, where lamin C is expressed and lamin B2 is distributed homogeneously along the nuclear rim, NM ruptures could be detected but were infrequent (*SI Appendix*, Fig. S5).

NM Ruptures in Cultured Neurons Deficient in B-Type Lamins. To further explore the susceptibility of lamin B1- or lamin B2-deficient cells to NM ruptures, we prepared cultures of *Lmnb1*-deficient (B1KO) and *Lmnb2*-deficient (B2KO) neuronal progenitor cells (NPCs). As expected, undifferentiated and differentiated B1KO and B2KO neurons lacked lamin B1 and lamin B2, respectively (Fig. 2 *A*–*E*). Lamin C expression levels in neurons were very low relative to levels in fibroblasts (Fig. 2*A*). Prelamin A expression was even lower (Fig. 2*A*). Prelamin A mRNA expression in neurons is virtually abolished by a neuron-specific microRNA (miR-9) (28, 29). Nuclei in B1KO neurons were slightly smaller and more circular than wild-type or B2KO neurons (Fig. 2*F*).

To examine the susceptibility of cultured neurons to NM ruptures, we transduced NPCs with a nuclear-localized green fluorescent cell reporter (NLS-GFP). We then quantified NM ruptures (escape of the NLS-GFP into the cytoplasm) in wild-type, B1KO, and B2KO neurons during 50 h of live-cell imaging. NM ruptures were frequent in B1KO neurons (Movie S1), occurring in >60% of neurons examined (Fig. 3*B*). In many neurons, NM ruptures occurred repetitively, with multiple cycles of NM rupture (escape of NLS-GFP into the cytoplasm) and NM repair (return of NLS-GFP into the nucleus) (Movies S2 and S3). Thus, the total number of NM ruptures was ∼2.7-fold greater than the number of neurons examined (Fig. 3*C* and *SI Appendix*, Fig. S6). The average duration of NM ruptures was 2.9 h (Fig. 3*D*). The increased susceptibility of B1KO neurons to NM ruptures was documented in 5 independent experiments (*SI Appendix*, Fig. S6). No ruptures were detected in wild-type neurons (Fig. 3 *B* and *C*). One-third of the B1KO neurons that exhibited a NM rupture (50 of 150 neurons) died during the 50-h period of observation (*SI Appendix*, Fig. S7).

NM ruptures were also observed in B2KO neurons (Fig. 3*A*), but the pattern was distinct. First, NM ruptures were infrequent in B2KO neurons, occurring in only 7.8% of neurons during 50 h of imaging (25 NM ruptures in 321 neurons examined) (Fig. 3*B*). Second, NM repair never occurred in B2KO neurons (Fig. 3*C* and Movies S4 and S5); thus, the mean duration of NM ruptures in B2KO neurons was much longer than in B1KO neurons (38.9 h) (Fig. 3*D*). Third, NM ruptures in B2KO cells led to cell death (with fragmentation of the nucleus and detachment of the neuron from the plate) (*SI Appendix*, Fig. S7). The majority of B2KO neurons that exhibited a NM rupture died during the 50-h period of observation (17 of 25 neurons) (Fig. 3*E*). The other 8 neurons with a NM rupture remained alive, without evidence of NM repair, when the experiment was terminated after 50 h of imaging.

Cell death in cultured B1KO and B2KO neurons was evident by caspase 3 staining and staining with the LIVE/DEAD vital dye (Fig. 4 *A* and *B* and *SI Appendix*, Fig. S8). As expected, the cell death phenotype was more severe in B1KO neurons. We also observed DNA damage in B1KO and B2KO neurons, as judged by staining for γH2AX, a marker for double-stranded DNA breaks (Fig. 4*C*).

Overexpression of Lamin B2 in B1KO Neurons Does Not Eliminate NM Ruptures. Lee et al. (31) showed previously that overexpression of lamin B2 in *Lmnb1*-deficient mouse embryos did not prevent neurodevelopmental abnormalities or the perinatal death. However, the overexpression of lamin B2 significantly increased the size of *Lmnb1*-deficient mouse embryos (31), implying that the surplus lamin B2 improved the viability of *Lmnb1*-deficient cells. To test the ability of lamin B2 to compensate for the loss of lamin B1, we used a doxycycline (Dox)-inducible lentiviral vector to overexpress lamin B2 in B1KO and B2KO neurons. In the presence of doxycycline, lamin B2 expression in B1KO neurons was robust (Fig. 5*A*), such that the lamin B2 covered the entire nuclear rim rather than only 1 pole of the nucleus (Fig. 5*B*). Overexpression of lamin B2 reduced the frequency of NM ruptures in B1KO cells, but many of the neurons continued to have NM ruptures (Fig. 5 *C* and *D*). Indeed, some B1KO neurons had repetitive NM ruptures (Fig. 5 *C* and *D*). In contrast, overexpression of lamin B2 in B2KO cells eliminated NM ruptures (Fig. 5 *C* and *D*). Lamin B2 overexpression also abolished cell death in B2KO cells (reduced the frequency of cell death to that observed in wild-type neurons) (Fig. 5 *E* and *F* and *SI Appendix*, Fig. S9). Overexpression of lamin B2 in B1KO neurons

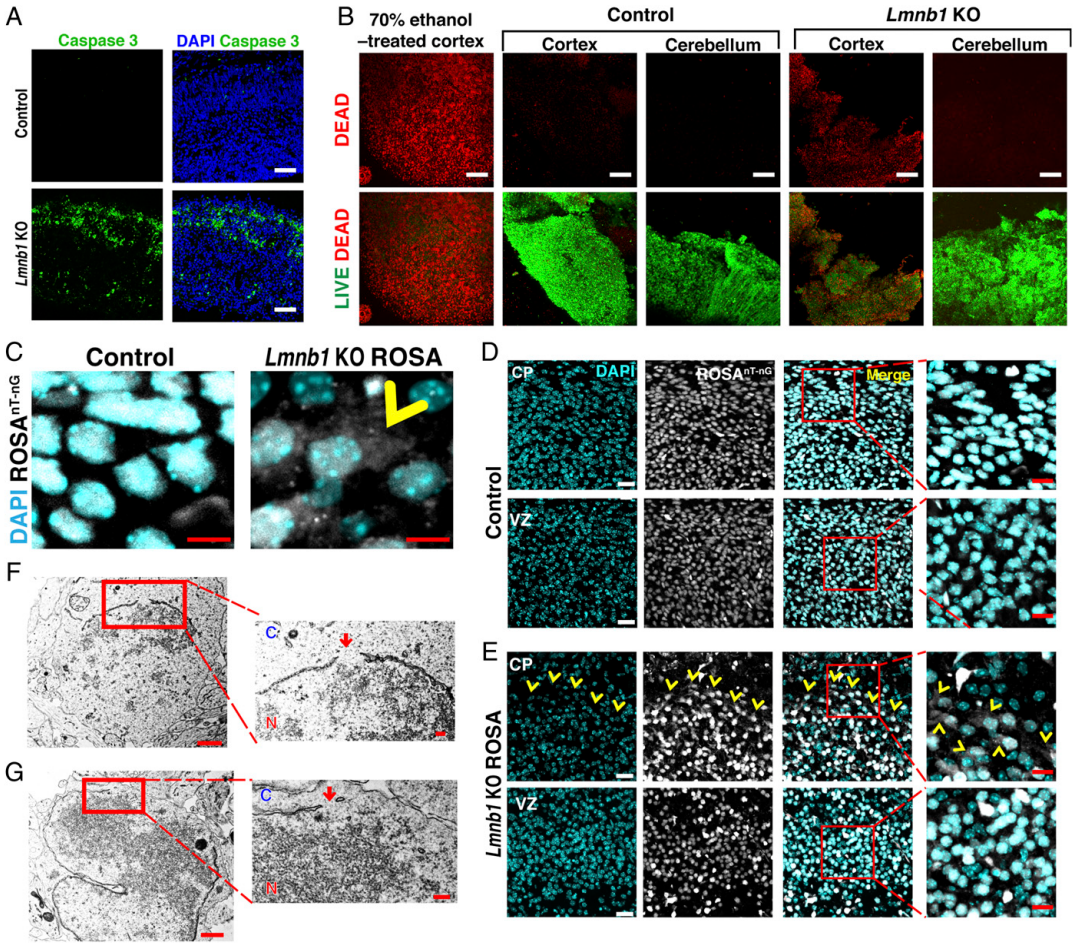

Fig. 1. Forebrain-specific inactivation of *Lmnb1* causes neuronal cell death in the cerebral cortex of mouse embryos and leads to NM ruptures. (*A*) Immunofluorescence microscopy of the cerebral cortex of E18.5 control (*Lmnb1*$^{+/+}$) and *Lmnb1* KO (*Emx1-Cre Lmnb1*$^{fl/fl}$) embryos after staining for a marker of programmed cell death (caspase 3, green). DNA was stained with DAPI (blue). (Scale bars, 50 μm.) (*B*) Immunofluorescence microscopy of the cerebral cortex and cerebellum of control (*Lmnb1*$^{+/+}$ *Lmnb2*$^{fl/fl}$) and *Lmnb1* KO (*Emx1-Cre Lmnb1*$^{fl/fl}$) E18.5 embryos after staining tissues with the LIVE/DEAD fluorescent vital dye. The LIVE/DEAD dye yields a green signal in live cells and a red signal in dead cells. As a positive control for dead cells, a wild-type mouse embryo brain was treated with 70% ethanol. (Scale bars, 100 μm.) (*C*–*E*) Fluorescence microscopy images of cortical neurons in control (*Lmnb1*$^{+/+}$ ROSA$^{nT\text{-}nG}$) and *Lmnb1* KO ROSA (*Emx1-Cre Lmnb1*$^{fl/fl}$ ROSA$^{nT\text{-}nG}$) E18.5 embryos. The ROSA$^{nT\text{-}nG}$ transgene produces a nuclear-targeted tdTomato reporter in the absence of *Cre* and a nuclear-targeted GFP in the presence of *Cre*. In these images, both tdTomato and GFP are colored white and the DNA (stained with DAPI) is colored cyan. *C* shows high-magnification images of cortical plate neurons in a control embryo and a *Lmnb1* KO ROSA embryo; the yellow arrowhead points to a neuron with a NM rupture (escape of the ROSA$^{nT\text{-}nG}$ reporter into the cytoplasm). (Scale bars, 5 μm.) (*D* and *E*) Images of the cortical plate (CP) and ventricular zone (VZ) of forebrains from a control embryo (*D*) and a *Lmnb1* KO ROSA embryo (*E*). In the control embryo, the ROSA$^{nT\text{-}nG}$ reporter is confined to the nucleus in CP and VZ neurons. Many CP neurons in the *Lmnb1* KO ROSA embryo had NM ruptures, with escape of the reporter protein into the cytoplasm (yellow arrowheads), but the reporter remained confined to the nucleus in VZ neurons. (Scale bars, 50 μm, except in the *Insets* where the scale bar is 10 μm.) (*F* and *G*) Electron micrographs showing NM discontinuities in cortical plate neurons of E18.5 *Lmnb1* KO (*Emx1-Cre Lmnb1*$^{fl/fl}$) embryos (red arrows). (Scale bar for low magnification images on the *Left*, 1 μm; scale bar for images on the *Right*, 200 nm.) N, nuclei; C, cytoplasm.

reduced but did not eliminate cell death (Fig. 5 *E* and *F* and *SI Appendix*, Fig. S9).

NM Ruptures and Cell Death in B1KO Cells as They Migrate into and across Tight Constrictions. We suspected that the NM ruptures and cell death in the cortical neurons of *Lmnb1*-deficient embryos resulted from mechanical forces on the cell nucleus—both internal forces associated with nucleokinesis and the constrictive forces as cells migrated between other cells within the cortical plate (32). To explore this idea, we plated wild-type and B1KO neurons onto the flat portion of a silicon wafer and observed the cells as they migrated into an adjacent field of tightly spaced pillars (exposing both the cells and cell nuclei to external constrictive forces) (Fig. 6*A* and *SI Appendix*, Fig. S10*A*). As B1KO neurons entered the

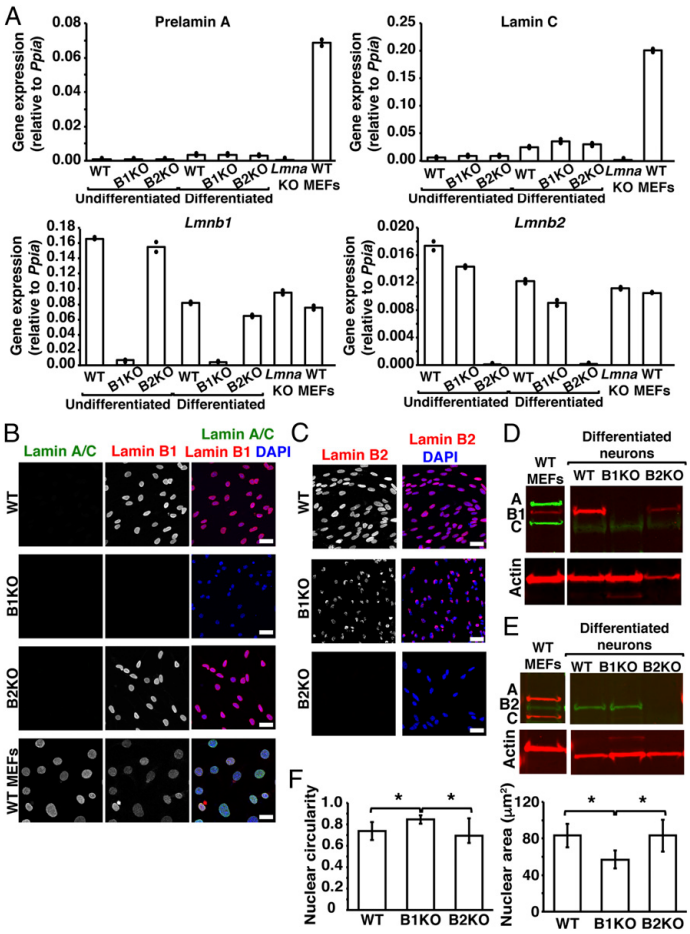

Fig. 2. Nuclear lamin expression in neuronal progenitor cells lacking lamin B1 or lamin B2. (*A*) Transcript levels for prelamin A, lamin C, lamin B1, and lamin B2 in *Lmnb1*$^{+/+}$*Lmnb2*$^{+/+}$ (WT), *Lmnb1*$^{-/-}$*Lmnb2*$^{+/+}$ (B1KO), and *Lmnb1*$^{+/+}$*Lmnb2*$^{-/-}$ (B2KO) undifferentiated and differentiated neurons. Controls included *Lmna*$^{+/+}$*Lmnb1*$^{+/+}$*Lmnb2*$^{+/+}$ mouse embryonic fibroblasts (WT MEFs) and *Lmna*$^{-/-}$ MEFs (*Lmna* KO). Expression levels were normalized to *Ppia*; bar graphs show means for 2 independent experiments and dots represent values from individual experiments. (*B* and *C*) Immunofluorescence microscopy of neurons after staining with antibodies against lamin A/C and lamin B1 (*B*) or an antibody against lamin B2 (*C*). DNA was stained with DAPI (blue). (Scale bars, 25 μm.) (*D* and *E*) Western blots of neuronal protein extracts with antibodies against lamin A/C (green) and lamin B1 (red) (*D*) or with antibodies against lamin A/C (red) and lamin B2 (green) (*E*). Actin was used as a loading control. (*F*) Bar graphs depicting nuclear circularity and nuclear area in WT, B1KO, and B2KO neurons. More than 200 cells from 3 neurospheres of each genotype were analyzed. Mean ± SD; *$P < 0.05$ by an unpaired Student's *t* test.

field of pillars, we observed NM ruptures (Fig. 6*B*). No NM ruptures were observed when wild-type neurons entered the field of pillars. Also, we observed widespread caspase 3 staining of B1KO neurons after they had migrated into the field of pillars (Fig. 6*C* and *SI Appendix*, Fig. S10*B*). Cell death was also observed with the LIVE/DEAD vital dye (Fig. 6*D*).

Discussion

In earlier studies, we documented defective migration of cortical neurons in *Lmnb1* and *Lmnb2* knockout embryos, along with a second abnormality—reduced density of neurons within the cerebral cortex (12). The mechanism for the neuronal migration defect was reasonably well understood, but a mechanism for the reduced cellularity of neurons was not. In the current study, we observed frequent NM ruptures in migrating neurons in the cortical plate of E18.5 *Lmnb1*-deficient embryos, evident by the escape of a nuclear-localized fluorescent reporter protein into the cytoplasm and by electron micrographs revealing discontinuities in the nuclear membranes, but did not observe NM ruptures in the more stationary cells of the ventricular zone. The regions of the brain with NM ruptures also had many dead and dying neurons, as judged by staining for caspase 3 or by staining with the LIVE/DEAD fluorescent vital dye. Consistent with the findings in *Lmnb1*-deficient embryos, we observed NM ruptures, accompanied by DNA damage and cell death, in B1KO neurons as they migrated away from cultured neurospheres. Thus, both mouse embryo and cultured neuron observations strongly imply

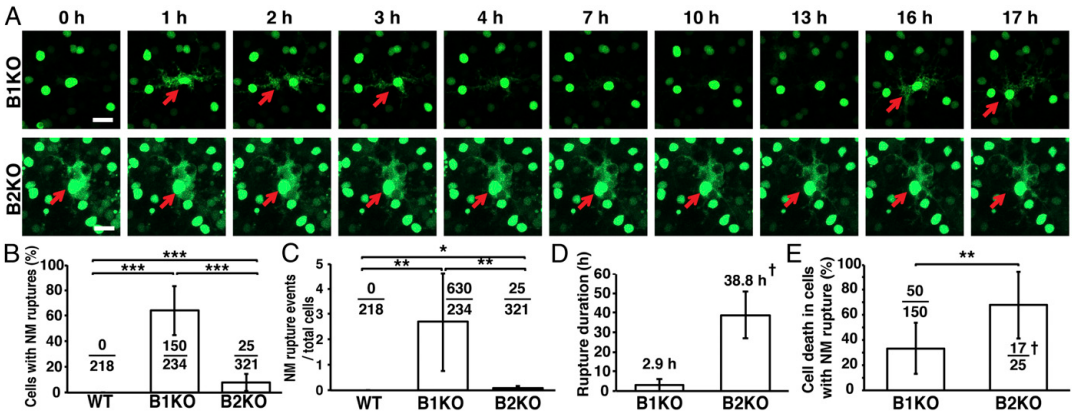

Fig. 3. NM ruptures in B1KO and B2KO neurons. (*A*) Live-cell fluorescence microscopy images of B1KO and B2KO neurons expressing a NLS-GFP. Red arrows point to a NM rupture (escape of the nuclear-localized GFP into the cytoplasm). (Scale bars, 20 μm.) (*B*) Percentages of neurons with NM ruptures in 5 independent experiments during 50 consecutive hours of imaging. The ratio depicts numbers of NM ruptures relative to total numbers of cells observed. ***$P <$ 0.0001. (*C*) Numbers of NM rupture events in 5 independent experiments, each with 50 h of imaging. Mean ± SD; *$P < 0.01$. **$P < 0.001$. One of the 5 experiments was an outlier, with 2 to 3 times more NM ruptures than in the other 4 experiments. When the outlier experiment was excluded (*SI Appendix*, Fig. S6), the SD was smaller and the levels of statistical confidence were greater. (*D*) Average duration of NM ruptures. †Repair of a NM rupture was never observed in a B2KO neuron; thus, the duration of 38.8 h represents the average length of time that NM ruptures were observed over the 50-h period of imaging. (*E*) Percentages of cells with NM ruptures that died during 50 h of imaging. The ratio depicts numbers of cells with NM ruptures that died relative to total numbers of cells with NM ruptures. †Cell death was observed in 17 of 25 B2KO neurons with a NM rupture; 8 of the 25 cells with a NM rupture remained alive, without evidence of NM repair, at the end of the 50-h period of imaging. *B*–*E* show mean ± SD **$P < 0.001$.

that the reduced density of cortical neurons in *Lmnb1*-deficient mice is due to NM ruptures and the accompanying cell death.

The susceptibility of *Lmnb1*-deficient neurons to NM ruptures is likely due to several factors. First, neither the cortical neurons in E18.5 embryos nor cultured neurons express *Lmna*, the gene for lamin A and lamin C. The minimal amounts of lamin A and lamin C expression in cortical neurons probably increase the likelihood of NM ruptures. On the other hand, the high levels of lamins A and C expression in skin and liver likely explains why keratinocyte- or hepatocyte-specific *Lmnb1*/*Lmnb2* knockout mice are free of pathology (8, 9). Second, while lamin B2 is expressed in neurons, it has little ability to compensate for the loss of lamin B1 (30, 31). In migrating neurons of *Lmnb1*-deficient embryos, lamin B2 is asymmetrically distributed along 1 pole of the nucleus, leaving most of the nuclear rim devoid of any nuclear lamin (*SI Appendix*, Fig. S4*B*).

NM ruptures and cell death were never observed in cells of the ventricular zone but were frequent in neurons within the cortical plate. We suspect that the higher susceptibility of cortical plate neurons to NM ruptures relates to deformational forces on the cell nucleus during neuronal migration. Neuronal migration is a saltatory process that depends on nucleokinesis—the motor-driven translocation of the nucleus into the leading edge of the cell. Following translocation of the nucleus, the trailing edge of the neuron is remodeled, resulting in net forward movement of the cell in the direction of the cortical plate. The mechanical forces involved in pulling the cell nucleus forward, together with the virtual absence of nuclear lamins over a large portion of the nucleus, likely triggers NM ruptures. Two observations favor a role for mechanical forces in eliciting NM ruptures. First, NM ruptures were not observed in more stationary cells of the ventricular zone, where the long-distance migration of neurons along glial-directed guides is not in play. Second, NM ruptures, along with cell death, were elicited when cultured B1KO neurons migrated into a field of tightly spaced silicon pillars. The nuclear membrane ruptures in the "silicon pillar experiments" could be a result of nucleokinesis forces and/or a direct consequence of the compressive forces that accompany cellular migration through the field of narrowly spaced pillars.

Lamin B1 and lamin B2 are ∼60% identical at the amino acid level (33), and their temporal and spatial patterns of expression in the brain are very similar (12). Those considerations, along with the fact that deficiencies in either protein cause neuronal layering abnormalities in the cerebral cortex, might lead one to suspect that the 2 nuclear lamins have identical functions. Any such view, however, would be inconsistent with other observations. First, the properties of the 2 proteins are different. For example, lamin B1 is essential for a uniform distribution of lamin B2 along the nuclear rim, whereas the distribution of lamin B1 is quite normal in the absence of lamin B2 (12). Second, lamin B1's farnesyl lipid anchor is required for development of the brain and for survival, whereas lamin B2's farnesyl lipid anchor appears to be utterly dispensable (22). *Lmnb1* knockin embryos that express a nonfarnesylated lamin B1 manifest severe neuronal layering abnormalities in the cerebral cortex as well as perinatal death—like conventional *Lmnb1* knockout mice (22). In contrast, *Lmnb2* knockin mice that express a nonfarnesylated lamin B2 are entirely healthy, free of both neurodevelopmental abnormalities and perinatal mortality (22). Third, the characterization of "reciprocal *Lmnb1*/*Lmnb2* knockin mice" revealed that lamin B1 and lamin B2, despite high levels of amino acid identity, have minimal capacities to substitute for each other during development. For example, $Lmnb2^{+/+}Lmnb1^{B2/B2}$ embryos, where the gene-regulatory elements of *Lmnb1* drive the expression of lamin B2 (resulting in substantially increased levels of lamin B2 expression but no lamin B1), manifest severe neuronal migration defects, reduced neuronal density in the cerebral cortex, and perinatal death. However, brain weights in $Lmnb2^{+/+}Lmnb1^{B2/B2}$ embryos were ∼60% higher than in conventional *Lmnb1* knockout embryos (31), implying that greater-than normal amounts of lamin B2 expression have at least some capacity to improve the survival of *Lmnb1*-deficient neurons.

Our cultured neuron studies underscored the limited capacity of lamin B2 to substitute for lamin B1. Overexpression of lamin

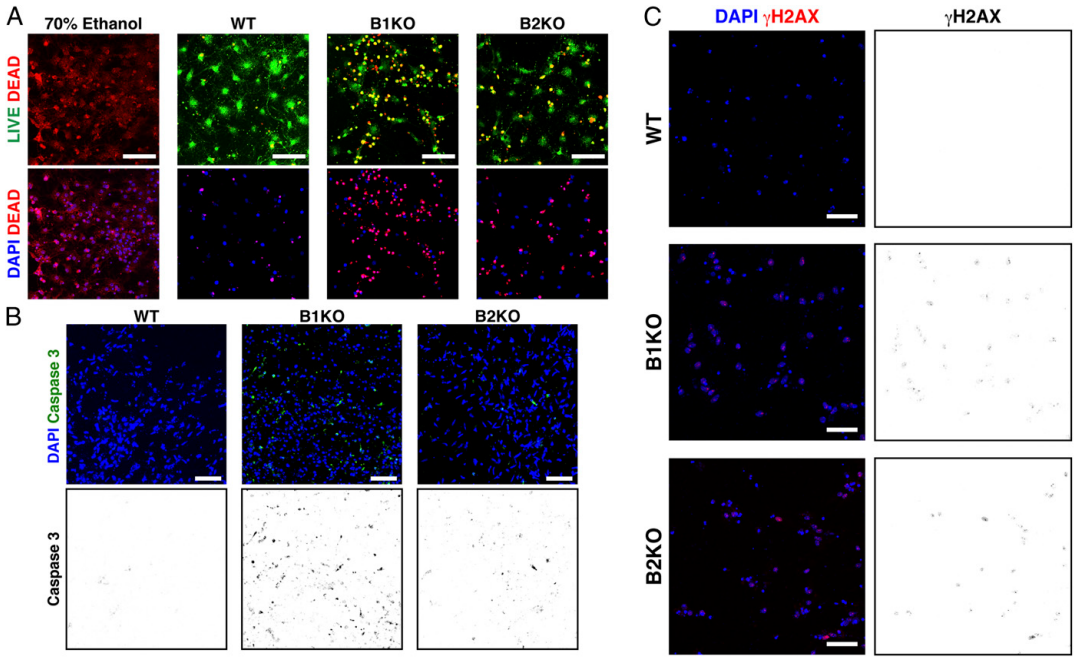

Fig. 4. Cell death in cultured B1KO and B2KO neurons. (*A*) Fluorescence microscopy of WT (*Lmnb1*$^{+/+}$ *Lmnb2*$^{fl/fl}$), B1KO, and B2KO neurons after staining with the LIVE/DEAD vital dye. The LIVE/DEAD dye fluoresces green in live cells and red in dead cells. As a control for dead cells, we treated wild-type neurons with 70% ethanol. DNA was stained with DAPI (blue). (Scale bars, 20 μm.) (*B*) Immunofluorescence microscopy of WT, B1KO, and B2KO neurons that had been cultured in Matrigel for 7 d and stained with an antibody marker of programmed cell death (caspase 3, green). DNA was stained with DAPI (blue). (Scale bars, 25 μm.) The *Lower* shows caspase 3 staining in black against a white background. (*C*) Immunofluorescence microscopy of WT, B1KO, and B2KO differentiated neurons that had been cultured for 30 d and then stained with an antibody against the DNA damage marker γH2AX (red). DNA was stained with DAPI (blue). (Scale bars, 50 μm.) The panels on the *Right* show caspase 3 staining in black against a white background.

B2 in B1KO neurons reduced but did not prevent NM ruptures and cell death, despite the fact that the lamin B2 covered the entire nuclear rim. In contrast, lamin B2 overexpression in B2KO neurons abolished NM ruptures.

Our analysis of NM ruptures in B1KO and B2KO neurons by live-cell microscopy suggested distinct functions for lamin B1 and lamin B2. NM ruptures occurred in most B1KO neurons and repetitively in a subset of neurons, with repeated cycles of NM rupture and repair (escape of the fluorescent reporter into the cytoplasm followed by return of the reporter into the nucleus). The mean duration of NM ruptures in B1KO neurons was 2.9 h. Some B1KO neurons with NM ruptures died, but the majority survived. The behavior of B2KO neurons was different. NM ruptures were much less frequent but when they occurred they were never repaired and resulted in cell death. We do not understand the phenotypic differences, but our studies suggest that lamin B1 is more important for the structural integrity of the nuclear envelope, whereas lamin B2 is crucial for NM repair. Perhaps lamin B2 is the "mortar" that binds together the key building blocks in the nuclear lamina (i.e., lamin B1), and perhaps lamin B2 (or a lamin B2-interacting protein) plays a key role in sealing holes in the nuclear membranes.

The phenotype observed in B2KO neurons—infrequent NM ruptures but an absence of NM repair—may help to explain phenotypes observed in *Lmnb2* mouse models. In conventional *Lmnb2* knockout embryos, the reduction in the size of the cerebral cortex is modest (only ~5 to 10% smaller than in wild-type embryos) (11). In contrast, the reduction in the size of the forebrain in 4-mo-old forebrain-specific *Lmnb2* knockout mice is more substantial (20% smaller than in wild-type mice) (12). The subtle decrease in cortical size in E18.5 *Lmnb2* knockout embryos may reflect infrequent NM ruptures (and the resulting cell death), whereas the more substantial decrease in cortical size in the adult forebrain-specific *Lmnb2* knockout mice could reflect loss of neurons due to an absence of NM repair. Even if NM ruptures are infrequent, the failure to repair the ruptures would be expected to result in a progressive loss of neurons and brain size.

Finally, we would point out that the 2 principal phenotypes associated with deficiencies of B-type lamins, neuronal layering defects in the cortex and decreased neuronal survival, are mechanistically related. Fundamental to both are a weakened nuclear lamina and mechanical forces on migrating neurons during development. Interestingly, B-type lamin deficiencies have only minor effects on stationary, postmitotic, *Lmna*-expressing neurons (13, 28). Inactivating *Lmnb1* in photoreceptor neurons of the retina early in development leads to neuronal layering abnormalities and a dramatic loss of neurons, whereas inactivating both *Lmnb1* and *Lmnb2* in postmitotic photoreceptor cells after birth has minimal consequences (minor effects on the positioning of the nucleus within the cell) (34, 35). The B-type lamins are long-lived proteins with a half-life of over 5 mo in postmitotic cells (36), making it challenging to define the functional relevance of the proteins in adult mice (37).

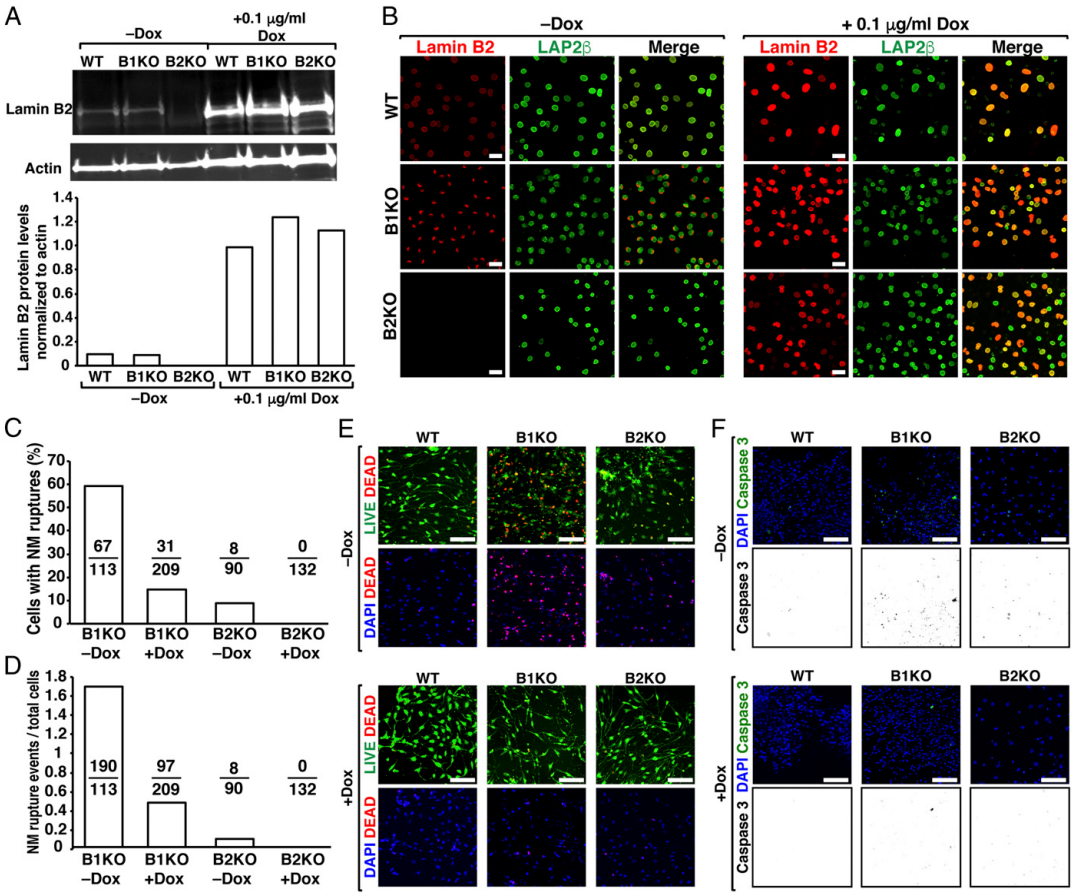

Fig. 5. Overexpression of lamin B2 reduces cell death and NM ruptures in B1KO and B2KO neurons. (*A*) Western blots of extracts from WT, B1KO, and B2KO neurons; the neurons had been transduced with a doxycycline-inducible lamin B2 lentiviral vector (pTRIPZ-*LMNB2*) and then incubated in the presence or absence of Dox. Actin was used as a loading control. The bar graph shows lamin B2 protein levels normalized to actin. (*B*) Immunofluorescence microscopy of WT, B1KO, and B2KO neurons that had been transduced with pTRIPZ-*LMNB2*. In the presence of Dox, the cells expressed lamin B2. Immunofluorescence microscopy was performed after staining neurons with antibodies against lamin B2 (red) and LAP2β (green). (Scale bars, 20 μm.) (*C*) Percentages of B1KO and B2KO neurons exhibiting NM ruptures during 20 h of live-cell imaging. Ratios show numbers of neurons with NM ruptures over the total number of neurons examined. (*D*) Total numbers of NM rupture events relative to the total number of neurons examined. In these studies, the neurons had been transduced with NLS-GFP and pTRIPZ-*LMNB2* and incubated in the presence or absence of Dox. NM ruptures (escape of NLS-GFP in the cytoplasm) were observed by fluorescence microscopy. Data show totals from 2 independent experiments. (*E*) Overexpression of lamin B2 in B1KO and B2KO neurons reduces cell death, as judged by staining with the LIVE/DEAD fluorescent vital dye. WT, B1KO, and B2KO neurons that had been transduced with pTRIPZ-*LMNB2* were incubated in the presence or absence of Dox for 24 h and then incubated with the LIVE/DEAD dye, which fluoresces green in live cells and red in dead cells. DNA was stained with DAPI (blue). (Scale bars, 50 μm.) (*F*) Overexpression of lamin B2 in B1KO and B2KO neurons reduces programmed cell death, as judged by staining for caspase 3. WT, B1KO, and B2KO neurons that had been transduced with pTRIPZ-*LMNB2* were incubated in the presence or absence of Dox for 24 h and then stained with a caspase 3-specific antibody (green). No caspase 3 staining was observed in WT cells. DNA was stained with DAPI (blue). (Scale bars, 50 μm.) The *Lower* shows caspase 3 staining in black against a white background.

Materials and Methods

Cell Culture Models. NPCs were isolated from E13.5 embryos derived from intercrossing *Lmnb1*$^{+/-}$ mice and used to generate *Lmnb1*$^{+/+}$*Lmnb2*$^{+/+}$ (WT) and *Lmnb1*$^{-/-}$*Lmnb2*$^{+/+}$ (B1KO) neurospheres. Explants from the cerebral cortex were placed in DMEM/F-12 medium (Corning) and dissociated with TrypLE Select (Gibco); the NPCs were resuspended in DMEM/F-12 (Corning). To generate *Lmnb1*$^{+/+}$*Lmnb2*$^{-/-}$ (B2KO) neurospheres, we intercrossed *Emx1-Cre Lmnb2*$^{fl/fl}$ mice and isolated forebrain NPCs from *Emx1-Cre Lmnb2*$^{fl/fl}$ embryos. To be certain that *Lmnb2* was completely inactivated, the NPCs were treated twice with *Cre* adenovirus (1,000 multiplicity of infection). Neurospheres were generated by culturing NPCs in DMEM/F-12 medium containing 2% B-27 supplement (Thermo Fisher Scientific), 100 U/mL of penicillin, and 100 μg/mL of streptomycin at 37 °C in 5 to 7% CO_2. Neurospheres were supplemented with 3 μL of a heparin–embryonic growth factor (EGF)–fibroblast growth factor (FGF) mix (described below) for every milliter of medium. NPCs were transduced (in University of California, Los Angeles [UCLA]'s Vector Core Facility) with a lentiviral vector for NLS-GFP (26).

Preparing the Heparin–EGF–FGF Supplement. One milligram of FGF was resuspended in 1 mL of FGF buffer (0.1% BSA [Sigma] in PBS) and diluted in 39 mL of DMEM/F-12 (Corning); 1 mg EGF (Thermo Fisher Scientific) was

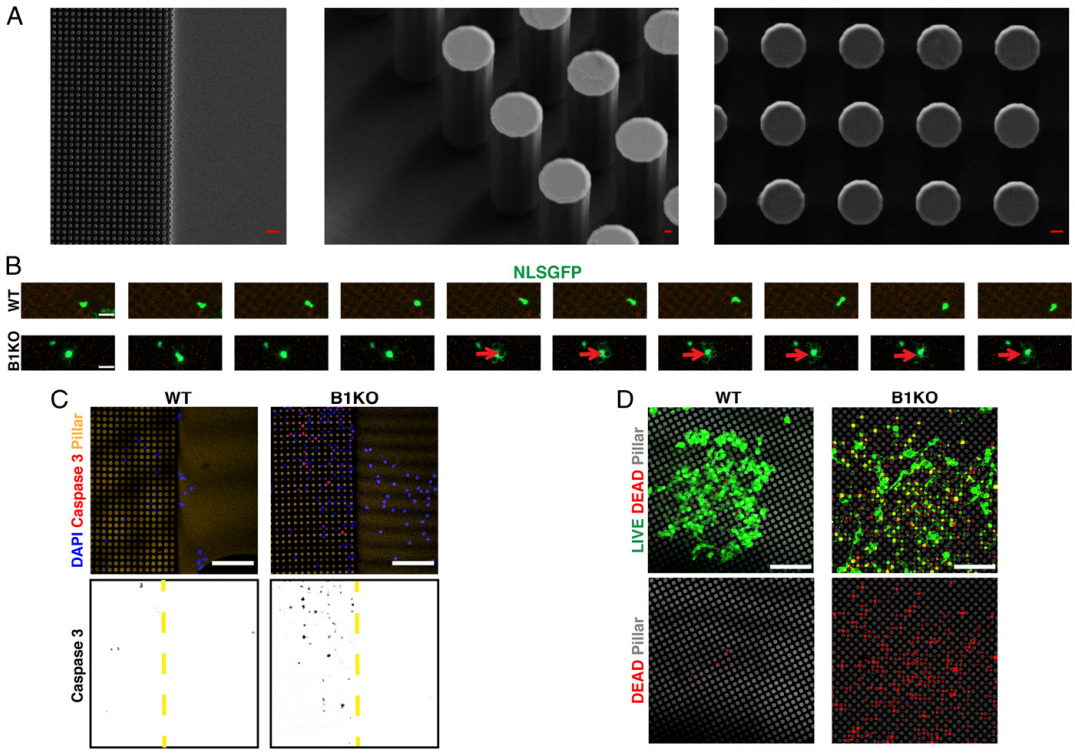

Fig. 6. NM ruptures and cell death during the migration of B1KO neurons into a field of silicon pillars (8 μm in diameter; 22 μm in height; spaced 4 μm apart). (*A*, *Left*) Scanning electron micrograph of a silicon wafer (with one side flat and the other side patterned with uniformly spaced silicon pillars). (Scale bar, 30 μm.) (*A*, *Middle* and *Right*) Scanning electron micrographs of the uniformly spaced silicon pillars. (Scale bars, 2 μm.) (*B*) Live-cell fluorescence microscopy images (20-min intervals) of NLS-GFP–expressing WT and B1KO neurons after the cells had migrated into the field of pillars. NM ruptures (escape of the NLS-GFP into the cytoplasm) were observed in B1KO neurons (red arrows; *Bottom*) but not in WT neurons (*Top*). (Scale bars, 20 μm.) (*C*) Immunofluorescence microscopy of WT and B1KO neurons with a caspase 3-specific antibody (a marker of apoptotic cell death). Neurospheres were pipetted onto the smooth portion of the silicon wafer, and individual neurons were allowed to migrate into the field of pillars. The migration of neurons into the field of pillars subjects the cells as well as the cell nucleus to constrictive forces. Cell death, as judged by caspase 3 staining, was observed in B1KO neurons (but not WT neurons) after the cells had migrated into the field of pillars. DNA was stained with DAPI (blue). (Scale bars, 50 μm.) The panels below show caspase 3 staining in black against a white background. The edge of the field of pillars is marked by a yellow dashed line. (*D*) Fluorescence microscopy with the LIVE/DEAD fluorescent vital dye, revealing cell death in B1KO neurons (but not WT neurons) after the migration of cells into the field of pillars. The LIVE/DEAD fluorescent vital dye fluoresces green in live cells and red in dead cells. (Scale bar, 50 μm.)

resuspended in EGF buffer (10% BSA in PBS) and diluted in 9 mL of fresh DMEM/F-12; 500 mg of heparin sodium salt (Sigma-Aldrich) was dissolved in 100 mL DMEM/F-12. To prepare 25 mL of the heparin–EGF–FGF supplement, 8 mL of the FGF solution, 5 mL of the EGF solution, and 10 mL of the heparin solution were mixed with 2 mL of DMEM/F-12.

Neuronal Differentiation. Cultured neurospheres were carefully removed with polyethylene pipets (Fisher) and pipetted into a single drop of laminin (Sigma-Aldrich) on poly-L-ornithine–coated plates Neurospheres were allowed to settle for 30 min at 37 °C and then incubated with the DMEM/F-12 containing 2% B-27 supplement, 100 U/mL of penicillin, and 100 μg/mL of streptomycin. Neurospheres were differentiated for up to 30 d.

Quantitative RT-PCR Studies. RNA was isolated from undifferentiated and differentiated neurospheres, treated with DNase I (Ambion), and reverse transcribed with random primers, oligo(dT), and SuperScript III (Invitrogen). qPCR reactions were performed on a 7900 Fast Real-Time PCR system (Applied Biosystems) with SYBR Green PCR Master Mix (Bioline). Transcript levels were determined by the comparative cycle threshold method and normalized to levels of cyclophilin A. All primers used are listed in the *SI Appendix*, Table S1.

Immunocytochemistry. Neurons that had been differentiated on coverslips were fixed with 4% paraformaldehyde in PBS or ice-cold methanol, dipped once in acetone, and permeabilized with 0.2% Triton. The fixed cells were then processed for confocal immunofluorescence microscopy (8) with the antibodies listed in *SI Appendix*, Table S2. For confocal immunofluorescence microscopy, images were recorded with a Zeiss LSM 700 laser-scanning microscope with a Plan Apochromat 20×/0.80 objective (air) or a Plan Apochromat 100×/1.40 oil-immersion objective. Images along the *z* axis were processed with Zen 2010 software (Zeiss).

Western Blots. Urea-soluble protein extracts from cells were size fractionated on 4 to 12% gradient polyacrylamide Bis-Tris gels (Invitrogen) and then transferred to a nitrocellulose membrane for Western blots. Membranes were blocked with Odyssey Blocking solution (LI-COR Biosciences) for 1 h at room temperature (RT) and then incubated with primary antibodies at 4 °C overnight (antibodies are listed in *SI Appendix*, Table S2). After washing the membranes with PBS containing 0.1% Tween-20, the membranes were incubated with infrared dye (IR)-labeled secondary antibodies (LI-COR Biosciences) for 1 h at RT. The IR signals were quantified with an Odyssey infrared scanner (LI-COR Biosciences).

Nuclear Shape Analyses. To assess the area and circularity of cell nuclei, WT, B1KO, and B2KO neurospheres were stained with an antibody against the inner nuclear membrane protein LAP2β, and images of cells were recorded with a Zeiss LSM700 laser-scanning microscope (20× objective), focusing on individual neurons that had migrated away from the main body of the neurosphere. Nuclear area was assessed using ImageJ software; nuclear circularity ($4\pi \times$ area/perimeter^2) was assessed by measuring nuclear areas and perimeters for 100 cells/genotype ($n = 3$ independent experiments). Nuclear circularity reaches a maximum value of 1.0 for a perfect circle (38).

Live-Cell Imaging. Neurospheres were plated on a poly-L-ornithine–coated 6-well plate containing 2-mm glass wells (MatTek), and live-cell imaging was performed with a Zeiss LSM 800 confocal microscope equipped with a Plan Apochromat 10×/0.45 or a Plan Apochromat 20×/0.80 objective at 37 °C with 5% CO_2 (maintained with TempModule S1 CO_2 Module S1 from Zeiss). *Z* stacks were acquired from both fluorescence and transmission channels. Image sequences were analyzed with ZEN (Zeiss) using linear adjustments applied uniformly to the entire image. For confocal image stacks, images were 3-dimensionally reconstructed and displayed as maximum intensity projections. A nuclear rupture event was defined as NLS-GFP entry into the cytoplasm in interphase cells.

Fluorescent Vital Dye. Neurons were allowed to differentiate on poly-L-ornithine–coated 6-well plates containing 2-mm glass wells (MatTek) for 7 d. After washing cells with PBS (Gibco), cell viability was assessed with the LIVE/DEAD Cell Imaging Kit (Thermo Fisher). Neurons were incubated with the LIVE/DEAD dye for 15 min at 20 to 25 °C and then fixed with 4% paraformaldehyde in PBS and stained with DAPI. Cells were imaged immediately with a Zeiss LSM700 laser-scanning microscope with a Plan Apochromat 20×/0.80 objective (air). As a positive control for cell death, cells or tissue sections were treated with 70% ethanol for 15 min before staining.

Plating of Neurospheres on Matrigel. A vial of Matrigel (Corning) was thawed overnight by submerging it in ice in a 4 °C refrigerator. Using prechilled pipet tips, Matrigel was pipetted into glass-bottom 6-well culture plates (MatTek) and then incubated at 37 °C for 30 min to allow a gel to form. Neurospheres were resuspended in Matrigel and plated on top of the gel layer, allowing 30 min at 37 °C for the gel to solidify. Each well was then flooded with DMEM/F-12 medium containing 2% B-27 supplement (Thermo Fisher), 100 U/mL of penicillin, and 100 μg/mL of streptomycin. Neurons were allowed to differentiate and migrate into the Matrigel for 7 d. The neurospheres were then prepared for immunocytochemistry as described earlier.

Silicon Pillar Fabrication. Prime quality 4-inch Si (100) wafers (P/B, 1 to 10 Ω-cm) were purchased from UniversityWafer (Boston, MA). A quartz photomask (PhotomaskPortal) was designed with LayoutEditor software to fabricate a custom array of circles with 4-μm spacings and used for conventional photolithography. Positive photoresist SPR700-1.2 was spin-coated on the Si surface, followed by a 90-s soft bake at 90 °C on a hotplate. A Karl Suss contact aligner was used to expose the photoresist on the wafer selectively with the pattern on the photomask with an optimal exposure time of 2 s (UV wavelength 365 nm, intensity 12 mW/cm^2). The exposed wafer was post-exposure baked at 110 °C for 90 s, immersed in MF-26A developer for 1 min (development), rinsed with deionized water, and blown dry with N_2. After photolithography, the patterned silicon wafer was reactive-ion etched (Plasma-Thermo FDRIE DSE II) for 6 min and 30 s to remove silicon in the exposed regions, forming 22-μm-deep silicon pillars. The pillar depth, diameter, and pitch were characterized with a Zeiss Supra 40VP scanning electron microscope (SEM) and Dektak 6 Surface Profilometer.

Fluorescent Labeling of APTES-Functionalized Pillar Substrates. The silicon micropillar substrates were functionalized with (3-aminopropyl) triethoxysilane (APTES, Sigma-Aldrich) using chemical vapor deposition. Silanol groups were formed on the silicon surface by ozone treatment for 15 min. The substrate and a Teflon cap filled with 100 μL of APTES was then placed in a vacuum flask and suspended in a 40 °C water bath with a vacuum line attached. House vacuum was engaged for 1 min, reducing the pressure in the flask to vaporize APTES, promoting covalent binding between the APTES silane termination and surface silanol functionalities during a 1-h incubation. Substrates were removed from the flask and rinsed with 100% ethanol. The silicon was then labeled with a fluorescent dye (Texas Red). To generate a stock solution, 1 mg of Texas Red sulfonyl chloride was mixed with 100 μL of 99% *N,N*-dimethylformamide (Sigma-Aldrich). A total of 50 μL of the stock was added dropwise to 10 mL of a 0.1- to 0.2-M sodium bicarbonate (Sigma-Aldrich) buffer (pH ~ 9). The APTES-functionalized substrate was then incubated in the buffered dye solution for 2 h at 4 °C on a shaking stage. The silicon substrates were then rinsed with Milli-Q ultrapure 18 MΩ water to remove physisorbed dye and stored at −20 °C until use. To plate neurospheres for differentiation, laminin (Sigma-Aldrich) was first pipetted onto the silicon wafer substrates; the neurospheres were removed with a polyethylene pipets (Fisher) and pipetted into a drop of laminin. Neurospheres were allowed to settle for 30 min at 37 °C and then incubated with DMEM/F-12 medium containing 2% B-27 supplement, 100 U/mL of penicillin, and 100 μg/mL of streptomycin.

Mouse Studies. Forebrain-specific *Lmnb1* and *Lmnb2* knockout mice (*Emx1-Cre Lmnb1*$^{fl/fl}$, *Emx1-Cre Lmnb2*$^{fl/fl}$) were generated as described (12) and bred with *ROSA*$^{nT\text{-}nG}$ mice (B6;129S4-*Gt(ROSA)26Sor*$^{tm1(CAG\text{-}tdTomato^*,\text{-}EGFP^*)Ees}$/J) from The Jackson Laboratory (Bar Harbor, ME). All mouse studies were carried out in accordance with the recommendations in the *Guide for the Care and Use of Laboratory Animals* of the National Institutes of Health. All mice were fed a chow diet and housed in a virus-free barrier facility with a 12-h light/dark cycle. Animal protocols were reviewed and approved by the Animal Research Committee of UCLA.

Immunohistochemistry. Mouse tissues were prepared for immunohistochemical studies as described (12). Embryonic brains were fixed in 4% paraformaldehyde in PBS for 2 h at room temperature, incubated in 30% sucrose in PBS at 4 °C overnight, and then frozen in O.C.T. (Tissue-Tek, Sakura Finetek). Sections (10 μm thick) were fixed for 5 min in 4% paraformaldehyde or ice-cold methanol, followed by 5 dips in acetone and permeabilization with 0.1% Tween-20. Background staining with mouse antibodies was minimized with the Mouse-on-Mouse Kit (Vector Laboratories, Burlingame, CA). Tissue sections were blocked with 2.5% horse serum for 1 h at room temperature and incubated overnight at 4 °C with primary antibodies at the dilutions indicated in *SI Appendix*, Table S2. Alexa Fluor 488- and Alexa Fluor 568-conjugated secondary antibodies (Molecular Probes, Invitrogen, Carlsbad, CA) were used at a 1:2,000 dilution; DyLight 649-conjugated streptavidin (Vector Laboratories) was used at 5 μg/mL. After counterstaining with DAPI, sections were mounted with Prolong Gold antifade (Invitrogen) and images were obtained with a Zeiss LSM700 laser-scanning microscope with a Plan Apochromat 20×/0.80 objective (air) or a Plan Apochromat 100×/1.40 oil-immersion objective. Images along the *z* axis were processed by Zen 2010 software (Zeiss).

Fluorescent Vital Dye Staining of Embryonic Tissues. Cerebral cortex explants were harvested from E18.5 mouse embryos and placed in PBS containing 1% BSA. Cell viability was assessed by incubating 2-mm-thick pieces of explants with the LIVE/DEAD fluorescent dye (Thermo Fisher) for 15 min at 20 to 25 °C. After fixation with 4% paraformaldehyde in PBS and staining with DAPI, the tissues were immediately imaged with a Zeiss LSM 700 laser-scanning microscope with a Plan Apochromat 20×/0.80 objective (air).

Preparation of Tissues for Electron Microscopy. The cerebral cortex from E18.5 embryos was excised and fixed overnight at 4 °C in a solution containing 4% paraformaldehyde, 2.5% glutaraldehyde, 2.1% sucrose, and 0.1 M sodium cacodylate. On the next day, the samples were rinsed 5 times for 3 min each with 0.1 M sodium cacodylate and then incubated in a solution containing 2% osmium tetroxide, 1.5% potassium ferricyanide, and 0.1 M sodium cacodylate for 1 h at 4 °C. Next, the samples were rinsed 5 times for 3 min each with H_2O and then incubated with 1% thiocarbohydrazide for 20 min at room temperature. Next, samples were rinsed again 5 times for 3 min each with H_2O and then incubated with 2% osmium tetroxide for 30 min at room temperature. The samples were then rinsed 5 times for 3 min with H_2O and incubated with 2% uranyl acetate at 4 °C overnight. On the following day, tissue samples were rinsed with H_2O and dehydrated with a series of increasing ethanol concentrations (30, 50, 70, 85, 95, and 100%) for 10 min each, followed by 2 10-min incubations with 100% ethanol. Next, the samples were infiltrated with Embed812 resin (Electron Microscopy Sciences) by incubating samples in 33% resin (diluted in anhydrous acetone) for 2 h, 66% resin overnight, and 100% resin for 4 h. Samples were then embedded in fresh resin using polypropylene molds (Electron Microscopy Sciences) and polymerized in a vacuum oven at 65 °C for 48 h. After polymerization, samples were removed from the molds; block faces were trimmed, faced, and 65-nm sections were cut using a Leica UC6 μLtramicrotome equipped with a Diatome diamond knife. Sections were collected onto glow-discharged copper grids coated with formvar and carbon (Electron Microscopy Sciences) and stained with Reynold's lead citrate solution for 10 min. Finally, samples were imaged with a FEI Tecnai T12 transmission electron microscope set at 120 kV and equipped with a Gatan CCD camera.

Statistical Analyses. Statistical analyses were performed with GraphPad QuickCalcs (https://www.graphpad.com/). Differences in nuclear morphologies (blebs, irregularly shaped nuclei) and the frequency of NM ruptures were analyzed with a χ^2 test. Differences in nuclear circularity and numbers of γH2AX foci were assessed with a 2-tailed Student's *t* test.

See *SI Appendix, SI Materials and Methods* for more details on the methods we used.

Data Availability. All data are available in the manuscript and *SI Appendix*.

ACKNOWLEDGMENTS. This work was supported by NIH Grants HL126551 (S.G.Y.) and AG047192 (L.G.F.), a NIH Ruth L. Kirschstein National Research Service Award T32GM065823 (N.Y.C.), a Whitcome Fellowship Award from UCLA's Molecular Biology Institute, and a Vascular Biology Training Grant. We acknowledge support provided by NIH/National Center for Advancing Translational Science UCLA Clinical and Translational Science Institute Grant KL2TR001882 as well as Young Investigator Awards from the Alex's Lemonade Stand Foundation for Childhood Cancer Research, Hyundai Hope on Wheels, and the Tower Cancer Research Foundation. We acknowledge Chiara Bertipaglia and Richard Vallee (Columbia University) for helpful discussions. We thank Dr. Janel LeBelle and Dr. Harvey Kornblum (UCLA) for sharing methods for culturing neurospheres. We thank Dr. Jan Lammerding for sharing the NLS-GFP plasmid. We thank Ms. Lisa Kawakami for help with microfabrication and Ms. Liv Heidenreich for help with microstructure functionalization. Virus production and transduction were performed by the Integrated Molecular Technologies Core/UCLA Vector Core, which is supported by CURE/P30 DK041301. Nano- and microfabrication were performed at the Integrated Systems Nanofabrication Cleanroom of the California NanoSystems Institute.

1. J. Harborth, S. M. Elbashir, K. Bechert, T. Tuschl, K. Weber, Identification of essential genes in cultured mammalian cells using small interfering RNAs. *J. Cell Sci.* **114**, 4557–4565 (2001).
2. L. Vergnes, M. Péterfy, M. O. Bergo, S. G. Young, K. Reue, Lamin B1 is required for mouse development and nuclear integrity. *Proc. Natl. Acad. Sci. U.S.A.* **101**, 10428–10433 (2004).
3. R. D. Moir, M. Montag-Lowy, R. D. Goldman, Dynamic properties of nuclear lamins: Lamin B is associated with sites of DNA replication. *J. Cell Biol.* **125**, 1201–1212 (1994).
4. R. I. Lopez-Soler, R. D. Moir, T. P. Spann, R. Stick, R. D. Goldman, A role for nuclear lamins in nuclear envelope assembly. *J. Cell Biol.* **154**, 61–70 (2001).
5. M. Y. Tsai *et al.*, A mitotic lamin B matrix induced by RanGTP required for spindle assembly. *Science* **311**, 1887–1893 (2006).
6. T. Dechat *et al.*, Nuclear lamins: Major factors in the structural organization and function of the nucleus and chromatin. *Genes Dev.* **22**, 832–853 (2008).
7. C. J. Hutchison, Lamins: Building blocks or regulators of gene expression? *Nat. Rev. Mol. Cell Biol.* **3**, 848–858 (2002).
8. S. H. Yang *et al.*, An absence of both lamin B1 and lamin B2 in keratinocytes has no effect on cell proliferation or the development of skin and hair. *Hum. Mol. Genet.* **20**, 3537–3544 (2011).
9. S. H. Yang, H. J. Jung, C. Coffinier, L. G. Fong, S. G. Young, Are B-type lamins essential in all mammalian cells? *Nucleus* **2**, 562–569 (2011).
10. C. Coffinier, L. G. Fong, S. G. Young, LINCing lamin B2 to neuronal migration: Growing evidence for cell-specific roles of B-type lamins. *Nucleus* **1**, 407–411 (2010).
11. C. Coffinier *et al.*, Abnormal development of the cerebral cortex and cerebellum in the setting of lamin B2 deficiency. *Proc. Natl. Acad. Sci. U.S.A.* **107**, 5076–5081 (2010).
12. C. Coffinier *et al.*, Deficiencies in lamin B1 and lamin B2 cause neurodevelopmental defects and distinct nuclear shape abnormalities in neurons. *Mol. Biol. Cell* **22**, 4683–4693 (2011).
13. S. G. Young, H. J. Jung, C. Coffinier, L. G. Fong, Understanding the roles of nuclear A- and B-type lamins in brain development. *J. Biol. Chem.* **287**, 16103–16110 (2012).
14. T. Shimi *et al.*, The A- and B-type nuclear lamin networks: Microdomains involved in chromatin organization and transcription. *Genes Dev.* **22**, 3409–3421 (2008).
15. R. D. Moir *et al.*, Review: The dynamics of the nuclear lamins during the cell cycle–relationship between structure and function. *J. Struct. Biol.* **129**, 324–334 (2000).
16. C. W. Tang *et al.*, The integrity of a lamin-B1-dependent nucleoskeleton is a fundamental determinant of RNA synthesis in human cells. *J. Cell Sci.* **121**, 1014–1024 (2008).
17. R. B. Vallee, J. W. Tsai, The cellular roles of the lissencephaly gene LIS1, and what they tell us about brain development. *Genes Dev.* **20**, 1384–1393 (2006).
18. J. W. Tsai, K. H. Bremner, R. B. Vallee, Dual subcellular roles for LIS1 and dynein in radial neuronal migration in live brain tissue. *Nat. Neurosci.* **10**, 970–979 (2007).
19. D. J. Hu *et al.*, Dynein recruitment to nuclear pores activates apical nuclear migration and mitotic entry in brain progenitor cells. *Cell* **154**, 1300–1313 (2013).
20. A. Gupta, L. H. Tsai, A. Wynshaw-Boris, Life is a journey: A genetic look at neocortical development. *Nat. Rev. Genet.* **3**, 342–355 (2002).
21. A. Wynshaw-Boris, Lissencephaly and LIS1: Insights into the molecular mechanisms of neuronal migration and development. *Clin. Genet.* **72**, 296–304 (2007).
22. H. J. Jung *et al.*, Farnesylation of lamin B1 is important for retention of nuclear chromatin during neuronal migration. *Proc. Natl. Acad. Sci. U.S.A.* **110**, E1923–E1932 (2013).
23. J. D. Vargas, E. M. Hatch, D. J. Anderson, M. W. Hetzer, Transient nuclear envelope rupturing during interphase in human cancer cells. *Nucleus* **3**, 88–100 (2012).
24. E. M. Hatch, A. H. Fischer, T. J. Deerinck, M. W. Hetzer, Catastrophic nuclear envelope collapse in cancer cell micronuclei. *Cell* **154**, 47–60 (2013).
25. E. Hatch, M. Hetzer, Breaching the nuclear envelope in development and disease. *J. Cell Biol.* **205**, 133–141 (2014).
26. C. M. Denais *et al.*, Nuclear envelope rupture and repair during cancer cell migration. *Science* **352**, 353–358 (2016).
27. N. Y. Chen *et al.*, Fibroblasts lacking nuclear lamins do not have nuclear blebs or protrusions but nevertheless have frequent nuclear membrane ruptures. *Proc. Natl. Acad. Sci. U.S.A.* **115**, 10100–10105 (2018).
28. H. J. Jung *et al.*, Regulation of prelamin A but not lamin C by miR-9, a brain-specific microRNA. *Proc. Natl. Acad. Sci. U.S.A.* **109**, E423–E431 (2012).
29. H. J. Jung, J. M. Lee, S. H. Yang, S. G. Young, L. G. Fong, Nuclear lamins in the brain - new insights into function and regulation. *Mol. Neurobiol.* **47**, 290–301 (2013).
30. S. G. Young, H. J. Jung, J. M. Lee, L. G. Fong, Nuclear lamins and neurobiology. *Mol. Cell. Biol.* **34**, 2776–2785 (2014).
31. J. M. Lee *et al.*, Reciprocal knock-in mice to investigate the functional redundancy of lamin B1 and lamin B2. *Mol. Biol. Cell* **25**, 1666–1675 (2014).
32. B. Nadarajah, P. Alifragis, R. O. Wong, J. G. Parnavelas, Neuronal migration in the developing cerebral cortex: Observations based on real-time imaging. *Cereb. Cortex* **13**, 607–611 (2003).
33. B. S. J. Davies *et al.*, Posttranslational processing of nuclear lamins. *Enzymes* **29**, 21–41 (2011).
34. D. Razafsky, N. Blecher, A. Markov, P. J. Stewart-Hutchinson, D. Hodzic, LINC complexes mediate the positioning of cone photoreceptor nuclei in mouse retina. *PLoS One* **7**, e47180 (2012).
35. D. Razafsky *et al.*, Lamin B1 and lamin B2 are long-lived proteins with distinct functions in retinal development. *Mol. Biol. Cell* **27**, 1928–1937 (2016).
36. B. H. Toyama *et al.*, Identification of long-lived proteins reveals exceptional stability of essential cellular structures. *Cell* **154**, 971–982 (2013).
37. C. M. Gigante *et al.*, Lamin B1 is required for mature neuron-specific gene expression during olfactory sensory neuron differentiation. *Nat. Commun.* **8**, 15098 (2017).
38. A. C. Rowat *et al.*, Nuclear envelope composition determines the ability of neutrophil-type cells to passage through micron-scale constrictions. *J. Biol. Chem.* **288**, 8610–8618 (2013).

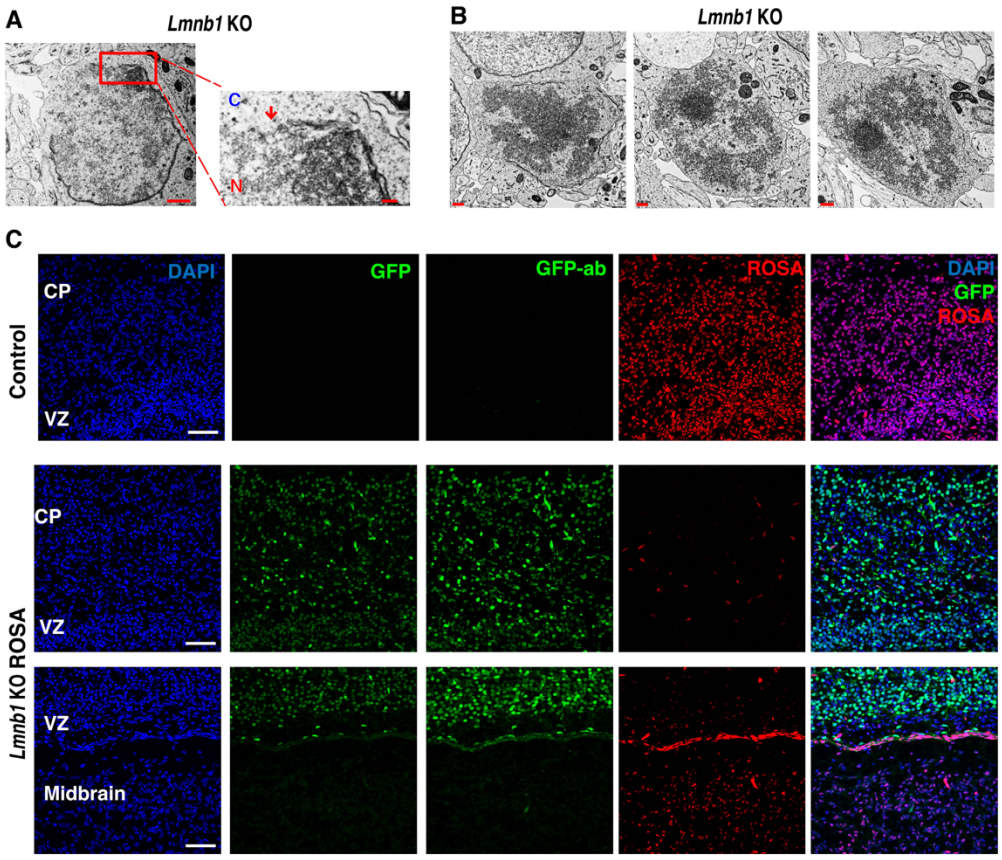

Supplemental Figure 1. Forebrain-specific inactivation of *Lmnb1* in cortical neurons results in nuclear membrane (NM) ruptures and cell death. (*A*) Electron micrograph showing a discontinuity in the nuclear membranes (red arrow) in a cortical plate neuron from an E18.5 *Lmnb1* KO (*Emx1-Cre Lmnb1*$^{fl/fl}$) embryo. N, nuclei; C, cytoplasm. Scale bar on the left, 1 µm; scale bar on the right, 200 nm. (*B*) Electron micrograph showing dead cortical plate neurons (condensed chromatin; no obvious nuclear membranes) in the forebrain of an E18.5 forebrain-specific *Lmnb1* KO embryo. Scale bars, 500 nm. (*C*) Immunofluorescence microscopy of the forebrain of E18.5 control (*Lmnb1*$^{+/+}$ ROSA$^{nT\text{-}nG}$) (top) and *Lmnb1* KO ROSA (*Emx1-Cre Lmnb1*$^{fl/fl}$ ROSA$^{nT\text{-}nG}$) (bottom) embryos with an antibody against GFP (green). Images were recorded from the cortical plate (CP) and ventricular zone (VZ) of the forebrain and the adjacent midbrain. DNA was stained with DAPI (blue). In control mice, the tdTomato reporter from the ROSA$^{nT\text{-}nG}$ transgene fluoresces red and is confined to the nucleus. In forebrain-specific *Lmnb1* KO mice, *Cre* expression in the forebrain activates a GFP reporter and inactivates the tdTomato reporter. Thus, forebrain neurons fluoresce green, whereas neurons in the adjacent midbrain (where *Cre* is absent) fluoresce red. Scale bars, 50 µm.

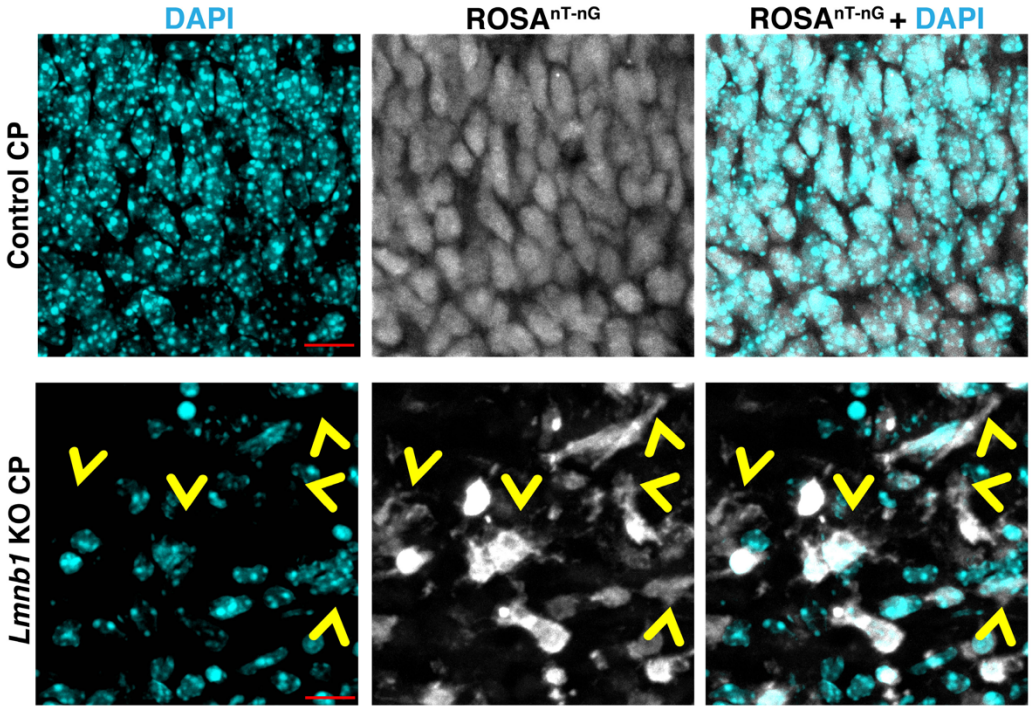

Supplemental Figure 2. Fluorescence micrographs, recorded with a 100× objective, of the cortical plate (CP) from an E18.5 control (*Lmnb1*$^{+/+}$ ROSA$^{nT\text{-}nG}$) embryo (top) and an E18.5 *Lmnb1* KO ROSA (*Emx1-Cre Lmnb1*$^{fl/fl}$ ROSA$^{nT\text{-}nG}$) embryo (bottom). The tdTomato and GFP signals from the ROSA$^{nT\text{-}nG}$ transgene were colored white. DNA was stained with DAPI (cyan). Yellow arrowheads point to *Lmnb1* KO ROSA neurons in which the GFP reporter had escaped into the cytoplasm (a result of nuclear membrane ruptures). Scale bars, 10 μm.

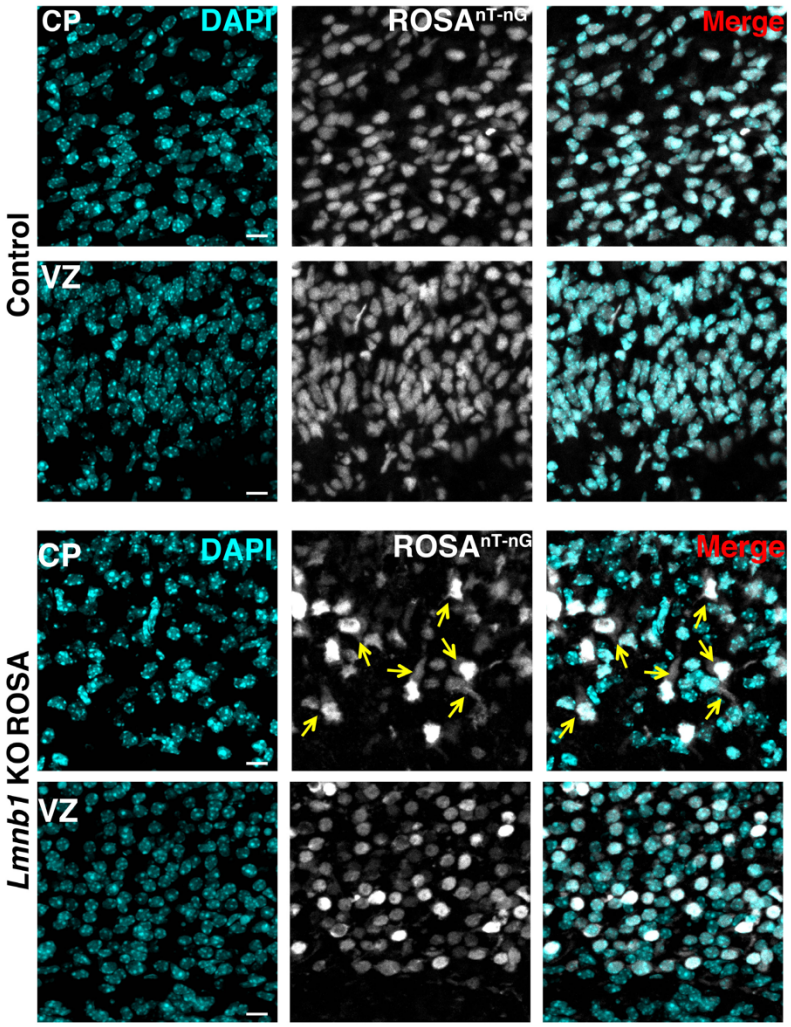

Supplemental Figure 3. Fluorescence micrographs, recorded with a 63× objective, of the cortical plate (CP) and ventricular zone (VZ) neurons from an E18.5 control (*Lmnb1*$^{+/+}$ ROSA$^{nT\text{-}nG}$) embryo (top) and an E18.5 *Lmnb1* KO ROSA (*Emx1-Cre Lmnb1*$^{fl/fl}$ ROSA$^{nT\text{-}nG}$) embryo (bottom). The tdTomato and GFP signals from the ROSA$^{nT\text{-}nG}$ transgene were colored white. DNA was stained with DAPI (cyan). Yellow arrows point to *Lmnb1* KO ROSA neurons in which the GFP reporter had escaped into the cytoplasm (a result of nuclear membrane ruptures). Scale bars, 10 μm.

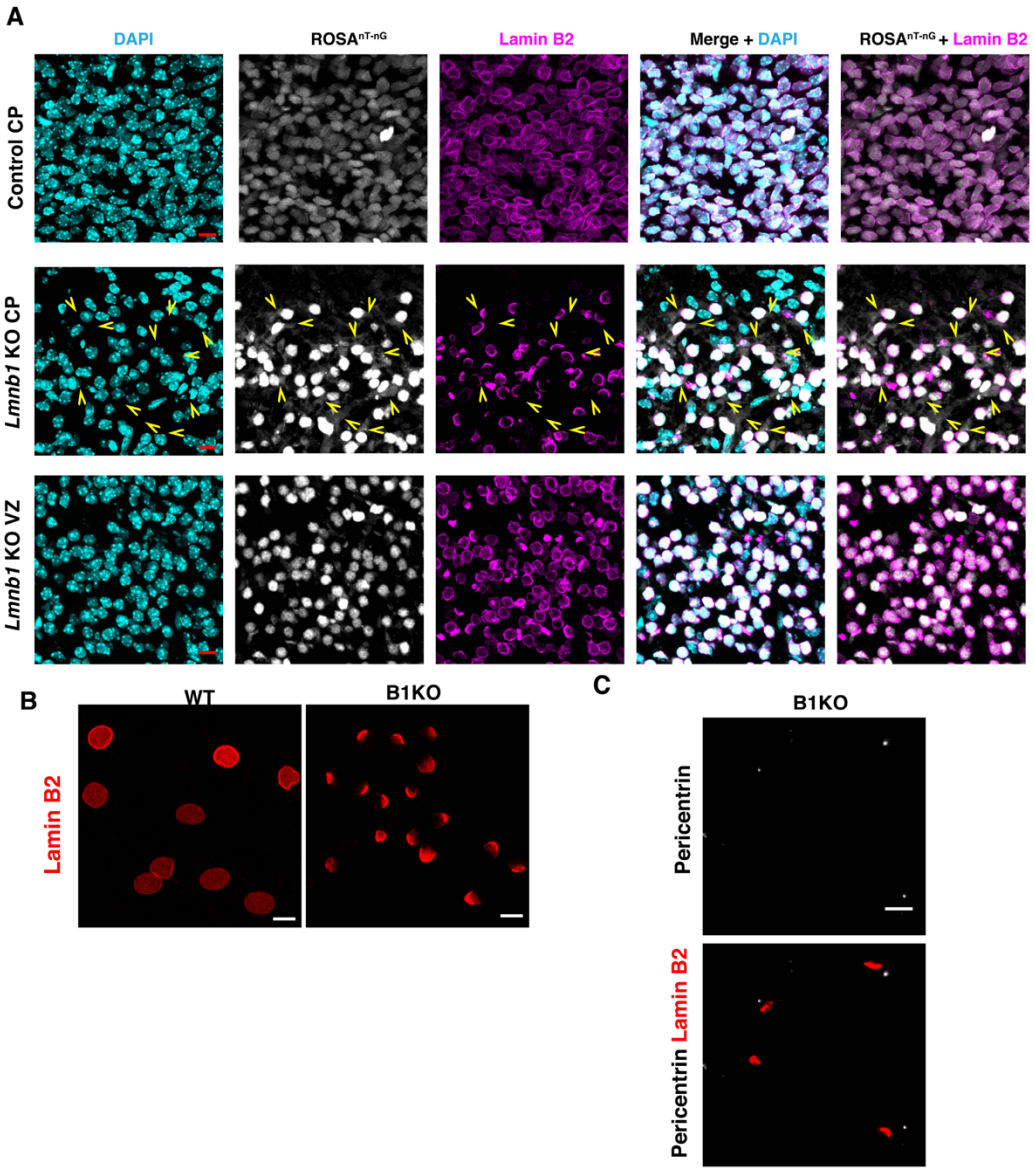

Supplemental Figure 4. Asymmetric distribution of lamin B2 in the cerebral cortex of lamin B1–deficient embryos and lamin B1–deficient neurospheres. (*A*) Fluorescence micrographs revealing an asymmetric distribution of lamin B2 and nuclear membrane (NM) ruptures in the cortical plate (CP) neurons of

forebrain-specific *Lmnb1* knockout embryos. The CP of an E18.5 control embryo (*Lmnb1*$^{+/+}$ ROSA$^{nT\text{-}nG}$) and both the CP and ventricular zone (VZ) neurons of a *Lmnb1* KO ROSA embryo (*Emx1-Cre Lmnb1*$^{fl/fl}$ ROSA$^{nT\text{-}nG}$) were stained with an antibody against lamin B2 (magenta). The tdTomato and GFP signals from the ROSA$^{nT\text{-}nG}$ transgene were colored white. In CP neurons from the control embryo, lamin B2 was distributed evenly along the nuclear rim, and no NM ruptures were observed. In CP neurons from the *Lmnb1* KO ROSA embryo, lamin B2 was distributed asymmetrically, and there were many NM ruptures (escape of GFP into the cytoplasm) (yellow arrowheads). In VZ neurons of the *Lmnb1* KO ROSA embryo, lamin B2 was distributed evenly, and no NM ruptures were observed. Scale bars, 10 μm. (*B*) Immunofluorescence microscopy of WT and B1KO neurons after staining with an antibody against lamin B2 (red). Scale bars, 10 μm. (*C*) Immunofluorescence microscopy of B1KO neurons after staining with antibodies against pericentrin (white) and lamin B2 (red). Scale bars, 10 μm.

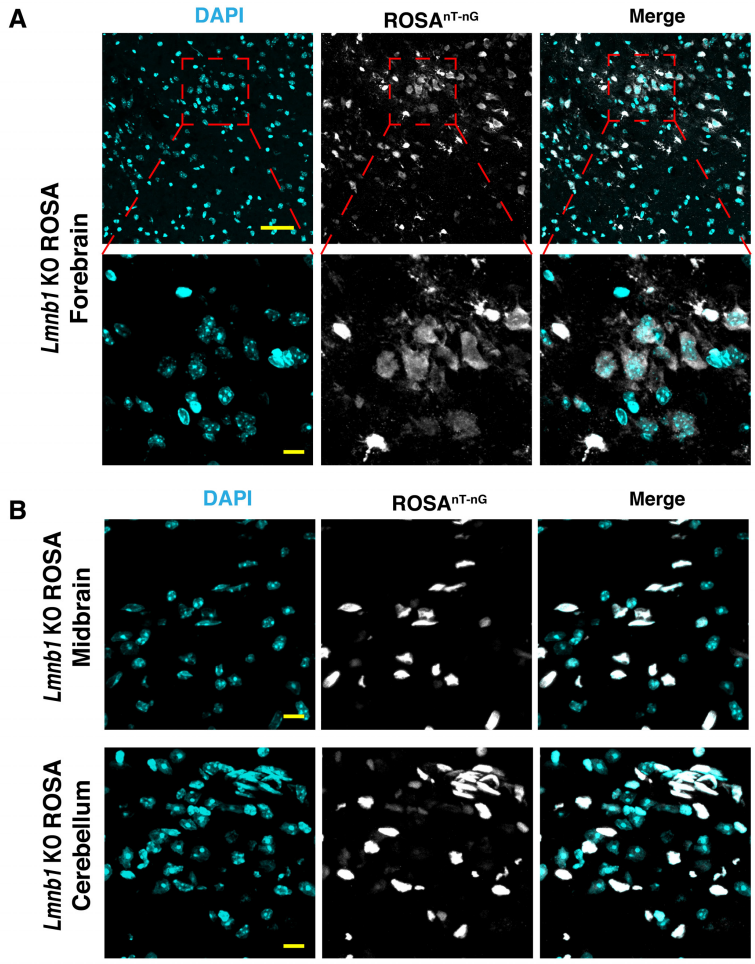

Supplemental Figure 5. Nuclear membrane (NM) ruptures in forebrain-specific *Lmnb1* KO mice. (*A*) Immunofluorescence microscopy images from the forebrain of a 3.5-month-old *Lmnb1* KO ROSA (*Emx1-Cre Lmnb1*$^{fl/fl}$ ROSA^{nT-nG}). In the *Lmnb1* KO ROSA mice, *Cre* expression in the forebrain activates a GFP reporter (white). DNA was stained with DAPI (cyan). (Top) NM ruptures (escape of GFP into the cytoplasm) were observed in the forebrain of *Lmnb1* KO ROSA mice (red box). (Bottom) Higher magnification view of the boxed region. Scale bar top, 50 µm. Scale bar bottom, 10 µm. (*B*) Immunofluorescence microscopy images from the midbrain and cerebellum of a 3.5-month-old *Lmnb1* KO ROSA (*Emx1-Cre Lmnb1*$^{fl/fl}$ ROSA^{nT-nG}) showing that the product of the ROSA^{nT-nG} transgene is completely localized to the nucleus. Scale bar, 10 µm.

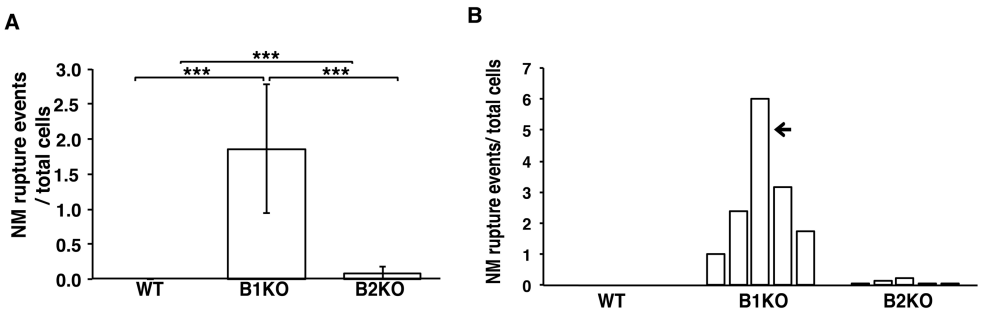

Supplemental Figure 6. Nuclear membrane (NM) ruptures in B1KO and B2KO neurons. (*A*) Numbers of nuclear membrane (NM) rupture events over 50 h of imaging in four of five independent experiments (excluding an outlier experiment in which the number of NM rupture events was 2–3 times more than in the other four experiments). ***$P < 0.0001$. Data from all five experiments, including the outlier experiment, are shown in Fig. 3. (*B*) Bar graph showing numbers of NM rupture events normalized to the total numbers of cells imaged over 50 h of imaging in all five independent experiments. NM rupture events were never observed in WT neurons. The arrow points to the outlier experiment in which higher numbers of NM ruptures were observed in B1KO neurons.

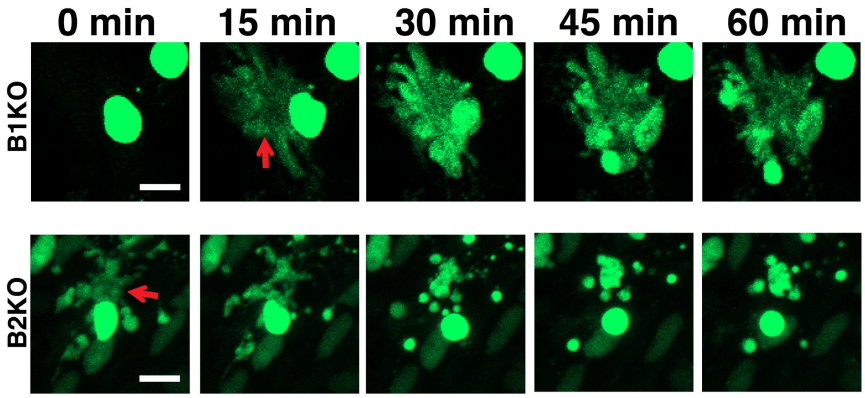

Supplemental Figure 7. Live-cell fluorescence microscopy images at (15-min intervals) of B1KO and B2KO neurons expressing a nuclear-localized green fluorescent protein (NLS-GFP). Red arrows point to a nuclear membrane (NM) rupture (escape of the nuclear-localized GFP into the cytoplasm). Scale bars, 10 μm. In both image sequences, the NM rupture event resulted in cell death.

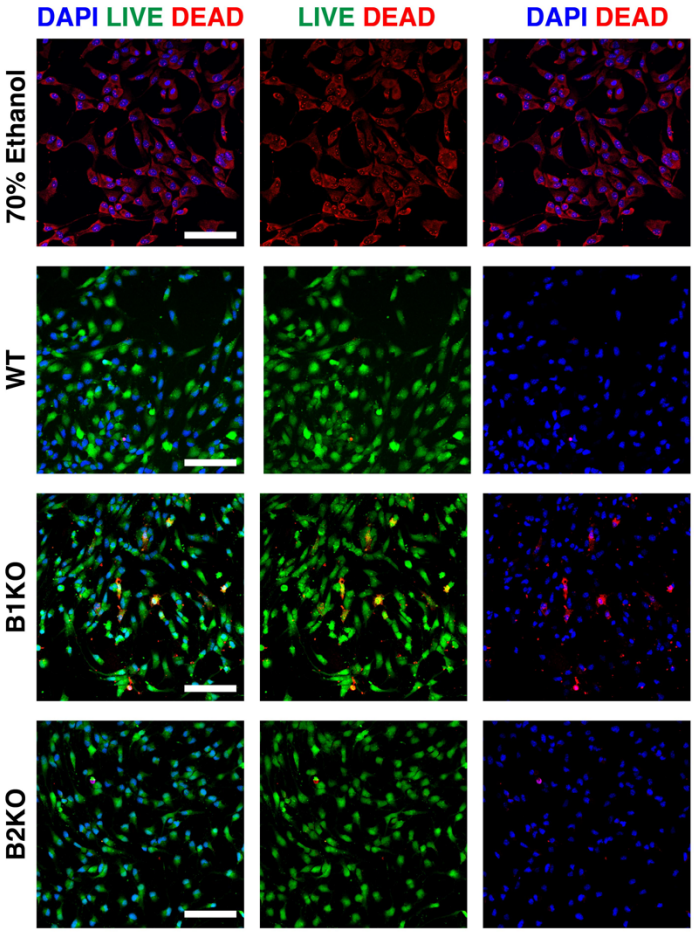

Supplemental Figure 8. Confocal fluorescence microscopy of WT, B1KO, and B2KO differentiated neurons after staining with the LIVE/DEAD vital dye. The LIVE/DEAD dye fluoresces green in live cells and red in dead cells. As a control for dead cells, one batch of neurons was killed with 70% ethanol. Scale bars, 20 μm.

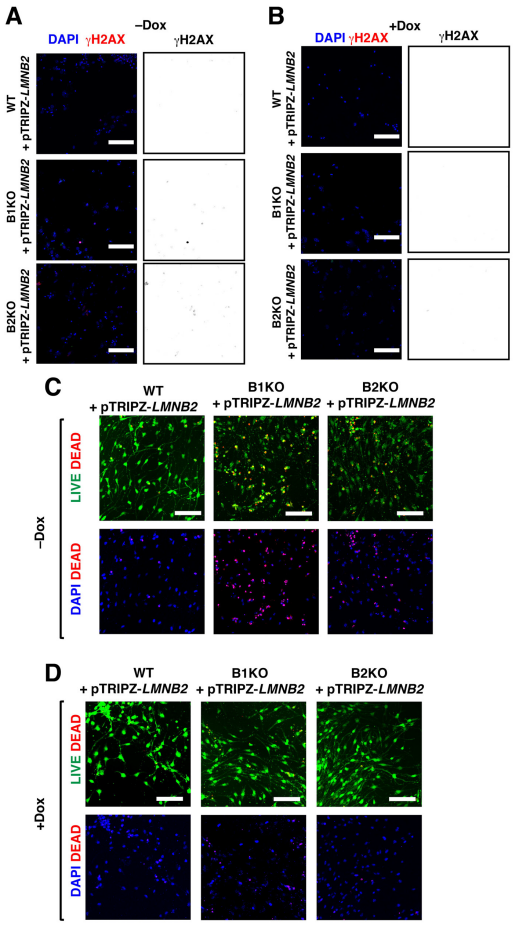

Supplemental Figure 9. Overexpression of lamin B2 in B1KO and B2KO neurons reduces DNA damage and neuronal cell death. (*A–B*) Immunofluorescence microscopy of WT, B1KO, and B2KO neurons that had been transduced with pTRIPZ-*LMNB2* and then incubated in the absence (*A*) or presence (*B*) of Dox for 24 h. The cells were then stained with an antibody against γH2AX (red). DNA was stained with DAPI (blue). Scale bars, 50 µm. Panels on the right show γH2AX staining in black against a white background. (*C–D*) Immunofluorescence microscopy of WT, B1KO, and B2KO neurons that had been transduced with pTRIPZ-*LMNB2* and then incubated in the absence (*C*) or presence (*D*) of Dox for 24 h. The neurons were then stained with the LIVE/DEAD fluorescent vital dye, which fluoresces green in live cells and red in dead cells. DNA was stained with DAPI (blue). The data shown in this figure represents another experiment besides what is shown in Figure 5. Scale bars, 50 µm.

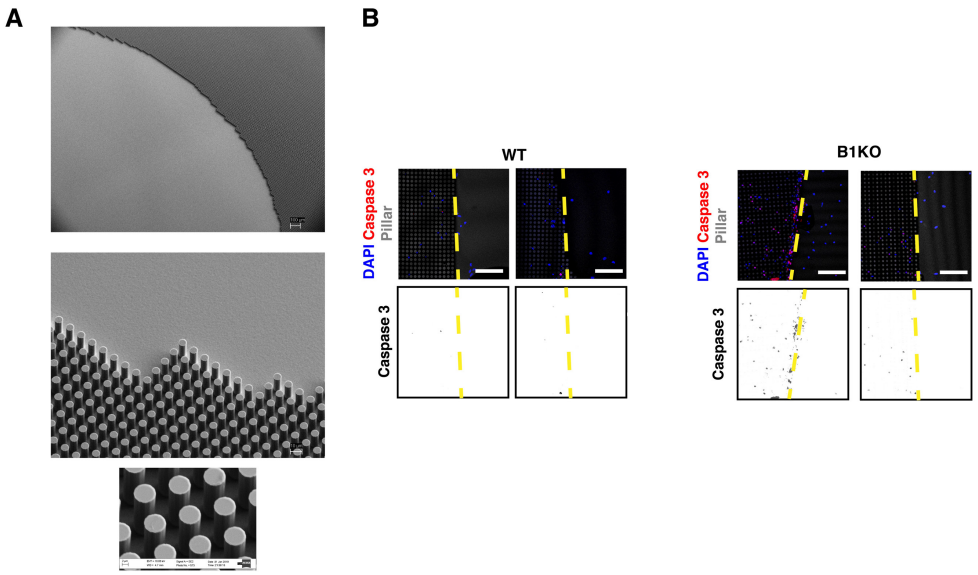

Supplemental Figure 10. Death of B1KO neurons after migrating into a field of silicon pillars (8 μm in diameter; 22 μm in height; spaced 4 μm apart). (*A*) (Top) Scanning electron micrograph of a silicon wafer (with a flat area and a field uniformly spaced silicon pillars). Scale bar, 100 μm. (Middle) Scanning electron micrograph of the silicon wafer at the edge of a field of pillars. Scale bar, 10 μm. (Bottom) A higher magnification image of the uniformly spaced silicon pillars. Scale bar, 2 μm. (*B*) Death in B1KO neurons after migrating into the field of silicon pillars. Cells were plated onto the smooth portion of the silicon wafer and allowed to migrate into the field of pillars. After 24 h, WT and B1KO neurons (two silicon wafers each) were stained with a caspase 3–specific antibody (a marker of apoptotic cell death) and imaged by confocal microscopy. Cell death was observed in B1KO neurons but not in WT neurons after the cells had migrated into the field of pillars. DNA was stained with DAPI (blue). Scale bars, 50 μm. The panels below show caspase 3 staining in black against a white background. The edge of the field of pillars is marked by a yellow dashed line.

Supplementary Tables

Table S1

Gene	Species	Sequences (5′–3′)
Lamin A	Mouse	ggttgaggacaatgaggatga tgagcgcaggttgtactcag
Lamin B1	Mouse	caactgacctcatctggaagaac tgaagactgtgcttctctgagc
Lamin B2	Mouse	aggtgcaggctgagctagag tgattccagatccttcactcg
Lamin C	Mouse	cctatcgaaagctgctggag cctgagactgggatgagtgg
Cyclophilin A	Mouse	tgagcactggagagaaagga ccattatggcgtgtaaagtca
LAP2	Mouse	ggagtgaatcctggtccattg gactgttggaagaggagtagagg

Table S2

Antigen	Antibody	Species	Company	WB	ICC	IHC
Lap2β [27]	Monoclonal	Mouse	BD Transduction Laboratories		1:500	
Lamin B1 [M-20]	Polyclonal	Goat	Santa Cruz Biotech.	1:2000	1:500	
Cleaved Caspase-3	Polyclonal	Rabbit	Cell Signaling Technology		1:1000	1:1000
Lamin A/C	Polyclonal	Goat	Santa Cruz Biotech.		1:500	
Lamin A	Monoclonal	Mouse	Santa Cruz Biotech.	1:2000		
Lamin B2	Monoclonal	Rabbit	Abcam		1:1000	
Lamin B2	Monoclonal	Mouse	Invitrogen		1:50	
Lamin B2	Polyclonal	Rabbit	Proteintech	1:300		
Actin	Polyclonal	Goat	Santa Cruz Biotech.	1:5000		
GFP	Polyclonal	Rabbit	Invitrogen			1:1000
γ-H2AX	Monoclonal	Rabbit	EMD Millipore		1:1000	

Supplementary Movie Legends

Movie S1. B1KO neurons exhibit transient nuclear membrane ruptures. B1KO neurons expressing NLS-GFP (green) were imaged over 18 h. Repeated transient nuclear membrane ruptures were observed (arrow), as judged by the flooding of NLS-GFP into the cytoplasm.

Movie S2. B1KO neurons exhibit frequent nuclear membrane ruptures. B1KO neurons expressing NLS-GFP (green) were imaged over 44 h. Repeated transient nuclear membrane ruptures were observed, as judged by the flooding of NLS-GFP into the cytoplasm. Nuclear membrane ruptures were observed in majority of B1KO neurons.

Movie S3. Migrating B1KO neurons exhibit nuclear membrane ruptures. B1KO neurons expressing NLS-GFP (green) were imaged over 36 h. Some nuclear membrane ruptures occurred in migrating cells (arrows).

Movie S4. B2KO neurons exhibit prolonged, nonhealing nuclear membrane ruptures. B2KO neurons expressing NLS-GFP (green) were imaged over 19 h. A B2KO neuron exhibited nuclear membrane rupture (white arrow). That rupture persisted, without evidence of healing for the entire duration of the movie.

Movie S5. A migrating B2KO neuron with a nuclear membrane rupture. B2KO neurons expressing NLS-GFP (green) were imaged over 18 h. A B2KO neuron (arrow) exhibited a nuclear membrane rupture as it moved across the field of view. The nuclear membrane rupture persisted, without evidence of repair, and the neuron died.

Chapter 4:

Increased Expression of LAP2β, an Inner Nuclear Membrane Protein, Eliminates Nuclear Membrane Ruptures in Nuclear Lamin–Deficient Neurons and Fibroblasts

ABSTRACT

Defects or deficiencies in nuclear lamins cause pathology in many cell types, and recent studies have implicated nuclear membrane (NM) ruptures as a cause of cell toxicity. We previously observed NM ruptures and progressive cell death in the developing brain of lamin B1–deficient mouse embryos. We also observed frequent NM ruptures and DNA damage in nuclear lamin–deficient fibroblasts. Factors modulating susceptibility to NM ruptures remain unclear, but we noted low levels of LAP2β, a chromatin-binding inner NM protein, in fibroblasts with NM ruptures. Here, we explored the apparent link between LAP2β and NM ruptures in nuclear lamin–deficient neurons and fibroblasts, and we tested whether manipulating LAP2β expression levels would alter NM rupture frequency. In cortical plate neurons of lamin B1–deficient embryos, we observed a strong correlation between low LAP2β levels and NM ruptures. We also found low LAP2β levels and frequent NM ruptures in neurons of cultured *Lmnb1*$^{-/-}$ neurospheres. Reducing LAP2β expression in *Lmnb1*$^{-/-}$ neurons with an siRNA markedly increased the NM rupture frequency (without affecting NM rupture duration), whereas increased LAP2β expression eliminated NM ruptures and reduced DNA damage. Consistent findings were observed in nuclear lamin–deficient fibroblasts. Reduced LAP2β expression increased NM ruptures, whereas increased LAP2β expression virtually abolished NM ruptures. Increased LAP2β expression nearly abolished NM ruptures in cells subjected to mechanical stress (an intervention that increases NM ruptures). Our studies showed that increasing LAP2β expression bolsters NM integrity in nuclear lamin–deficient cells and markedly reduces NM rupture frequency.

INTRODUCTION

We recently examined mouse embryonic fibroblasts (MEFs) that were homozygous for knockout

mutations in the three nuclear lamin genes (*Lmnb1, Lmnb2, Lmna*) (1). These "triple-knockout fibroblasts" (TKO MEFs) lacked nuclear blebs but nevertheless had frequent nuclear membrane (NM) ruptures (1). The NM ruptures were associated with increased DNA damage (1). The frequency of NM ruptures in TKO MEFs increased when cells were subjected to mechanical stress (uniaxial stretching) and decreased when cells were subjected to interventions that interfere with the transmission of cytoskeletal forces to the nucleus (1). In follow-up studies, we observed frequent NM ruptures, along with DNA damage and cell death, in migrating neurons within the cortical plate of lamin B1–deficient mouse embryos (2). Cortical plate neurons are particularly susceptible to NM ruptures because neuronal migration subjects the cell nucleus to mechanical stress (2) and because embryonic neurons do not express lamin A or lamin C (3-6). In the studies of TKO MEFs and *Lmnb1*$^{-/-}$ neurons (1, 2), NM ruptures were identified by the escape of a nuclear-localized fluorescent reporter into the cytoplasm.

In our studies of NM ruptures in TKO MEFs (1), the outline of the cell nucleus was visualized with an antibody against the inner nuclear membrane protein LAP2β (lamina-associated polypeptide 2, β isoform). LAP2β contains a transmembrane helix that anchors it to the inner nuclear membrane (7–9), and it interacts, *via* nucleoplasmic LEM (LAP2, emerin, Man1) domains (10, 11), with the DNA-bridging protein BAF (barrier-to-autointegration factor). This LEM–BAF complex is thought to tether chromatin to the nuclear periphery (12). In TKO MEFs, we found, by confocal microscopy, reduced amounts of LAP2β in TKO MEFs with NM ruptures. In those cells, there were also gaps in the distribution of LAP2β along the nuclear rim (1). In TKO MEFs without NM ruptures, LAP2β was distributed evenly along the nuclear periphery (1). In our initial study of TKO MEFs (1), we focused on the impact of mechanical stress on NM ruptures and did not pursue the possibility that LAP2β expression might modulate susceptibility of cells to NM

ruptures.

In the current studies, we investigated the possibility of a link between LAP2β expression and NM ruptures in nuclear lamin–deficient cells. We had two goals. The first was to investigate the potential association between abnormalities in LAP2β expression and distribution and NM ruptures—both in tissues of a nuclear lamin–deficient mouse and in a second nuclear lamin–deficient cell line. We began by studying the developing brain of *Lmnb1*$^{-/-}$ embryos. We reasoned that we would be able to assess LAP2β expression, LAP2β distribution, and NM ruptures in migrating neurons of the cortical plate (where cells are subjected to mechanical stress during neuronal migration) and in the germinal cells of the ventricular zone (where cells have not migrated) (2). We further reasoned that *Lmnb1*$^{-/-}$ embryos would be a useful source of primary neurons for cell culture studies of NM ruptures (2).

Our second goal was to examine whether LAP2β expression levels in nuclear lamin–deficient cells are directly relevant to the susceptibility to NM ruptures. Specifically, we wanted to test the hypothesis that manipulating LAP2β expression levels would change NM rupture frequency. Initially, we were skeptical that we would find any effect of LAP2β expression levels. Earlier studies identified indirect effects of other LEM domain proteins on the *repair* of NM ruptures (12–16), but no one had considered the idea that altering LAP2β expression levels would influence the *frequency* of NM ruptures. Despite our initial skepticism, we tested whether manipulating LAP2β expression would affect the frequency of NM ruptures in TKO fibroblasts and *Lmnb1*$^{-/-}$ neurons. To our surprise, we found that reducing LAP2β expression levels markedly increased the frequency—but not the duration—of NM ruptures. Increasing LAP2β expression virtually abolished NM ruptures.

RESULTS

NM ruptures and LAP2β distribution in cortical neurons of *Lmnb1*-deficient mouse embryos. We bred *Lmnb1*$^{fl/fl}$ mouse embryos (17) harboring the forebrain-specific *Emx1-Cre* transgene (18) and a nuclear-targeted ROSA$^{nT\text{-}nG}$ transgene (2). The ROSA$^{nT\text{-}nG}$ transgene produces a tdTomato fluorescent reporter in the absence of *Cre* and GFP in the presence of *Cre* (Fig. 1*A–B*). In E18.5 *Lmnb1*$^{fl/fl}$ ROSA$^{nT\text{-}nG}$ embryos (where lamin B1 expression is normal), the ROSA$^{nT\text{-}nG}$ reporter was located in the nucleus and LAP2β was distributed evenly along the nuclear rim (Fig. 1*C*). In migrating neurons in the cortical plate of *Emx1-Cre Lmnb1*$^{fl/fl}$ ROSA$^{nT\text{-}nG}$ embryos (where lamin B1 is absent), numerous NM ruptures were present, evident by escape of the fluorescent reporter into the cytoplasm (Fig. 1*D*). Also, the levels of LAP2β were reduced and/or unevenly distributed along the nuclear rim (Fig. 1*B* and *D*). In the germinal cells within the ventricular zone (which are not subjected to stresses of cell migration), we did not observe clear examples of NM rupture (the reporter was largely confined to the nucleus) (Fig. 1*D*). Also, LAP2β expression was robust and distributed evenly along the nuclear rim in ventricular zone cells (Fig. 1*D*). In cortical plate neurons of *Emx1-Cre Lmnb1*$^{fl/fl}$ ROSA$^{nT\text{-}nG}$ embryos, we observed increased amounts of caspase 3, a marker of apoptotic cell death (Fig. 1*E*). Caspase 3 staining was absent in cells of the ventricular zone (Fig. 1*E*).

In 3.5-month-old *Emx1-Cre Lmnb1*$^{fl/fl}$ ROSA$^{nT\text{-}nG}$ mice, LAP2β levels in the cerebral cortex were much lower than in wild-type mice, and the LAP2β was often distributed unevenly along the nuclear rim (*SI Appendix,* Fig. S1*A–B*).

Neurons harvested from the cerebral cortex of *Lmnb1*$^{-/-}$ embryos have frequent NM ruptures and reduced amounts of LAP2β. Neuronal progenitor cells from *Lmnb1*$^{+/+}$ (wild-type;

WT) and *Lmnb1*$^{-/-}$ (lamin B1 knockout; B1KO) were cultured as neurospheres and allowed to differentiate. In WT neurons, there was some variation in LAP2β levels but the protein was always distributed evenly along the nuclear rim. In some B1KO neurons, LAP2β was present in reduced amounts or was distributed unevenly (Fig. 2*A*). The reduced amounts of LAP2β in B1KO neurons may have been due, at least in part, to reduced levels of LAP2β transcripts (Fig. 2*B*). In B1KO neurons with a NM rupture, LAP2β staining was less intense and/or was distributed unevenly along the nuclear rim (Fig. 2*C*). Confocal microscopy revealed that LAP2β distribution in B1KO nuclei was polarized, with disproportionate amounts of LAP2β located on the side of the nucleus closest to the centrosome (*SI Appendix,* Fig. S2).

In cortical plate neurons of E18.5 *Emx1-Cre Lmnb1*$^{fl/fl}$ embryos, both LAP2β and lamin B2 were distributed disproportionately to one side of the nucleus (*SI Appendix,* Fig. S3*A*). LAP2β and lamin B2 were also distributed to one side of the nucleus in cultured B1KO neurons (*SI Appendix,* Fig. S3*B*). To assess the distributions of LAP2β and lamin B2 across the nuclear area, individual nuclei were analyzed uniaxially and the fluorescence intensities of LAP2β and lamin B2 were quantified along the diameter of the cell nucleus in the direction of polarization (*SI Appendix,* Fig. S4*A*). In wild-type neurons, all nuclei had even distributions of LAP2β and lamin B2 (*SI Appendix,* Fig. S4*B*). In the majority of B1KO neurons, LAP2β and lamin B2 were polarized towards the same half of the cell nucleus (*SI Appendix*, Fig. S4*C*).

Knocking down LAP2β expression in B1KO neurons increases NM ruptures. To explore the association between NM ruptures and LAP2β expression, we knocked down LAP2β expression in WT and B1KO neurons with siLAP2β (a *Tmpo*-specific small-interfering RNA). In parallel, neurons were also treated with a control siRNA (siControl). LAP2β transcript levels in siLAP2β-

transfected neurons were reduced by ~50% (Fig. 3*A*), and reduced amounts of LAP2β in the cell nucleus were apparent by immunofluorescence microscopy, consistent with transcript levels (Fig. 3*B*). Reduced LAP2β expression increased numbers of B1KO neurons that exhibited at least one NM rupture during video microscopy (91.8% of 150 siLAP2β-transfected neurons imaged total in 3 independent experiments had at least one NM rupture *vs.* 64.6% of 125 control siRNA–transfected neurons imaged in 3 independent experiments) ($P < 0.0005$; χ^2 test) (Fig. 3*C*). Reduced LAP2β also increased the total number of NM ruptures (502 ruptures in 150 siLAP2β-transfected neurons *vs.* 167 ruptures in 125 control siRNA–transfected neurons) ($P < 0.05$; unpaired Student's *t*-test) (Fig. 3*D*). Of note, knocking down LAP2β expression reduced the time between NM ruptures ($P < 0.0005$; unpaired Student's *t*-test) (Fig. 3*E*) but had little or no effect on NM rupture duration (Fig. 3*F*). Increased numbers of NM ruptures were apparent by confocal microscopy (Fig. 3*G*). The vast majority of neurons with NM ruptures ruptured and repaired during continuous video microscopy (obviating any concerns that apoptotic cells were counted as NM ruptures). The larger numbers of NM ruptures in siLAP2β-transfected B1KO neurons were accompanied by increased apoptotic cell death (as judged by caspase 3 staining) (Fig. 3*H*). Reduced LAP2β expression affected NM rupture frequency only in B1KO neurons. Transfection of WT neurons with siLAP2β resulted in reduced amounts of LAP2β in the cell nucleus by immunofluorescence microscopy (*SI Appendix,* Fig. S5*A*), but we found no NM ruptures in >100 siLAP2β-transfected WT neurons during 20 h of imaging (*SI Appendix,* Fig. S5*B*).

Overexpressing LAP2β abolishes NM ruptures in B1KO neurons. To examine the effect of increased LAP2β expression on NM ruptures, we transduced NLS-GFP–expressing B1KO neurons with a lentivirus encoding a LAP2β-tdTomato fusion protein. The transduced B1KO

neurons were not subjected to drug selection; hence, some cells expressed the fusion protein while others did not. After 48 h, the cells were stained with a LAP2β-specific antibody (to assess total levels of LAP2β) and imaged by confocal microscopy. The binding of the LAP2β antibody (as judged by the ratio of LAP2β pixel intensities to nuclear area) was significantly greater in the LAP2β-tdTomato–transduced cells (n = 85) than in nontransduced cells ($P < 0.0001$; unpaired Student's t-test) (Fig. 4*A*). In the LAP2β-tdTomato–transduced cells, LAP2β staining was detectable along the entire circumference of the nucleus (Fig. 4*B*). In nontransduced cells, LAP2β staining was less intense and was distributed unevenly along the nuclear rim (Fig. 4*B*). LAP2β-tdTomato expression did not alter nuclear shape.

To assess the effect of LAP2β-tdTomato expression on NM integrity, we counted NM ruptures in nontransduced and LAP2β-tdTomato–transduced B1KO neurons (Fig. 4*C*; *SI Appendix,* Movies S1 and S2). By live-cell microscopy, 60.6% of 148 nontransduced B1KO neurons analyzed over 3 independent experiments had at least one NM rupture ($P < 0.0005$; χ^2 test) (Fig. 4*D*). Some of the nontransduced B1KO neurons had more than one rupture (142 NM ruptures were observed in the 148 neurons) ($P < 0.0005$; unpaired Student's t-test) (Fig. 4*E*). In contrast, no NM ruptures were detected in 101 LAP2β-tdTomato–transduced B1KO cells (Fig. 4*D–E*). LAP2β-tdTomato expression protected B1KO neurons from DNA damage (Fig. 4*F–G*). Only 2.4% of 240 LAP2β-tdTomato–transduced B1KO neurons had γH2AX foci in the nucleus, whereas >80% of 156 nontransduced B1KO neurons analyzed had nuclear γH2AX foci ($P < 0.0005$; χ^2 test) (Fig. 4*F*). We assessed γH2AX foci in a mixed population of nontransduced and LAP2β-tdTomato–transduced B1KO neurons; γH2AX foci were rare in 240 LAP2β-tdTomato–expressing B1KO neurons but frequent in 156 nontransduced cells (Fig. 4*G*).

Reducing LAP2β expression in TKO MEFs results in more NM ruptures and cell death. Transfection of WT and TKO MEFs with siLAP2β decreased LAP2β transcript levels by 50–60% (Fig. 5*A*), and microscopy revealed reduced amounts of LAP2β in the nucleus, consistent with the transcript levels (Fig. 5*B*). Reducing LAP2β expression in TKO MEFs increased the percentage of cells with NM ruptures: 27.7% of siLAP2β-transfected TKO MEFs (210 total cells counted in three independent experiments) had NM ruptures, whereas only 16.7% (140 total cells counted in three independent experiments) of control siRNA–transfected cells had a NM rupture ($P = 0.009$; χ^2 test). Some TKO MEFs had more than one NM rupture; we detected 213 NM ruptures in 210 siLAP2β-transfected cells but only 58 ruptures in the 140 control siRNA–transfected cells ($P < 0.05$; unpaired Student's *t*-test) (Fig. 5*C–D*). The duration of NM ruptures in control siRNA–transfected and siLAP2β-transfected TKO MEFs was similar (Fig. 5*E*). In 60 siLAP2β-transfected TKO MEFs with at least one NM rupture, 16 of the cells died during 20 h of imaging whereas the remainder survived, only 1 of 23 control siRNA–transfected TKO MEFs with a NM rupture died ($P = 0.009$; χ^2 test) (Fig. 5*F*). The increased frequency of NM ruptures in siLAP2β-transfected TKO MEFs (Fig. 5*G*) was accompanied by increased DNA damage (25.4% of siLAP2β-transfected TKO MEFs had nuclear γH2AX foci *vs*. only 12.8% of TKO MEFs transfected with the control siRNA) (Fig. 5*H*).

Increased LAP2β expression in TKO MEFs abolishes NM ruptures and reduces DNA damage. We transduced NLS-GFP–expressing TKO MEFs with the LAP2β-tdTomato lentivirus, resulting in a 32.3% increase in LAP2β transcript levels ($P = 0.0079$; unpaired Student's *t*-test) (Fig. 6*A*). We analyzed transduced NLS-GFP–expressing TKO MEFs with high levels of LAP2β-tdTomato expression (cells in the top 10 percentile for both GFP and tdTomato fluorescence).

LAP2β-tdTomato had no effect on nuclear shape. In three independent experiments (>100 cells counted/group), ~24.5% of nontransduced TKO MEFs exhibited one or more NM ruptures *vs*. only 0.85% of LAP2β-tdTomato–transduced cells ($P < 0.0001$; χ^2 test) (Fig. 6*B*). We observed a total of 69 NM ruptures in 141 nontransduced TKO MEFs but only 1 rupture in 103 LAP2β-tdTomato–transduced cells ($P = 0.0055$; unpaired Student's *t*-test) (Fig. 6*C*). The lower number of NM ruptures in LAP2β-tdTomato–transduced TKO MEFs was accompanied by reduced DNA damage. In 50 nontransduced cells, we observed 14 cells with γH2AX foci. In 101 LAP2β-tdTomato–transduced TKO MEFs, we observed only 5 cells with γH2AX foci ($P < 0.0001$; χ^2 test) (Fig. 6*D*).

The fact that increased LAP2β expression prevented NM ruptures in TKO MEFs suggested that increased LAP2β expression bolsters the integrity of nuclear membranes. If this were the case, we reasoned that LAP2β overexpression in TKO MEFs would protect against NM ruptures in the setting of mechanical stress. To test this possibility, we counted NM ruptures in nontransduced and LAP2β-tdTomato–transduced TKO MEFs under static conditions (Fig. 6*E*) and under uniaxial stretching (Fig. 6*F*). As expected (1), stretching nontransduced TKO MEFs increased the frequency of NM ruptures (52.2% of stretched cells *vs*. 17% of cells tested under static conditions) (Fig. 6*E*–*G*). No NM ruptures were detected in LAP2β-tdTomato–expressing TKO MEFs under static conditions (195 cells scored) ($P < 0.0001$; χ^2 test) (Fig. 6*E* and *G*). When the TKO MEFs were subjected to uniaxial stretching, we observed three cells (from a total of 198 cells) with a NM rupture ($P < 0.0001$; χ^2 test) (Fig. 6*F*–*G*). Remarkably, NM rupture frequency in LAP2β-tdTomato–expressing TKO MEFs under *stretching conditions* (3 NM ruptures in 198 cells) was much lower than the NM rupture frequency in nontransduced TKO MEFs under *static conditions* (29 NM ruptures in 172 cells).

DISCUSSION

In earlier studies of TKO MEFs (1), we observed that LAP2β was present in reduced amounts or was abnormally distributed in cells with NM ruptures (1, 19). Initially, we thought that the finding might be inconsequential and simply represented another example of a nuclear envelope protein whose expression pattern was altered by a deficiency of a nuclear lamin (17, 20–25). In the end, however, we investigated this finding further, motivated by the fact that the abnormality in LAP2β distribution was not observed in every TKO fibroblast but was restricted to cells with NM ruptures (1). We hypothesized that LAP2β expression might actually influence the structural integrity of nuclear membranes. Our first goal was to determine if the association of NM ruptures with reduced LAP2β was a peculiarity of TKO MEFs. We began by studying the forebrain of lamin B1–deficient mouse embryos. We had shown previously that lamin B1 deficiency disrupts the migration of neurons to the cortical plate and reduces neuronal survival (2, 17). Neuronal migration depends on nucleokinesis, a process in which the nucleus is pulled by cytoplasmic motors into the leading edge of the cell (26, 27). In the setting of lamin B1 deficiency, we suspected that the forces of nucleokinesis might induce NM ruptures. Indeed, NM ruptures were widespread in lamin B1–deficient cortical plate neurons. Moreover, virtually all cortical plate neurons had low levels of LAP2β and/or gaps or irregularities in LAP2β distribution. In contrast, LAP2β levels and distribution were normal—and NM ruptures were absent—in the germinal cells of the ventricular zone. We also observed frequent NM ruptures, accompanied by low levels of LAP2β and/or gaps in LAP2β distribution, in cultured *Lmnb1*$^{-/-}$ neurons. Thus, the association between NM ruptures and LAP2β abnormalities was not a peculiarity of TKO MEFs.

Our second objective was to determine whether manipulating LAP2β expression would

modulate the frequency of NM ruptures. In both *Lmnb1*$^{-/-}$ neurons and TKO MEFs, knocking down LAP2β expression resulted in more frequent NM ruptures and more DNA damage. Conversely, transducing *Lmnb1*$^{-/-}$ neurons and TKO MEFs with a LAP2β-tdTomato lentivirus virtually abolished NM ruptures. We suspected that higher levels of LAP2β expression bolstered the integrity of nuclear membranes. This suspicion was strongly supported by studies in which TKO MEFs were subjected to mechanical stretching. We found frequent NM ruptures in nontransduced TKO MEFs under static conditions, but the rupture frequency increased markedly when the cells were stretched. In LAP2β-tdTomato–transduced TKO MEFs, NM ruptures were abolished under static conditions and were extremely rare when the cells were stretched.

LEM domain proteins (9) have been implicated in the repair of NM ruptures (12–14, 16). Cytosolic barrier-to-autointegration factor (BAF) binds to chromatin at sites of NM ruptures and leads to rapid binding of several LEM domain proteins but not LAP2β (13, 16). LEMD2 binding to sites of NM ruptures was prolonged and led to recruitment of ESCRT-III nuclear membrane repair proteins (16). Recently, Young *et al.* (12) examined the *duration* of NM ruptures in a human osteosarcoma cell line in which lamin B1 expression had been knocked down with a shRNA. Depleting BAF—or depleting emerin or LEMD2—in those cells prolonged the duration of NM ruptures. In our studies, knocking down LAP2β expression in *Lmnb1*$^{-/-}$ neurons and TKO MEFs increased NM rupture *frequency* without affecting NM rupture *duration*. The observation that LAP2β expression levels did not alter NM rupture duration could relate to the fact that LAP2β, unlike other LEM domain proteins, did not associate with BAF at sites of NM ruptures in NIH3T3 cells (13, 16).

The fact that LAP2β expression prevented NM ruptures in TKO MEFs in response to

mechanical stretching suggested that LAP2β, either by itself or by associating with BAF and nuclear chromatin, bolsters the integrity of nuclear membranes in nuclear lamin–deficient cells. Our findings provide fresh insights into factors that modulate NM rupture frequency in nuclear lamin–deficient cells, but they also pose new questions. For example, does the protection against NM ruptures by LAP2β require its LEM domains? Would overexpression of other LEM domain proteins (*e.g.*, MAN1, emerin, LEMD2) also reduce NM rupture frequency? Would overexpression of other NM proteins—even those without LEM domains or chromatin-binding properties—influence NM rupture frequency? All of these questions need to be addressed in future studies.

The most important and most surprising discovery in the current studies is that a LAP2β-tdTomato fusion protein prevents NM ruptures in *Lmnb1*$^{-/-}$ neurons and TKO MEFs. The *Lmnb1*$^{-/-}$ neurons express lamin B2 and extremely low levels of lamins A/C (3–5). Whether the ability of the LAP2β-tdTomato to prevent NM ruptures in *Lmnb1*$^{-/-}$ neurons depends on the expression of the remaining nuclear lamins in those cells is unknown. Also, we would point out again here [as we have in the past (28)] that the TKO MEFs that we created contained the original *Lmna* knockout allele from Sullivan *et al.* (24). That knockout allele yields low amounts of an internally truncated lamin A that lacks amino acid sequences encoded by exons 8–11 (29). Those sequences have been reported to mediate interactions with LEM domain proteins (29). Thus far, we have not tested whether the capacity of the LAP2β-tdTomato fusion protein to abolish NM ruptures in TKO MEFs requires the expression of the internally truncated lamin A. These issues also need to be investigated in future studies.

MATERIALS AND METHODS

Mouse studies. Forebrain-specific *Lmnb1* knockout mice harboring a *ROSA*$^{nT\text{-}nG}$ fluorescent reporter (*Emx1-Cre Lmnb1*$^{fl/fl}$ ROSA$^{nT\text{-}nG}$) were generated as described (2). Mice were fed a chow diet and housed in a virus-free barrier facility with a 12-h light-dark cycle. All mouse studies were carried out according to the *Guide for the Care and Use of Laboratory Animals* of the National Institutes of Health. Animal protocols were reviewed and approved by the Animal Research Committee of the University of California, Los Angeles.

Immunohistochemistry. Mouse tissues were prepared for immunohistochemical studies as described (30). Adult and embryonic brains were fixed in 4% paraformaldehyde in phosphate-buffered saline (PBS) for 2 h at room temperature; incubated in 30% sucrose in PBS at 4°C overnight; and then frozen in O.C.T. (Tissue-Tek, Sakura Finetek). Sections (10-μm-thick) were fixed for 5 min in 4% paraformaldehyde or ice-cold methanol, followed by five dips in acetone and permeabilization with 0.1% Tween-20. Background staining with mouse antibodies was reduced with the Mouse-on-Mouse Kit (Vector Laboratories, Burlingame, CA). Tissue sections were blocked with 2.5% horse serum for 1 h at room temperature and incubated overnight at 4°C with primary antibodies at the dilutions indicated in Table S2. Alexa Fluor 488– and Alexa Fluor 568–conjugated secondary antibodies (Molecular Probes, Invitrogen, Carlsbad, CA) were used at a 1:2000 dilution; DyLight 649–conjugated streptavidin (Vector Laboratories) was used at 5 μg/ml. Following DAPI staining, sections were mounted with Prolong Gold antifade (Invitrogen), and images were recorded with a Zeiss LSM700 laser-scanning microscope with Plan Apochromat 20×/0.80 objective (air) or Plan Apochromat 100×/1.40 oil-immersion objectives. Images along the *z*-axis were processed by Zen 2010 software (Zeiss).

Cell Culture Models. Neuronal progenitor cells (NPCs) from E13.5 mouse embryos (derived from intercrosses of *Lmnb1*$^{+/-}$ mice) were used to generate *Lmnb1*$^{+/+}$ (wild-type; WT) and *Lmnb1*$^{-/-}$ (lamin B1 knockout; B1KO) neurospheres. Explants from the cerebral cortex were placed in DMEM/F-12 medium (Corning) and dissociated with TrypLE Select (Gibco); the NPCs were resuspended in DMEM/F-12 (Corning). Neurospheres were generated by culturing NPCs in DMEM/F-12 medium containing 2% B-27 Supplement (ThermoFisher), 100 U/ml penicillin, and 100 μg/ml streptomycin at 37°C in 5–7% CO_2. Neurospheres were supplemented with 3 μl of a heparin-EGF-FGF mixture for every ml of medium. Briefly, fibroblast growth factor (FGF) resuspended in PBS with 0.1% bovine serum albumin (BSA; Sigma) was mixed with embryonic growth factor (EGF) (ThermoFisher) that had been resuspended in PBS containing 10% BSA. The EGF and FGF solution was diluted in DMEM/F-12 (Corning) and mixed with heparin sodium salt (Sigma-Aldrich) that had been resuspended in DMEM/F-12.

We also transduced *Lmnb1*$^{+/+}$ and *Lmnb1*$^{-/-}$ neurons with a lentivirus encoding a mouse LAP2β-tdTomato fusion protein. To create the LAP2β-tdTomato fusion protein, the FUtdTW plasmid (#22478; Addgene) was digested with *Bam*HI and *Xba*I and gel-purified. A *Tmpo* cDNA was amplified from mouse cDNA with the CloneAMP HiFi PCR Kit (Takara Bio), forward primer 5′-ACGAGATGCCGGAGTTCCTAGAG-3′, and reverse primer 5′-CAATGCAGCACTAACTTTACTGAGGTG-3′. The *Tmpo* insert was purified with UltraClean15 (Qiagen; Germantown, MD) and introduced into the FUtdTW vector with the InFusion Cloning Kit (Takara Bio). The integrity of the plasmid encoding the LAP2β-tdTomato fusion was documented by DNA sequencing. Packaging of the lentivirus and cell transductions were performed by UCLA's Vector Core.

Triple-knockout (TKO) MEFs (*Lmna*$^{-/-}$ *Lmnb1*$^{-/-}$ *Lmnb2*$^{-/-}$) were created by Jung *et al.* (28)

by incubating *Lmna*$^{-/-}$*Lmnb1*$^{fl/fl}$*Lmnb*$^{fl/fl}$ MEFs with a *Cre* adenovirus. They also generated TKO keratinocytes. Jung *et al.* (28) emphasized that their TKO cells were generated with the first *Lmna* knockout allele created by Sullivan *et al.* (24). Jahn *et al.* (29) discovered that the *Lmna* knockout allele yielded *Lmna* transcripts with an in-frame deletion of sequences derived from exons 8–11. This mutant *Lmna* transcript resulted in the production of an internally truncated lamin A protein lacking several domains important for protein interactions, including interactions of lamin A with LEM domain proteins (29). Consistent with the report by Jahn and coworkers (29), Jung *et al.* (28) documented, by western blotting and immunohistochemistry, low levels of the internally truncated lamin A in their TKO cells. Subsequently, the properties of the TKO MEFs produced by Jung *et al.* (28) were studied by Chen *et al.* (1). As part of the latter studies, TKO MEFs were transduced with a lentiviral vector encoding a nuclear-localized GFP (NLS-GFP) (31). NLS-GFP–expressing TKO MEFs did not have nuclear blebs but displayed a high frequency of NM ruptures (1). In the current studies, we transduced the NLS-GFP–expressing TKO MEFs with the LAP2β-tdTomato lentivirus described earlier.

Neuronal Differentiation. Cultured neurospheres were removed with polyethylene pipets (Fisher) and pipetted into a single drop of laminin (Sigma-Aldrich) on poly-L-ornithine–coated plates. Neurospheres were allowed to settle for 30 min at 37°C and then incubated in DMEM/F-12 containing 2% B-27 Supplement, 100 U/ml penicillin, and 100 μg/ml streptomycin. Neurospheres were allowed to differentiate for up to 30 days.

Immunocytochemistry. Neurons that had been differentiated on coverslips were fixed with 4% paraformaldehyde in PBS or ice-cold methanol, dipped once in acetone, and permeabilized with 0.2% Triton. The fixed cells were then stained with antibodies listed in Table S2 and processed for confocal immunofluorescence microscopy (32). Confocal images were recorded with either a

Zeiss LSM700 laser-scanning microscope as described earlier or with a Zeiss LSM800 laser-scanning microscope with a 20×/0.80 objective (air). Images along the *z*-axis were processed with Zen 2010 or Zen Blue 2.3 software (all from Zeiss). All images shown in this paper are maximum intensity projections of *z*-stacks.

Quantitative RT-PCR. RNA was isolated from undifferentiated and differentiated neurospheres, treated with DNase I (Ambion), and reverse-transcribed with random primers, oligo(dT), and SuperScript III (Invitrogen). qPCR reactions were performed on a 7900 Fast Real-Time PCR system (Applied Biosystems) with SYBR Green PCR Master Mix (Bioline). Transcript levels were determined using the comparative cycle threshold method and normalized to levels of cyclophilin A transcripts. Primers are listed in Table S1.

siRNA transfections. In some studies, neurospheres that had been differentiated for 5 days were transfected with a MISSION esiRNA (endoribonuclease prepared siRNA) against mouse *Tmpo* (MilliporeSigma) (sequence in Table S3) with MISSION siRNA Transfection Reagent (MilliporeSigma). MEFs were allowed to adhere before being transfected with the esiRNA and transfection reagent.

Image Analysis. To quantify LAP2β fluorescence intensity in *Lmnb1*$^{-/-}$ neurons that had been transduced with the LAP2β–tdTomato lentivirus, cells were allowed to differentiate for 48 h and then fixed and processed for immunocytochemistry as described earlier. The fixed cells were stained with an antibody against LAP2β (*SI Appendix*, Table S2). Images were recorded with a Zeiss LSM800 laser-scanning microscope with a 20×/0.80 objective (air) and processed with Zen 2010 or Zen Blue 2.3 software (all from Zeiss). All images were maximum intensity projections of *z*-stacks. Images were exported into ImageJ (https://imagej.nih.gov/ij), and fluorescence

intensity was normalized to nuclear area (mm^2)

To quantify polarization of LAP2β and lamin B2, image stacks of wild-type and *Lmnb1*$^{-/-}$ neurons were analyzed using Zen software (Zeiss). Cells were stained with antibodies against lamin B2 and LAP2β (*SI Appendix,* Table S2), and DNA was stained with DAPI. Individual nuclei (defined by DAPI) were boxed with the Zen Profile Function (*SI Appendix*, Fig. S4*A*). The distribution of LAP2β and lamin B2 fluorescent signals were measured and plotted along the diameter of the cell nucleus in the direction of polarization. If the signal intensity of LAP2β or lamin B2 was higher on one side of the nucleus (relative to the midpoint of the diameter of the nucleus), they were considered polarized.

To quantify numbers of γH2AX foci in cell nuclei, cells were stained with an antibody against γH2AX (*SI Appendix,* Table S2) and DNA was stained with DAPI. Individual nuclei, defined by DAPI staining, were categorized as either having or lacking γH2AX foci.

Live-cell Imaging. Neurospheres were plated on a poly-L-ornithine–coated 6-well plate containing 2-mm glass wells (MatTek), and MEFs were plated on an uncoated 6-well plate containing 2-mm glass wells. Live-cell imaging was performed with a Zeiss LSM 800 confocal microscope equipped with a Plan Apochromat 20×/0.80 objective at 37°C with 5% CO_2 (maintained with TempModule S1 CO_2 Module S1 from Zeiss). *Z*-stacks were acquired from fluorescence and transmission channels. Image sequences were analyzed with Zen Blue 2.3 software (Zeiss) with linear adjustments applied uniformly to the entire image. Images were reconstructed and displayed as maximum intensity projections. Nuclear membrane ruptures in interphase cells were identified by escape of NLS-GFP into the cytoplasm. Even in cells with high levels of NLS-GFP expression, NLS-GFP was confined to the nucleus. Video microscopy images

were recored every 5 min or every 10 min, making it unlikely that we avoid detection of NM ruptures.

Flow Cytometry. Cells were sorted in the UCLA Jonsson Comprehensive Cancer Center (JCCC) and the Center for AIDS Research Flow Cytometry Core Facility on a FACSAria I(II) High-Speed Cell Sorter using a 488-nm blue laser (to sort for cells with NLS-GFP) and a 633-nm red laser to sort for cells transduced with the LAP2β-tdTomato lentivirus.

Cell Stretching. Stretching MEFs on polydimethylsiloxane (PDMS) membranes was performed as described (33). Cells were seeded on flexible PDMS membranes (1-mm-thick). The membranes were stretched 5 mm at 0.5 Hz for 2 h.

Statistical Analyses. Statistical analyses were performed with GraphPad QuickCalcs (www.graphpad.com). The percentages of cells with NM ruptures or γH2AX foci were analyzed with a χ^2 test. Differences in ratios of NM ruptures over the total number of cells imaged were analyzed with an unpaired Student's *t*-test.

Figures and Figure Legends

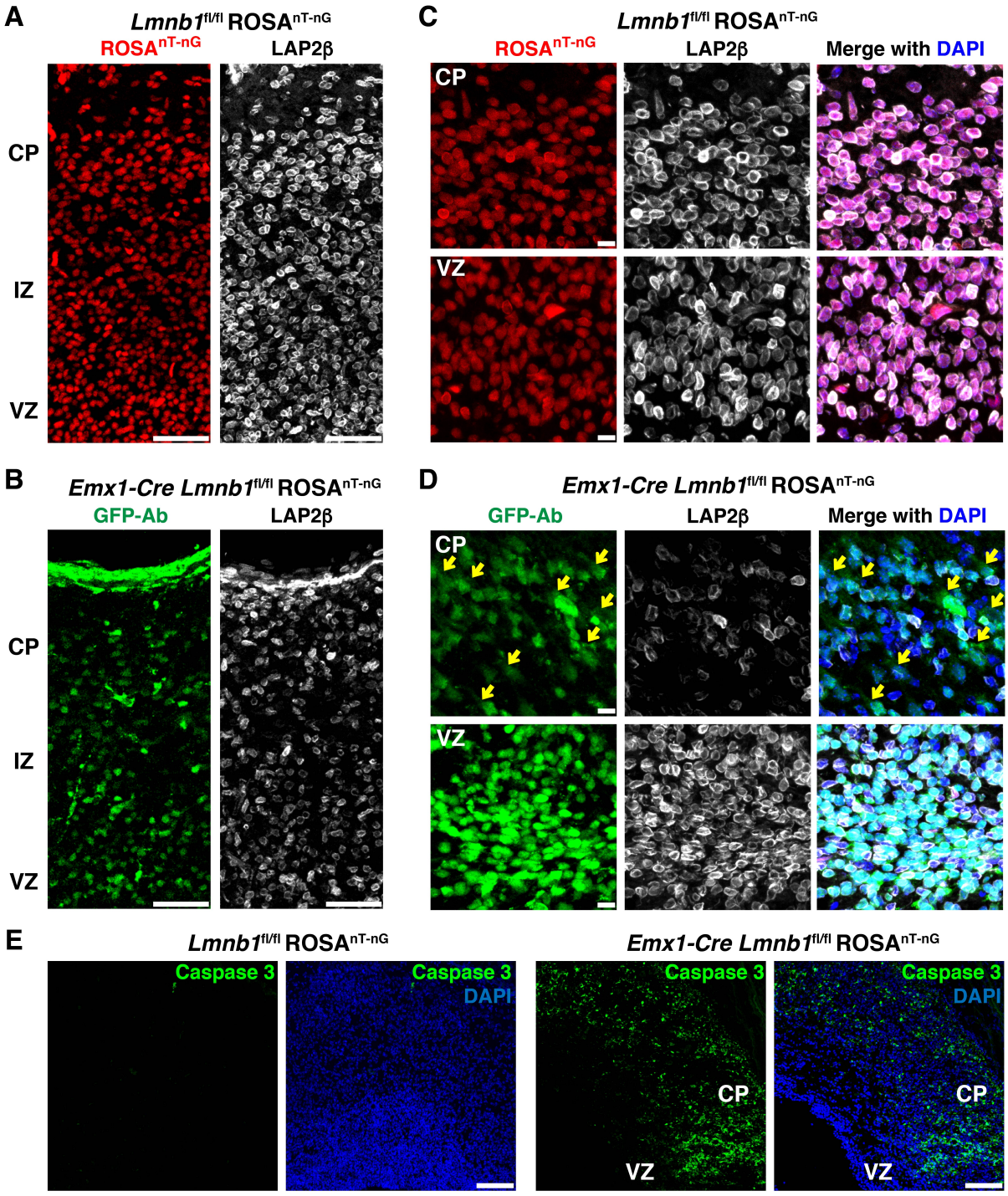

Fig. 1. Forebrain-specific inactivation of *Lmnb1* results in reduced neuronal cell density, reduced LAP2β expression, and nuclear membrane (NM) ruptures. (*A–B*) Fluorescence microscopy images

of the cerebral cortex of E18.5 *Lmnb1*$^{fl/fl}$ ROSA$^{nT\text{-}nG}$ (*A*) and *Emx1-Cre Lmnb1*$^{fl/fl}$ ROSA$^{nT\text{-}nG}$ (*B*) mouse embryos. The ROSA$^{nT\text{-}nG}$ transgene produces a nuclear-targeted tdTomato reporter in the absence of *Cre* and a nuclear-targeted GFP in the presence of *Cre*. tdTomato is colored red; GFP is colored green. Sections were stained with antibodies against the inner nuclear membrane protein LAP2β (white) and GFP (green). Scale bars, 50 μm. (*C–D*) Higher-magnification images of cortical plate (CP) neurons and ventricular zone (VZ) cells in E18.5 *Lmnb1*$^{fl/fl}$ ROSA$^{nT\text{-}nG}$ (*C*) and *Emx1-Cre Lmnb1*$^{fl/fl}$ ROSA$^{nT\text{-}nG}$ (*D*) mouse embryos. DNA was stained with DAPI (blue). Yellow arrows point to NM ruptures in CP neurons in the *Emx1-Cre Lmnb1*$^{fl/fl}$ ROSA$^{nT\text{-}nG}$ embryo. CP neurons with NM ruptures exhibited reduced levels of LAP2β and uneven LAP2β distribution along the nuclear rim. LAP2β distribution was normal in VZ cells of *Emx1-Cre Lmnb1*$^{fl/fl}$ ROSA$^{nT\text{-}nG}$ embryos, and the fluorescent reporter was largely confined to the nucleus. The VZ contains dividing cells; consequently, low levels of GFP were detected in the cytoplasm of some cells. Scale bars, 10 μm. (*E*) Immunofluorescence microscopy of the cerebral cortex in E18.5 *Lmnb1*$^{fl/fl}$ ROSA$^{nT\text{-}nG}$ and *Emx1-Cre Lmnb1*$^{fl/fl}$ ROSA$^{nT\text{-}nG}$ mouse embryos after staining sections with an antibody against caspase 3 (a marker of apoptotic cell death; green). Caspase 3 was confined to CP neurons and was absent from cells of the VZ. DNA was stained with DAPI (blue). Scale bars, 100 μm.

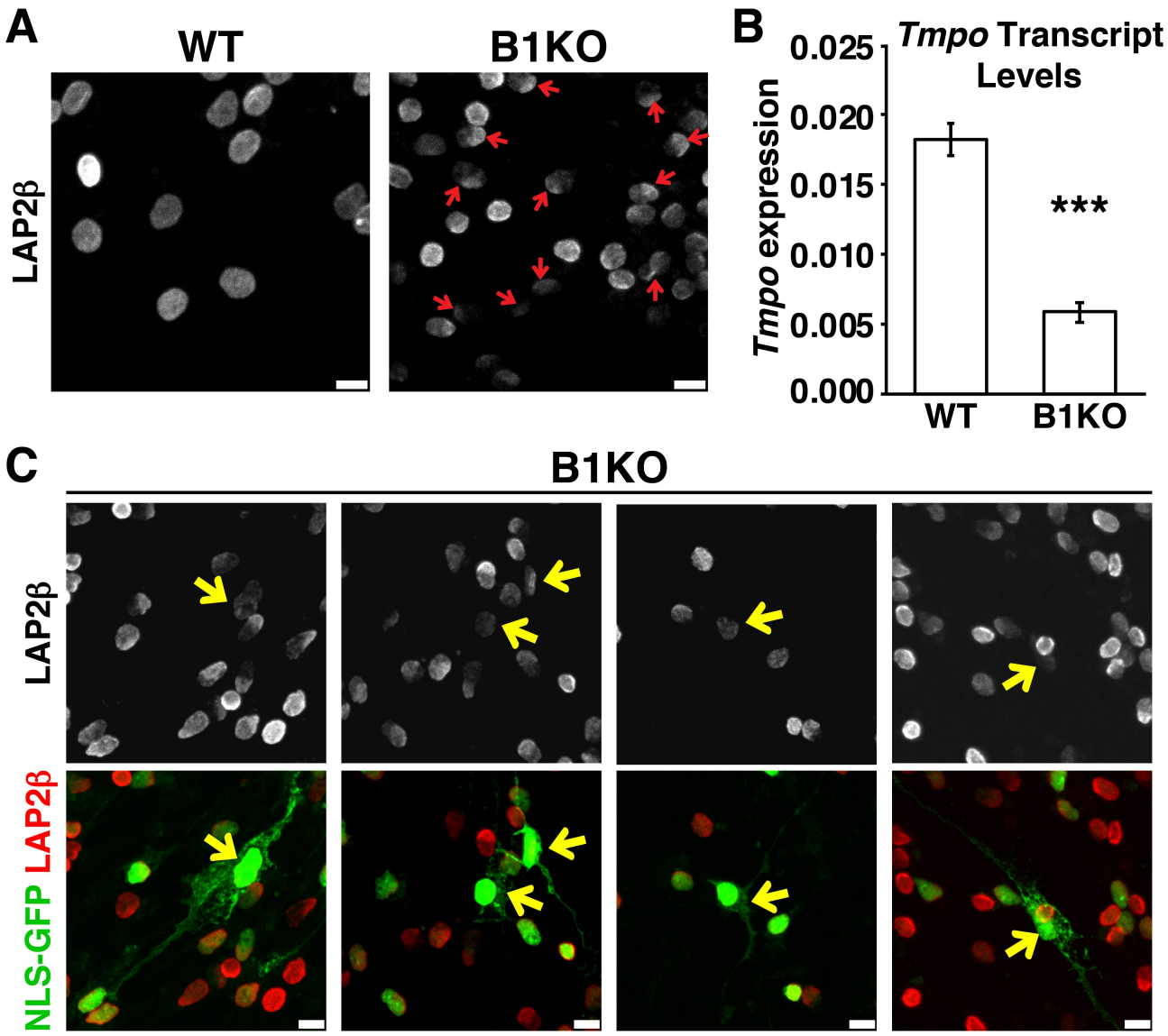

Fig. 2. LAP2β expression in *Lmnb1*$^{-/-}$ (lamin B1 knockout; B1KO) embryos. (*A*) Immunofluorescence microscopy of *Lmnb1*$^{+/+}$ (wild-type; WT) and *Lmnb1*$^{-/-}$ (B1KO) neurons after staining cells with an antibody against LAP2β (white). Red arrows point to B1KO neurons with low levels of LAP2β and/or abnormally distributed LAP2β along the nuclear rim. Scale bars, 10 μm. (*B*) Transcript levels for *Tmpo* (the gene for LAP2β) in WT and B1KO neurons. Neurons had been differentiated in culture for 48 h. Transcript levels were normalized to *Ppia* transcripts. Bar graph shows mean ± SEM; $n = 3$ independent experiments. ***$P < 0.0005$; unpaired Student's

t-test. (*C*) Immunofluorescence microscopy of B1KO neurons that expressed a nuclear-localized GFP (NLS-GFP, green) after staining the cells with an antibody against LAP2β. In the top row, LAP2β is white; in the bottom row, LAP2β is red. Yellow arrows point to neurons with a nuclear membrane (NM) rupture. LAP2β levels were low in neurons with a NM rupture. Scale bars, 10 μm.

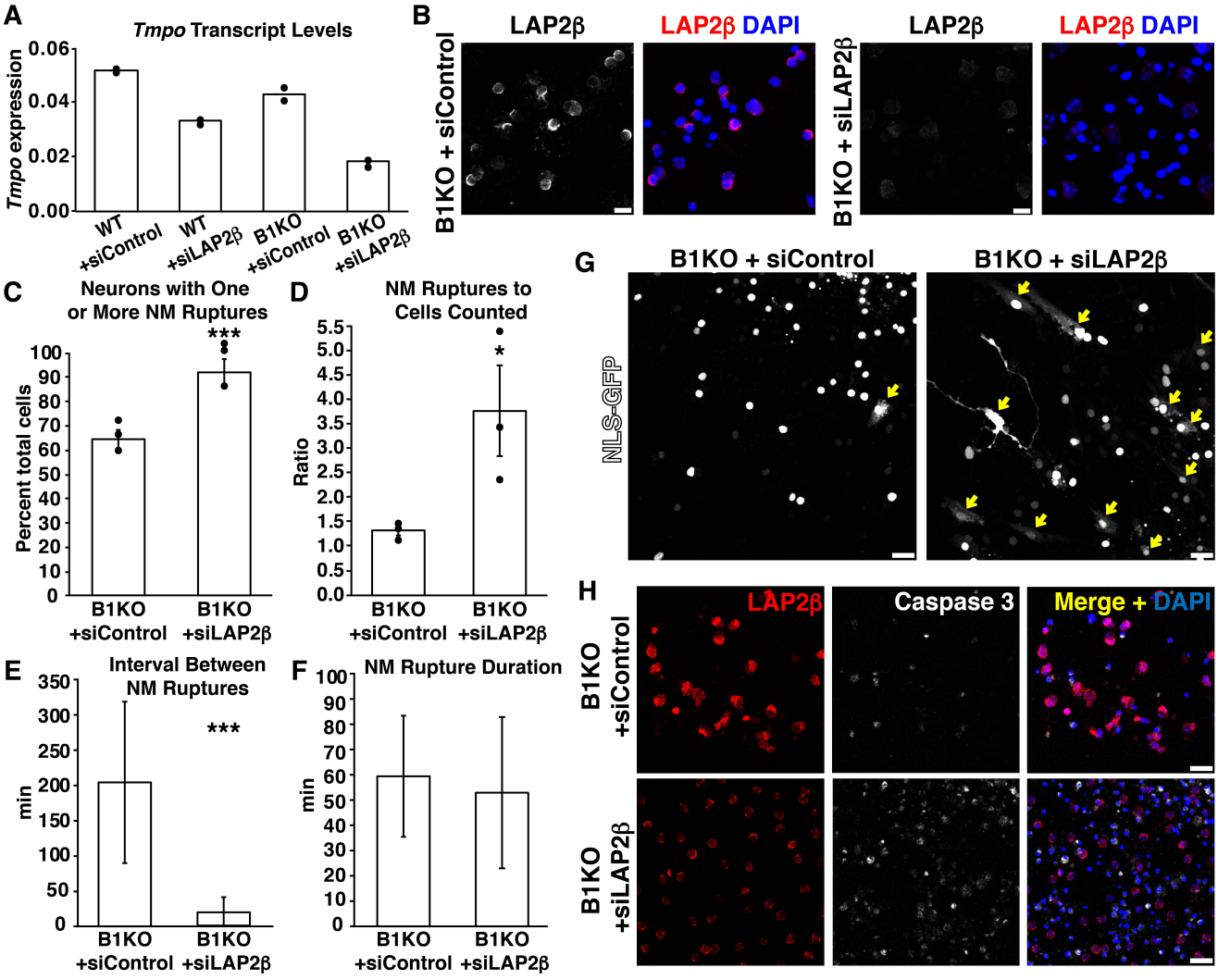

Fig. 3. Reducing LAP2β expression in lamin B1–deficient (B1KO) neurons with siLAP2β (a small-interfering RNA against *Tmpo*) increases nuclear membrane (NM) ruptures and results in more cell death. (*A*) Transcript levels for *Tmpo* in *Lmnb1*$^{+/+}$ (wild-type; WT) and B1KO neurons that had been transfected with siLAP2β or a control siRNA (siControl). Bar depicts the mean in two experiments; dots show results in two independent experiments; transcript levels were normalized to *Ppia* transcripts. Neurons were examined 24 h after transfections. (*B*) Confocal micrographs of B1KO neurons transfected with siLAP2β or siControl. Neurons were stained with an antibody against LAP2β (white in the left panels; red in the merged image). DNA was stained

with DAPI (blue). Scale bars, 10 μm. (*C*) Percentages of siLAP2β- or siControl-transfected B1KO neurons with a NM rupture. ***$P < 0.0005$; χ^2 test. Mean ± SEM; $n = 3$ independent experiments; 20 h of imaging/experiment. Dots depict percentages in three independent experiments. In three independent experiments, a total of 150 siLAP2β-transfected neurons and 125 control siRNA–transfected neurons were analyzed. (*D*) Ratio of the total number of NM ruptures to the number of neurons counted. Dots depict ratios in three independent experiments. *$P < 0.05$; unpaired Student's *t*-test. In three independent experiments, a total of 150 siLAP2β-transfected neurons and 125 control siRNA–transfected neurons were analyzed. (*E–F*) Bar graphs depict the mean time between NM ruptures (*E*) and the mean duration of NM ruptures (*F*) in siLAP2β- or siControl-transfected B1KO neurons (mean ± SD; >35 NM ruptures analyzed/group). ***$P<0.0005$; unpaired Student's *t*-test. (*G*) Confocal micrographs of siLAP2β- or siControl-transfected B1KO neurons that expressed NLS-GFP (white). Larger numbers of NM ruptures (evident by escape of GFP into the cytoplasm and/or sudden loss of GFP fluorescence within the cell nucleus; yellow arrows) were observed in siLAP2β-transfected B1KO neurons. Scale bars, 25 μm. (*H*) Confocal micrographs of siLAP2β- or siControl-transfected B1KO neurons after staining with antibodies against LAP2β (red) and caspase 3 (white); DNA was stained with DAPI (blue). Scale bars, 20 μm.

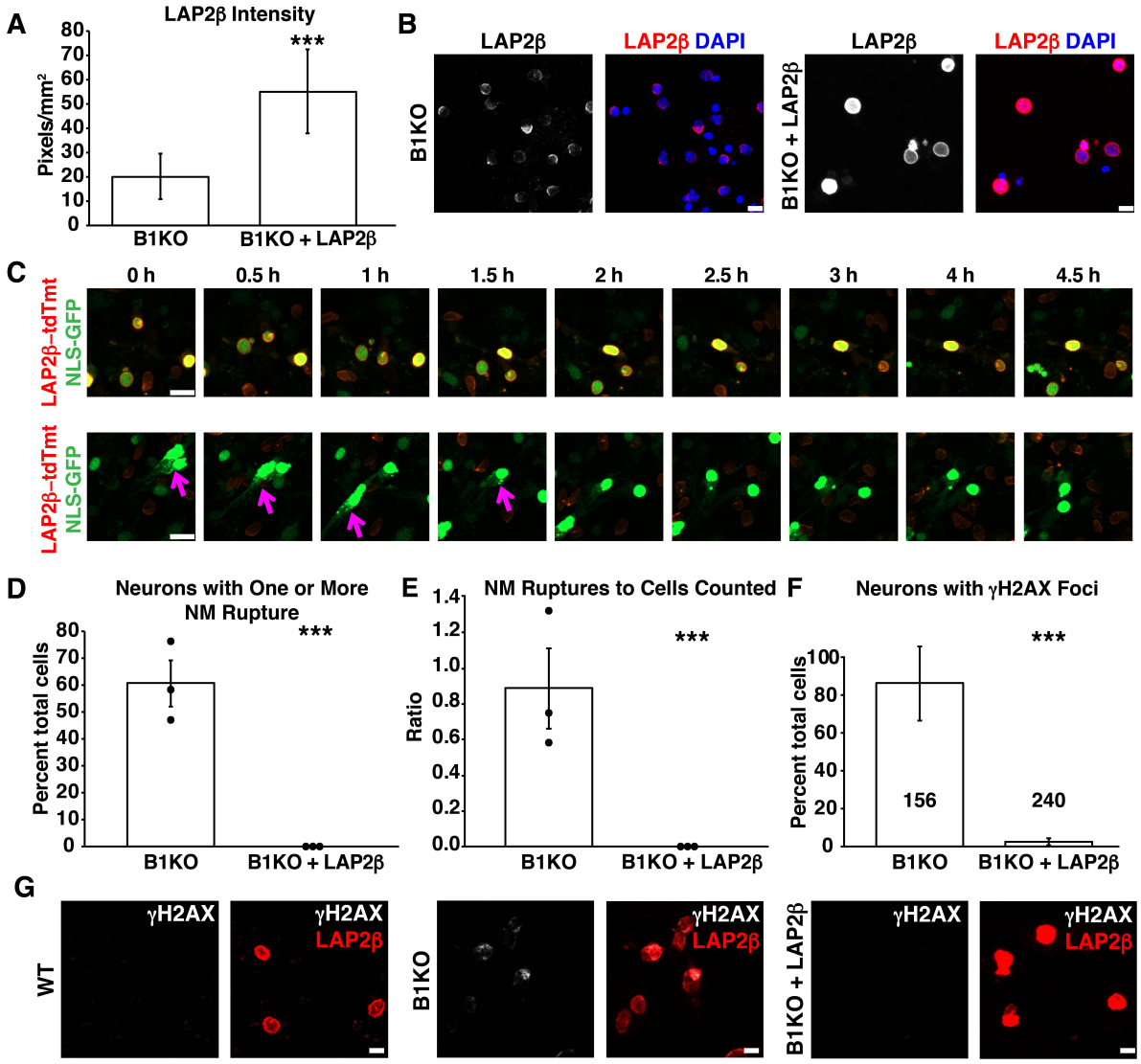

Fig. 4. Higher levels of LAP2β expression in differentiated B1KO neurons prevents nuclear membrane (NM) ruptures. WT and B1KO neurons were transduced with a lentivirus encoding a LAP2β-tdTomato fusion protein (LAP2β-tdTomato). (*A*) Fluorescence intensity in nontransduced and LAP2β-tdTomato–transduced B1KO neurons. Mean ± SD. ***$P < 0.0001$; unpaired Student's *t*-test. After staining neurons with an antibody against LAP2β, confocal micrographs were recorded and ten images were analyzed by ImageJ. Fluorescence intensity for each nucleus was quantified and normalized to nuclear area (in mm^2). (*B*) Immunofluorescence microscopy of

nontransduced and LAP2β-tdTomato–transduced B1KO neurons. Cells were stained with an antibody against LAP2β (white in the left panels; red in the merged image). DNA was stained with DAPI (blue). Scale bars, 10 μm. (*C*) Time-lapse microscopy study of NLS-GFP–expressing B1KO neurons (green) that had been incubated with a LAP2β-tdTomato lentivirus. The neurons were not subjected to drug selection; hence, some of the neurons did not express LAP2β-tdTomato (red). (*Top*) Micrographs of a field containing NLS-GFP–expressing neurons that were successfully transduced with LAP2β-tdTomato. NM ruptures were never observed in NLS-GFP–expressing neurons that expressed LAP2β-tdTomato. (*Bottom*) Confocal micrographs of another field in which several cells expressed NLS-GFP but no LAP2β-tdTomato. Neurons that expressed only NLS-GFP exhibited NM ruptures (evident by escape of GFP into the cytoplasm) (magenta arrows). Scale bars, 20 μm. (*D*) Percentages of NLS-GFP–expressing nontransduced neurons ($n = 148$) and LAP2β-tdTomato–transduced B1KO neurons ($n = 101$) that had at least one NM rupture (detected by escape of GFP into the cytoplasm). Mean ± SEM; $n = 3$ independent experiments; 20 h of imaging/experiment. Dots depict percentages in three independent experiments. ***$P < 0.0005$; χ^2 test. No NM ruptures were detected in 101 LAP2β-tdTomato–transduced B1KO neurons. A total of 148 nontransduced B1KO neurons were evaluated in the three experiments. (*E*) Ratio of the total number of NM ruptures in nontransduced and LAP2β-tdTomato–transduced B1KO neurons divided by the total number of neurons analyzed. Mean ± SEM; $n = 3$ independent experiments; ***$P < 0.0005$; unpaired Student's *t*-test. No NM ruptures were observed in LAP2β-tdTomato–transduced B1KO neurons. A total of 148 nontransduced B1KO neurons were evaluated. (*F*) Percentages of nontransduced and LAP2β-tdTomato–transduced B1KO neurons with γH2AX foci. 240 LAP2β-tdTomato–transduced B1KO neurons and 156 nontransduced B1KO neurons were analyzed. Mean ± SEM; $n = 3$ independent experiments. ***$P < 0.0005$; χ^2

test. The total number of neurons scored are recorded with each bar. (*G*) Confocal micrographs of nontransduced and LAP2β-tdTomato–transduced B1KO neurons after staining the cells with antibodies against LAP2β (red) and the DNA damage marker γH2AX (white). Scale bars, 10 μm.

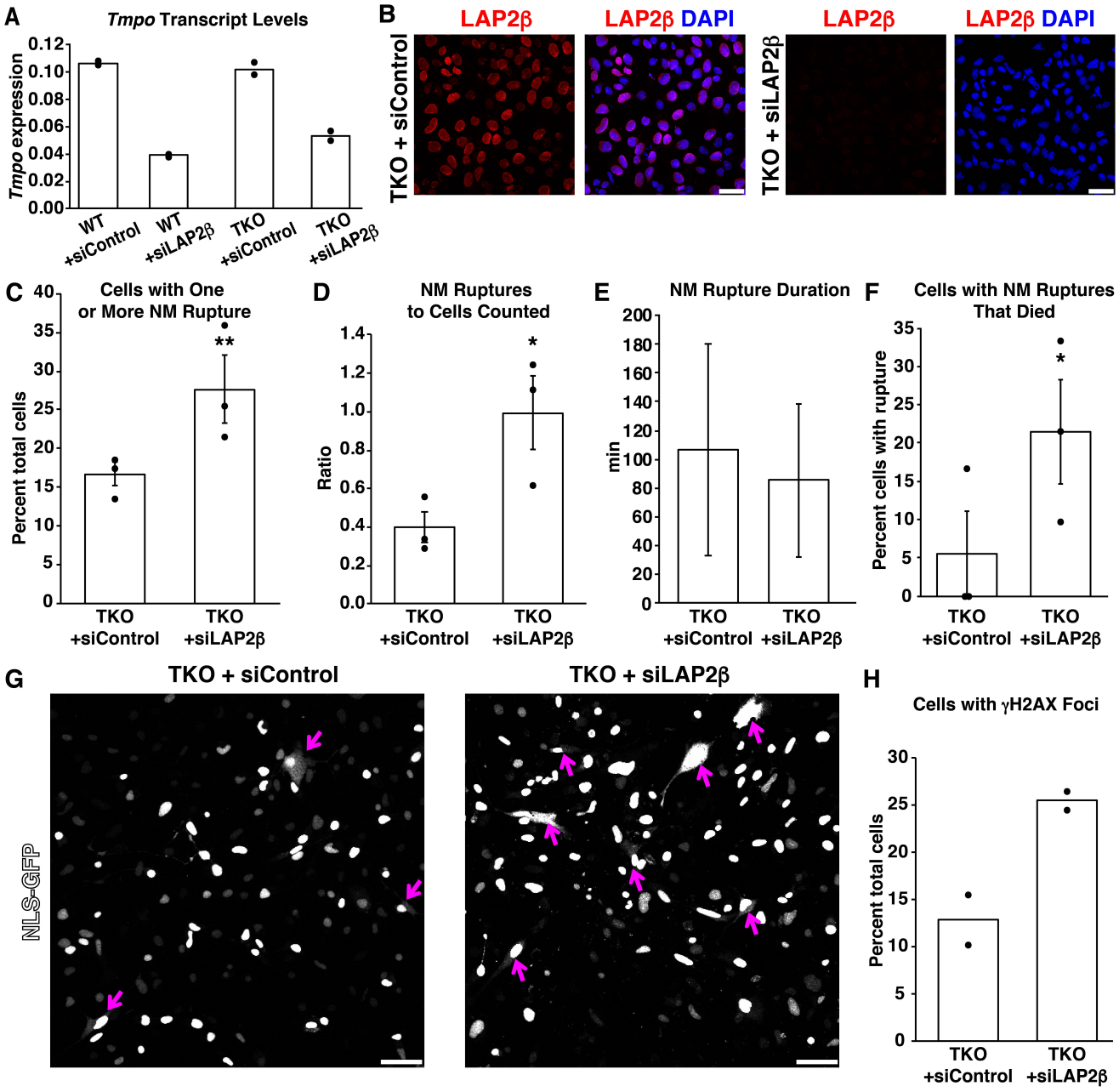

Fig. 5. Reducing LAP2β expression in *Lmnb1*$^{-/-}$*Lmnb2*$^{-/-}$*Lmna*$^{-/-}$ fibroblasts (triple knockout; TKO) with siLAP2β (a small-interfering RNA against *Tmpo*) increases the frequency of nuclear membrane (NM) ruptures and cell death. (*A*) Transcript levels for *Tmpo* (the gene for LAP2β) in wild-type (WT) and TKO MEFs transfected with siLAP2β or a control siRNA (siControl). Means from two independent experiments; dots show results in the two independent experiments;

transcript levels were normalized to *Ppia*. Analyses were performed 24 h after the transfection. $^{**}P < 0.005$; unpaired Student's *t*-test. (*B*) Immunofluorescence micrographs of TKO MEFs transfected with siLAP2β or siControl. MEFs were stained with an antibody against LAP2β (red). DNA was stained with DAPI (blue). Scale bars, 50 μm. (*C*) Percentages of siLAP2β- and control siRNA–transfected TKO MEFs with at least one NM rupture. In 140 control siRNA–transfected TKO MEFs analyzed in three independent experiments, NM ruptures were detected in 23 cells. In 210 siLAP2β-transfected TKO MEFs, 60 cells had a NM rupture. Mean ± SEM; $n = 3$ independent experiments, dots show the percentages in each experiment (20 h of imaging/experiment). $^{**}P = 0.009$; χ^2 test. (*D*) Ratio of total number of total NM ruptures over the total number of MEFs evaluated. Mean ± SEM; $n = 3$ independent experiments, dots show the ratio in each experiment (20 h of imaging/experiment). In 140 control siRNA–transfected TKO MEFs analyzed in three experiments, 58 NM ruptures were detected. In 210 siLAP2β-transfected TKO MEFs, 213 NM ruptures were detected. $^{*}P < 0.05$; unpaired Student's *t*-test. (*E*) NM rupture duration in siLAP2β- or siControl-transfected TKO MEFs (mean ± SD; >35 NM ruptures/group). (*F*) Percentages of siLAP2β- or control siRNA–transfected TKO MEFs that had a NM rupture and subsequently died during 20 h of imaging. Mean ± SEM; $n = 3$ independent experiments; dots show the percentage in each experiment. Of the 23 control siRNA–transfected TKO MEFs that exhibited a NM rupture, 1 died. Of 60 siLAP2β-transfected TKO MEFs that exhibited a NM rupture, 16 died. $^{*}P = 0.024$; χ^2 test. (*G*) Confocal micrographs of siLAP2β- or siControl-transfected TKO MEFs that expressed NLS-GFP (white). Numerous NM ruptures (magenta arrows) were observed in the siLAP2β-transfected TKO MEFs, evident by escape of GFP into the cytoplasm and/or sudden loss of GFP fluorescence within the cell nucleus. Scale bars, 25 μm. (*H*) Percentages of siLAP2β- or control siRNA–transfected TKO MEFs that exhibited nuclear γH2AX foci. Bars depict the mean from two

independent experiments (140 control siRNA–transfected TKO MEFs and 173 siLAP2β-transfected TKO MEFs scored); dots depict percentages in the two experiments.

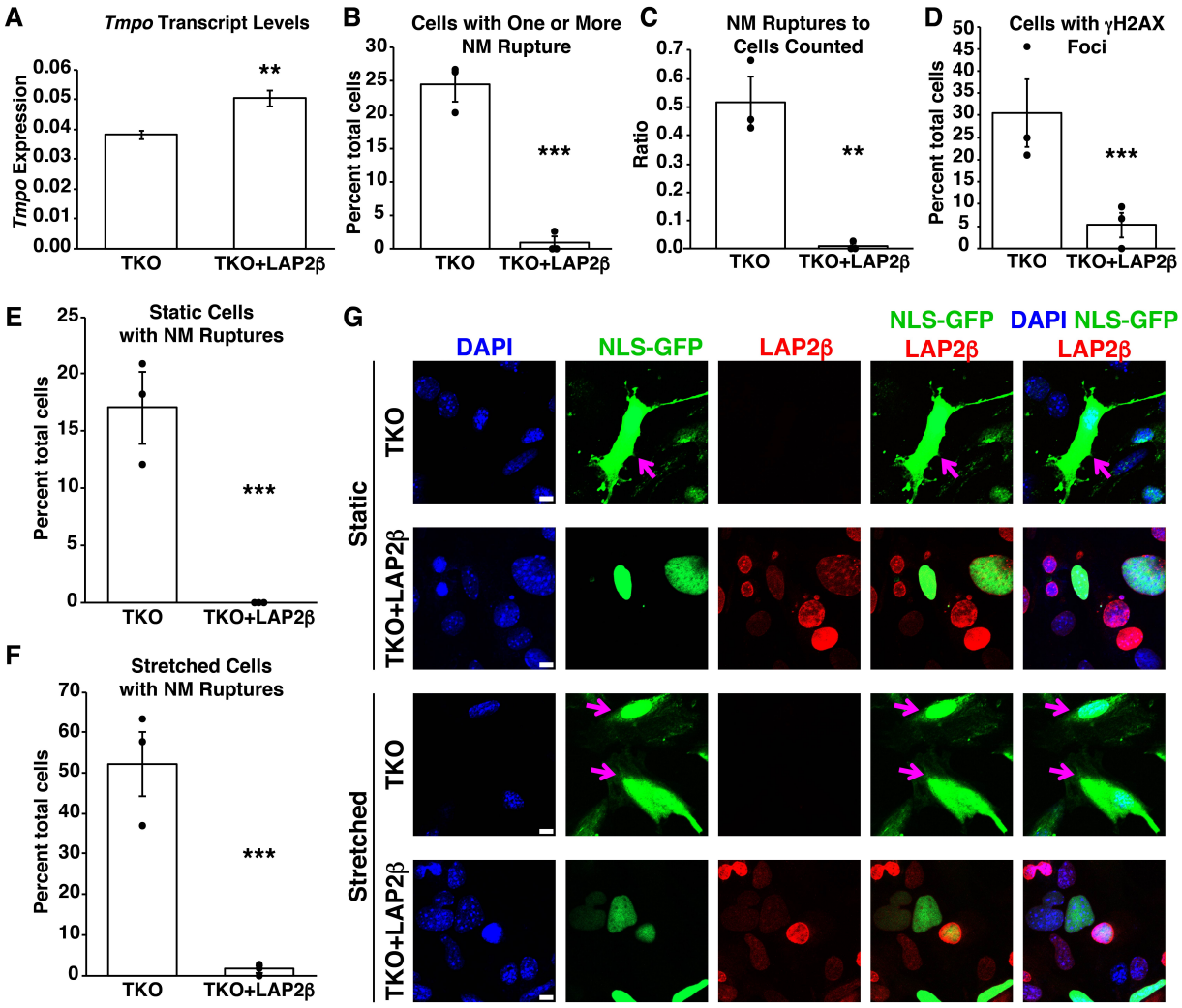

Fig. 6. Transduction of wild-type and TKO MEFs with a lentivirus encoding a LAP2β-tdTomato fusion protein prevents nuclear membrane (NM) ruptures and reduces DNA damage. (*A*) Transcript levels for *Tmpo* (the gene for LAP2β) in nontransduced or LAP2β-tdTomato–transduced TKO MEFs (mean ± SEM; $n = 3$ independent experiments). Transcript levels were normalized to *Ppia* transcripts. $^{**}P = 0.0079$; unpaired Student's *t*-test. (*B*) Percentages of nontransduced and LAP2β-tdTomato–transduced TKO MEFs that had a NM rupture event during 20 h of live-cell imaging. In 141 nontransduced TKO MEFs, 34 MEFs had a NM rupture. In 103 LAP2β-tdTomato–expressing MEFs, only 1 cell had a NM rupture. Mean ± SEM from three

independent experiments (20 h of imaging/experiment). ***$P < 0.0005$; χ^2 test. Black dots depict percentages in each experiment. (*C*) Ratio of the number of NM ruptures in TKO MEFs and LAP2β-tdTomato–transduced MEFs over the total number of cells analyzed. In 141 nontransduced TKO MEFs, there were 69 NM ruptures. In 103 LAP2β-tdTomato–expressing MEFs, there was only one NM rupture. Mean ± SEM from 3 independent experiments; **$P = 0.0055$; unpaired Student's *t*-test. Black dots depict ratios in each experiment. (*D*) Percentages of nontransduced and LAP2β-tdTomato–transduced TKO MEFs with γH2AX foci. Mean ± SEM from three independent experiments; ***$P<0.0005$; χ^2 test. Black dots depict ratios in each experiment. In three independent experiments, 50 nontransduced and 101 LAP2β-tdTomato–expressing MEFs were analyzed. (*E*) Percentages of nontransduced and LAP2β-tdTomato–transduced TKO MEFs with a NM rupture when plated on PDMS membranes under static conditions. In 172 nontransduced TKO MEFs, 29 MEFs had a NM rupture. In 195 LAP2β-tdTomato–expressing MEFs, there were no NM ruptures. Shown are mean percentages ± SEM from three independent experiments; ***$P<0.0001$; χ^2 test. Black dots depict percentages in each experiment. (*F*) Percentages of nontransduced and LAP2β-tdTomato–transduced TKO MEFs with a NM rupture when the cells were subjected to uniaxial stretching on a PDMS membrane for 2 h. In 151 nontransduced TKO MEFs, 79 MEFs had a NM rupture. Among 198 LAP2β-tdTomato–expressing MEFs, three cells had a NM rupture. Shown are mean ± SEM from three independent experiments; ***$P<0.0001$; χ^2 test. Black dots depict percentages in each experiment. (*G*) Immunofluorescence microscopy of nontransduced and LAP2β-tdTomato–transduced TKO MEFs under static and stretched conditions. The TKO MEFs expressed NLS-GFP (green) alone or NLS-GFP and LAP2β-tdTomato (red). DNA was stained with DAPI (blue). Magenta arrows point to NM ruptures. Scale bars, 10 μm.

References

1. Chen NY*, et al.* (2018) Fibroblasts lacking nuclear lamins do not have nuclear blebs or protrusions but nevertheless have frequent nuclear membrane ruptures. *Proc Natl Acad Sci USA* 115(40):10100–10105.

2. Chen NY*, et al.* (2019) An absence of lamin B1 in migrating neurons causes nuclear membrane ruptures and cell death. *Proc Natl Acad Sci USA* 116(51):25870–25879.

3. Young SG, Jung HJ, Coffinier C, & Fong LG (2012) Understanding the roles of nuclear A- and B-type lamins in brain development. *J Biol Chem* 287(20):16103–16110.

4. Jung HJ*, et al.* (2012) Regulation of prelamin A but not lamin C by miR-9, a brain-specific microRNA. *Proc Natl Acad Sci USA* 109(7):E423–431.

5. Jung HJ, Lee JM, Yang SH, Young SG, & Fong LG (2013) Nuclear lamins in the brain - new insights into function and regulation. *Mol Neurobiol* 47(1):290–301.

6. Young SG, Jung HJ, Lee JM, & Fong LG (2014) Nuclear lamins and neurobiology. *Mol Cell Biol* 34(15):2776–2785.

7. Berger R*, et al.* (1996) The characterization and localization of the mouse thymopoietin/lamina-associated polypeptide 2 gene and its alternatively spliced products. *Genome Res* 6(5):361–370.

8. Foisner R & Gerace L (1993) Integral membrane proteins of the nuclear envelope interact with lamins and chromosomes, and binding is modulated by mitotic phosphorylation. *Cell* 73(7):1267–1279.

9. Herrada I*, et al.* (2016) Purification and Structural Analysis of LEM-Domain Proteins. *Methods Enzymol* 569:43–61.

10. Furukawa K (1999) LAP2 binding protein 1 (L2BP1/BAF) is a candidate mediator of LAP2-chromatin interaction. *J Cell Sci* 112 (Pt 15):2485–2492.

11. Yang L, Guan T, & Gerace L (1997) Lamin-binding fragment of LAP2 inhibits increase in nuclear volume during the cell cycle and progression into S phase. *J Cell Biol* 139(5):1077–1087.

12. Young AM, Gunn AL, & Hatch EM (2020) BAF facilitates interphase nuclear membrane repair through recruitment of nuclear transmembrane proteins. *Mol Biol Cell* 31(15):1551–1560.

13. King MC & Lusk CP (2019) Loss of nuclear envelope integrity? No probLEM-BAF has it covered. *J Cell Biol* 218(7):2077–2079.

14. Lusk CP & Ader NR (2020) CHMPions of repair: Emerging perspectives on sensing and repairing the nuclear envelope barrier. *Curr Opp Cell Biol* 64:25–33.

15. Thaller DJ*, et al.* (2019) An ESCRT-LEM protein surveillance system is poised to directly monitor the nuclear envelope and nuclear transport system. *eLife* 8.

16. Halfmann CT*, et al.* (2019) Repair of nuclear ruptures requires barrier-to-autointegration factor. *J Cell Biol* 218(7):2136–2149.

17. Coffinier C*, et al.* (2011) Deficiencies in lamin B1 and lamin B2 cause neurodevelopmental defects and distinct nuclear shape abnormalities in neurons. *Mol Biol Cell* 22(23):4683–4693.

18. Gorski JA*, et al.* (2002) Cortical excitatory neurons and glia, but not GABAergic neurons, are produced in the Emx1-expressing lineage. *J Neurosci* 22(15):6309–6314.

19. Chen NY, Kim PH, Fong LG, & Young SG (2020) Nuclear membrane ruptures, cell death, and tissue damage in the setting of nuclear lamin deficiencies. *Nucleus* 11(1):237–249.

20. Guo Y & Zheng Y (2015) Lamins position the nuclear pores and centrosomes by modulating dynein. *Mol Biol Cell* 26(19):3379–3389.

21. Brachner A, Reipert S, Foisner R, & Gotzmann J (2005) LEM2 is a novel MAN1-related inner nuclear membrane protein associated with A-type lamins. *J Cell Sci* 118(Pt 24):5797–5810.

22. Jung HJ*, et al.* (2013) Farnesylation of lamin B1 is important for retention of nuclear chromatin during neuronal migration. *Proc Natl Acad Sci USA* 110(21):E1923–1932.

23. Vaughan A*, et al.* (2001) Both emerin and lamin C depend on lamin A for localization at the nuclear envelope. *J Cell Sci* 114(Pt 14):2577–2590.

24. Sullivan T*, et al.* (1999) Loss of A-type lamin expression compromises nuclear envelope integrity leading to muscular dystrophy. *J Cell Biol* 147(5):913–920.

25. Fong LG*, et al.* (2006) Prelamin A and lamin A appear to be dispensable in the nuclear lamina. *J Clin Invest* 116(3):743–752.

26. Vallee RB & Tsai JW (2006) The cellular roles of the lissencephaly gene LIS1, and what they tell us about brain development. *Genes Dev* 20(11):1384–1393.

27. Wynshaw-Boris A (2007) Lissencephaly and LIS1: insights into the molecular mechanisms of neuronal migration and development. *Clin Genet* 72(4):296–304.

28. Jung HJ, *et al.* (2014) An absence of nuclear lamins in keratinocytes leads to ichthyosis, defective epidermal barrier function, and intrusion of nuclear membranes and endoplasmic reticulum into the nuclear chromatin. *Mol Cell Biol* 34(24):4534–4544.

29. Jahn D, *et al.* (2012) A truncated lamin A in the Lmna -/- mouse line: implications for the understanding of laminopathies. *Nucleus* 3(5):463–474.

30. Coffinier C, *et al.* (2010) Abnormal development of the cerebral cortex and cerebellum in the setting of lamin B2 deficiency. *Proc Natl Acad Sci USA* 107(11):5076–5081.

31. Denais CM, *et al.* (2016) Nuclear envelope rupture and repair during cancer cell migration. *Science* 352(6283):353–358.

32. Yang SH, *et al.* (2011) An absence of both lamin B1 and lamin B2 in keratinocytes has no effect on cell proliferation or the development of skin and hair. *Hum Mol Genet* 20(18):3537–3544.

33. Kim PH, *et al.* (2018) Disrupting the LINC complex in smooth muscle cells reduces aortic disease in a mouse model of Hutchinson-Gilford progeria syndrome. *Sci Transl Med* 10(460).

Supplemental Figures and Figure Legends

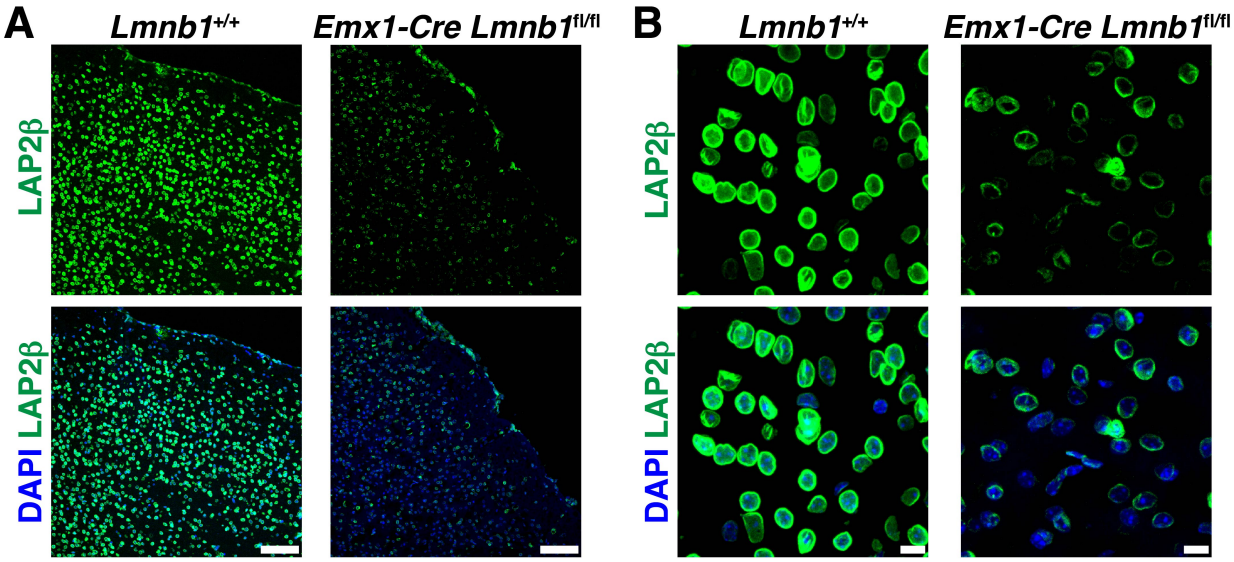

Supplemental Figure 1. Inactivation of *Lmnb1* in the forebrain results in low levels of LAP2β and an abnormal distribution of LAP2β along the nuclear rim. (*A–B)* Confocal micrographs of sections of the cerebral cortex in a wild-type mouse (*Lmnb1*$^{+/+}$) (*A*) and a forebrain-specific lamin B1–deficient mouse (*Emx1-Cre Lmnb1*$^{fl/fl}$) (*B*). Sections were stained with an antibody against LAP2β (green); DNA was stained with DAPI (blue). Scale bars: 50 μm in (*A*); 10 μm in (*B*).

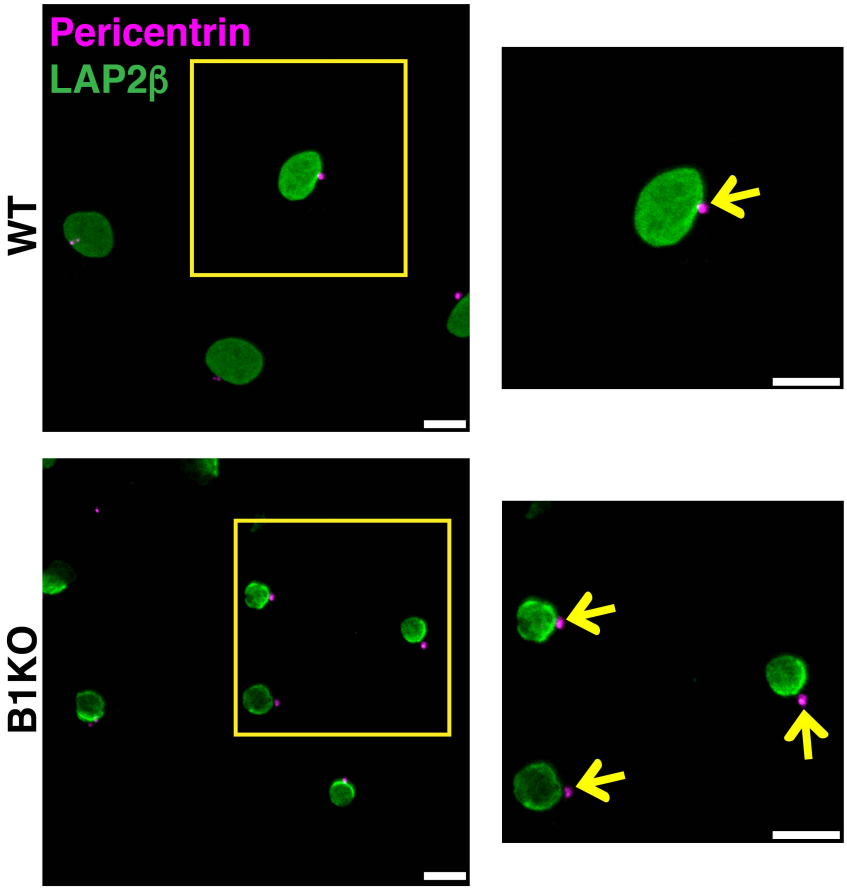

Supplemental Figure 2. *Lmnb1* deficiency in cortical neurons results in low levels of LAP2β in the nucleus and abnormally distributed LAP2β along the nuclear rim. Confocal micrographs show maximum intensity projections of *z*-stacks of wild-type (WT) and *Lmnb1*$^{-/-}$ (B1KO) neurons after staining with antibodies against LAP2β (green) and the centrosome marker pericentrin (magenta). The boxed regions are shown at higher magnification on the right. Yellow arrows point to the centrosome. Scale bars: 10 μm (left); 10 μm (right).

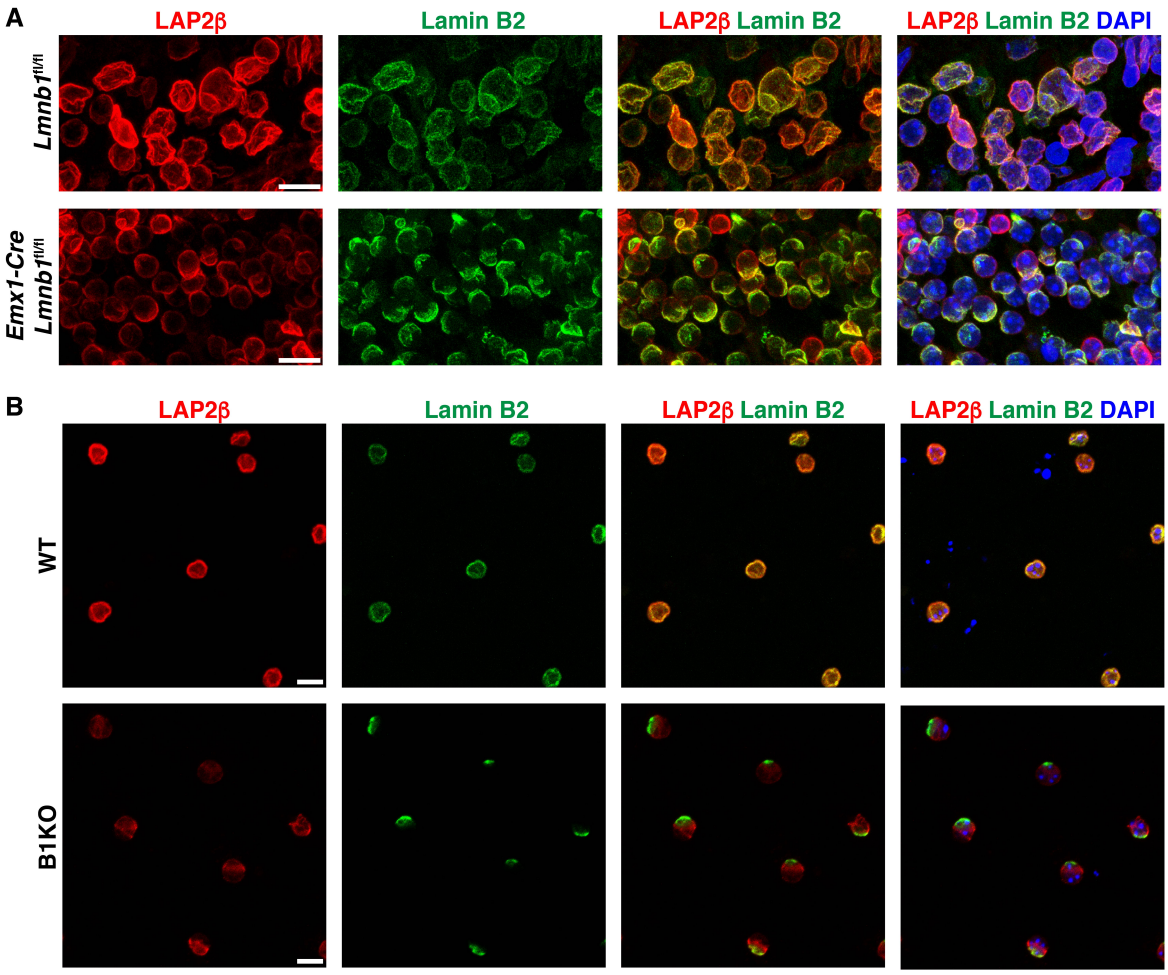

Supplemental Figure 3. LAP2β and lamin B2 are polarized to the same side of the nucleus in lamin B1–deficient neurons. (*A*) Immunofluorescence micrographs (maximum intensity projections of *z*-stacks) of the cortical plate of the forebrain of E18.5 wild-type (*Lmnb1*$^{fl/fl}$) and lamin B1–deficient (*Emx1-Cre Lmnb1*$^{fl/fl}$) mouse embryos. Sections were stained with antibodies against LAP2β red) and lamin B2 (green); DNA was stained with DAPI (blue). Scale bars, 10 μm. (*B*) Confocal micrographs (maximum intensity projections of *z*-stacks) of differentiated wild-type and *Lmnb1*$^{-/-}$ (B1KO) neurons after staining with antibodies against LAP2β (red) and lamin B2 (green); DNA was stained with DAPI (blue). LAP2β and lamin B2 were polarized to the same side of the nucleus, but the extent of lamin B2 polarization was greater. Scale bars, 10 μm.

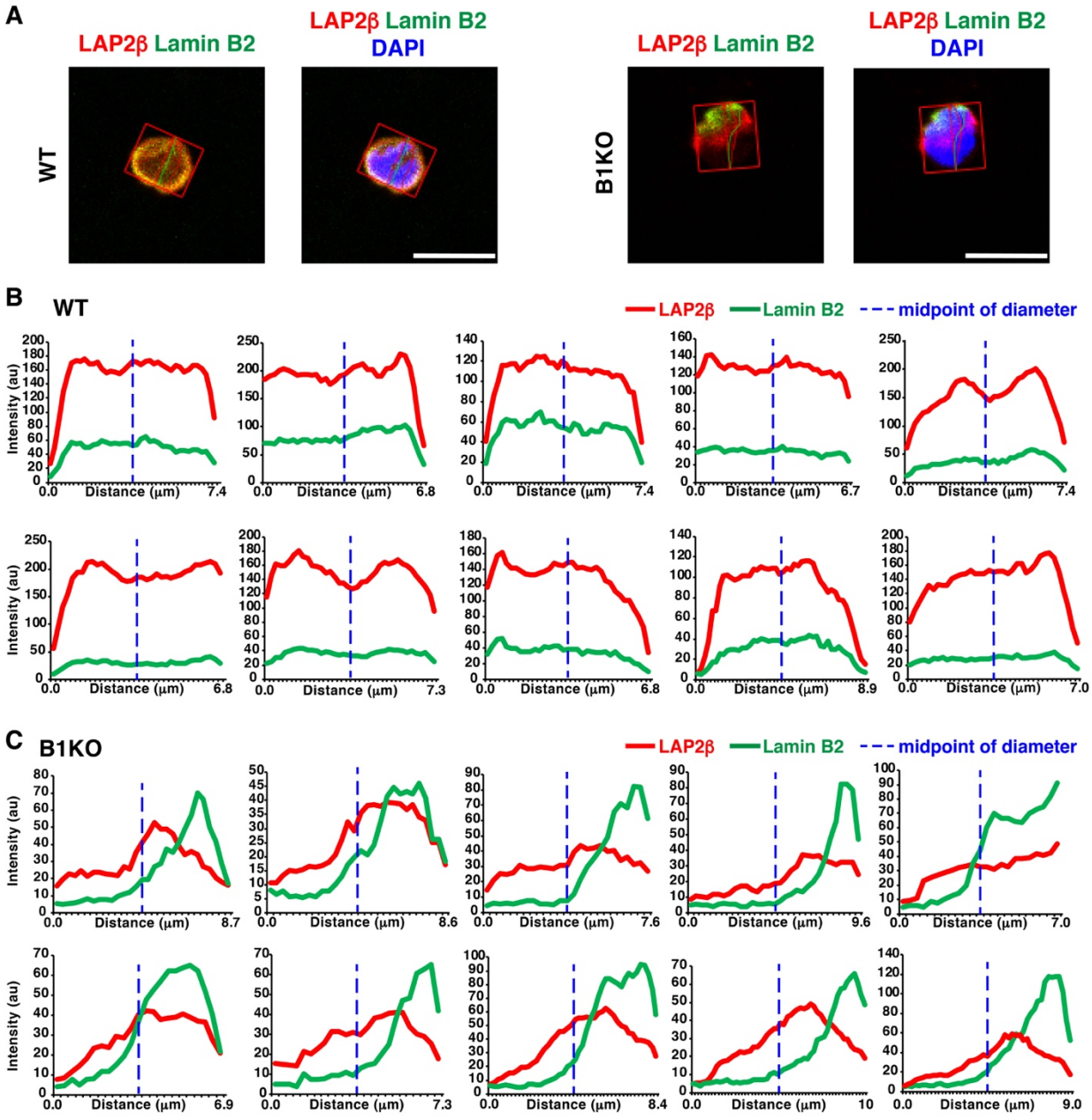

Supplemental Figure 4. The distribution of LAP2β and lamin B2 is polarized in lamin B1–deficient neurons. (*A*) Wild-type and *Lmnb1*$^{-/-}$ (B1KO) neurons were stained with antibodies against LAP2β (red) and lamin B2 (green) and DNA was stained with DAPI (blue). The distributions of LAP2β and lamin B2 in the nucleus were analyzed with the Zen Profile tool, where nuclei are individually boxed. The profiles of LAP2β and lamin B2 are superimposed on top of

confocal microscope images (maximum intensity projections of *z*-stacks). Scale bars, 10 μm. (*B*) Fluorescent intensity plots for LAP2β and lamin B2 in ten representative wild-type neurons. The midpoint of the nucleus is marked by a dotted blue line. The fluorescence intensities for LAP2β (red) and lamin B2 (green) are equally distributed on either side of the midline, indicating that there is no polarization. (*C*) Fluorescent intensity plots for LAP2β and lamin B2 in ten representative B1KO neurons. Note that the distribution of both LAP2β (red) and lamin B2 (green) is higher on one side of the midline, indicating that their distribution is polarized.

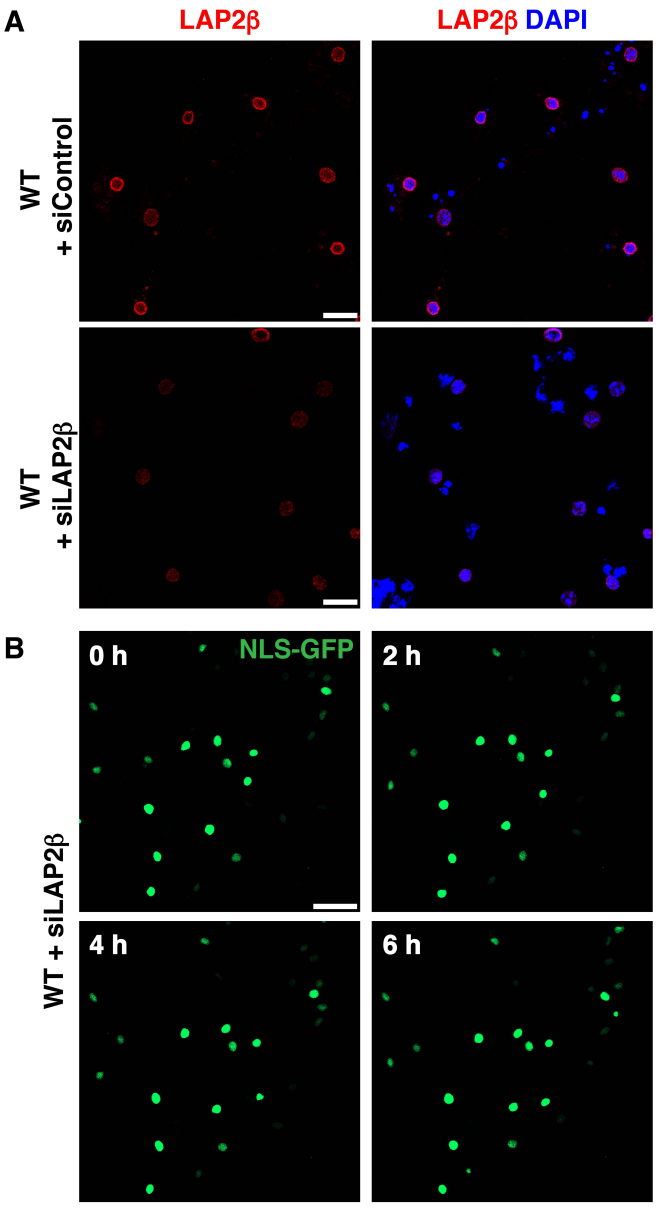

Supplemental Figure 5. LAP2β expression in wild-type (WT) neurons that had been transfected with siLAP2β (a small-interfering RNA against *Tmpo*) or a control siRNA (siControl). (*A*) Neurons were stained with an antibody against LAP2β (red); DNA was stained with DAPI (blue). Scale bars, 20 µm. (*B*) Time-lapse microscopy images of NLS-GFP–expressing wild-type (WT) neurons (green) that had been transfected with siLAP2β. No nuclear membrane ruptures were observed in NLS-GFP–expressing WT neurons. Scale bar, 50 µm.

Supplementary Tables

Table S1. Oligonucleotide primers for qRT-PCR

Gene	Species	Sequences (5′–3′)
Cyclophilin A (*Ppia*)	Mouse	tgagcactggagagaaagga ccattatggcgtgtaaagtca
LAP2 (*Tmpo*)	Mouse	ggagtgaatcctggtccattg gactgttggaagaggagtagagg

Table S2. Antibodies used for immunofluorescence microscopy

Antigen	Antibody	Species	Company	ICC*	IHC*
LAP2β [27]	Monoclonal	Mouse	BD Transduction Laboratories	1:500	1:500
Cleaved Caspase-3	Polyclonal	Rabbit	Cell Signaling Technology	1:1000	1:1000
Pericentrin	Polyclonal	Rabbit	Abcam	1:1000	
Lamin B2	Monoclonal	Rabbit	Abcam	1:1000	1:1000
GFP	Polyclonal	Rabbit	Invitrogen		1:1000
γ-H2AX	Monoclonal	Rabbit	EMD Millipore	1:1000	

*ICC, immunocytochemistry; IHC, immunohistochemistry

Table S3. Sequence of the siRNA used to knock down LAP2β expression

Gene	Species	siRNA cDNA target sequence (5′–3′)
Tmpo	Mouse	GCAGGAAAGCCACAAAGAAAACTGATAAGCCCAGGCTAGAAGATAA AGATGATCTGGATGTGACAGAGCTCTCTAATGAAGAACTTCTGGATCA GCTTGTAAGATATGGAGTGAATCCTGGTCCCATTGTGGGAACAACCAG GAAGCTATATGAGAAGAAGCTGTTGAAGCTGAGGGAGCAGGGAACTG AATCGAGATCCTCTACTCCTCTTCCAACAGTCTCTTCCTCTGCAGAAA ACACAAGGCAGAATGGAAGTAACGACTCTGACAGATACAGCGACAAT GATGAAGGAAAGAAGAAAGAACACAAGAAAGTGAAGTCCGCTAGGG ATTGTGTTCCTTTTTCTGAACTTGCATCTACTCCCTCTGGTGCATTTTTT CAGGGTATTTCTTTCCCTGAAATCTCCACCCGTCCTCCTTTGGGCAGGA CTGAACTG

Supplementary Movie Legends

Movie S1. B1KO neurons exhibit nuclear membrane ruptures in the absence of LAP2β - tdTomato expression. B1KO neurons expressing NLS-GFP (green) were imaged over 5 h. Nuclear membrane ruptures were present in two B1KO neurons, evident by the presence of NLS-GFP in the cytoplasm. Individual frames were collected every 10 min. This movie shows 3 frames per second.

Movie S2. B1KO neurons expressing the LAP2β-tdTomato fusion protein do not have nuclear membrane ruptures. B1KO neurons expressing LAP2β-tdTomato (red) and NLS-GFP (green) appear yellow or orange. Cells were imaged over 5 h. Individual frames were collected every 10 min. This movie shows 3 frames per second.